UNLV Theses, Dissertations, Professional Papers, and Capstones

6-2006

Petrogenesis of Pleistocene Basalts in the Norris-Mammoth Corridor, Yellowstone National Park

Kristeen Marie Bennett
University of Nevada, Las Vegas

Follow this and additional works at: https://digitalscholarship.unlv.edu/thesesdissertations

Part of the Geology Commons, and the Volcanology Commons

PETROGENESIS OF PLEISTOCENE BASALTS

IN THE NORRIS-MAMMOTH CORRIDOR,

YELLOWSTONE NATIONAL PARK

by

Kristeen Marie Bennett

Bachelor of Science
California State University, Chico
2002

Master of Science
University of Nevada, Las Vegas
200?

A thesis submitted in partial fulfillment
of the requirements for the

Master of Science Degree
Department of Geoscience
College of Sciences

Graduate College
University of Nevada, Las Vegas
June 200?

ABSTRACT

**Petrogenesis of Pleistocene basalts in the Norris-Mammoth Corridor,
Yellowstone National Park**

by

Kristeen Bennett

Dr. Eugene Smith, Examination Committee Chair
Professor of Geoscience
University of Nevada, Las Vegas

The basalts of the Norris-Mammoth corridor within the Yellowstone Plateau volcanic field have an outcrop erupted volume of ~94 km^3. Basalt in the Yellowstone Plateau volcanic field is minor in volume compared to 3,700 km^3 of felsic lavas, domes, and pyroclastic rocks. The tholeiitic eruptive products formed small Hawaiian-style shield volcanoes. A newly identified volcanic vent, called the Panther Creek vent, within the Swan Lake Flat basalt stratigraphic unit, was primarily Strombolian in its eruption style. This vent is the first recognized cinder cone in Yellowstone National Park.

All basaltic units within the Norris-Mammoth corridor, and the Yellowstone Plateau volcanic field, can be differentiated by isotopes and trace element geochemistry. This suggests that independent partial melting events of asthenospheric mantle were responsible for the petrogenesis of the basalts within the Norris-Mammoth corridor. The simplest model to explain the genesis of the youngest basalt unit (Swan Lake Flat basalt that erupted from the Panther Creek vent) in the Norris-Mammoth corridor is one of "source mixing." Partial melting produced EMORB-like basalt in the upper mantle. This basalt was contaminated

or mixed with older, fractionated basalt within the lithospheric mantle.

More precise ages for post-Yellowstone caldera basalts, along with accurate Nd and Sr isotopes show a general decrease in $^{87}Sr/^{86}Sr$ and increase in ε_{Nd} with decreasing age of Norris-Mammoth corridor basalts. This suggests that the basalts in the Norris-Mammoth corridor may be recording a new influx asthenospheric partial melts into the overlying lithosphere. Pooling of multiple basaltic partial melts in the lithosphere may be melting surrounding crust, generating rhyolitic magma that may coalesce to form a batholith-sized magma chamber and produce a new caldera cycle.

TABLE OF CONTENTS

LIST OF TABLES

CHAPTER 1

INTRODUCTION

Geologic Background

Volcanism within the Yellowstone Plateau volcanic field has been intermittently active for the past 2.2 Ma (Doe et al., 1982; Obradovich, 1992; Christiansen, 2001). The most voluminous products of this volcanism are represented by rhyolitic ash-flow tuffs related to a "caldera cycle" (Christiansen, 2001). Each caldera cycle began with the extrusion of pre-caldera rhyolite domes and flows, climaxed with the eruption of a caldera-forming ash-flow tuff, and ended with the extrusion of post-caldera rhyolite domes and/or flows. Eruptions of caldera-marginal basalts occurred throughout each cycle. The final stage of each caldera cycle is the infilling of each caldera with voluminous basalt flows, but this has yet to occur within Yellowstone National Park. Basalt fills older calderas in the smaller Henry's Fork caldera and the broad Snake River Plain basalt province, southeast of the Yellowstone National Park. Geophysical evidence suggests that there are numerous calderas buried beneath basalt flows of the Snake River Plain (Morgan et al., 1984; Josten et al., 1997).

Two of these caldera cycles have been identified within Yellowstone National Park, the third is to the southwest in the Island Park area (See Figure 1). The first caldera cycle began during the late Pliocene (2.1 Ma) with eruption of the Huckleberry Ridge Tuff (2,500 km^3) (Christiansen, 2001). The Junction Butte Basalt and the Basalt of the Narrows are associated with this tuff. Hepburn Mesa basalt, which crops out approximately ten kilometers north of

the town of Gardiner, may also be a part of this caldera cycle (Smith et al., 1997). The volume of rhyolite and basalt related to this cycle may have been more abundant but is not detectable because of younger volcanic cover associated with later caldera cycles.

The Henry's Fork Caldera (previously known as the Island Park Caldera) formed during the second caldera cycle at 1.2 Ma (Christiansen, 2001). The Henry's Fork Caldera eruption produced the Mesa Falls Tuff (280 km^3). The eruptions of Undine Falls Basalt, Fall River Basalt, Basalt of Warm River, and Basalt of Shotgun Valley are thought to be related to this caldera cycle (Christiansen, 2001). Gerrit Basalt occurs within the Henry's Fork Caldera and its eruption may indicate later stages of caldera development; the same progression that has been observed within the Snake River Plain (Christiansen, 2001).

The Yellowstone Caldera formed during the third, most recent cycle. This cycle culminated with the eruption of the Lava Creek Tuff in a single, 1,000 km^3 cooling unit during the middle Pleistocene (640 ka) (Christiansen, 2001). A number of exposures of basalt related to the third cycle are exposed to the north of the caldera rim. These include Osprey Basalt, Madison River Basalt, Basalt of Geode Creek, and Swan Lake Flat Basalt. Falls River Basalt and the Basalt of Mariposa Lake are exposed south of the present caldera (See Figure 2).

To the southwest, the Yellowstone Plateau merges with the Snake River Plain near the Henry's Fork Caldera. Hamilton (1960, 1963, 1964, and 1965) and Hamilton and Wilshire (1965) first suggested that there was a "volcanic association" linking the Snake River Plain and the Yellowstone Plateau. Basalts of the Snake River Plain overlap some of the older rocks of the Yellowstone Plateau field at its southwestern margin.

Basalts in the Norris-Mammoth corridor

This study focuses on the extracaldera basalts in the Norris-Mammoth corridor. These basalts are olivine tholeiites with sparse phenocrysts of plagioclase and rare olivine. The groundmass is composed of olivine, clinopyroxene, labradorite, and some iron and titanium oxides (Christiansen, 2001). For this study, the following basalt fields within the Norris-Mammoth corridor were studied: (1) Swan Lake Flat Basalt, (2) Madison River Basalt, and (3) Undine Falls Basalt. Swan Lake Flat and Madison River basalts are known to have erupted after the Lava Creek Tuff. Based upon volcanic stratigraphy and a K/Ar date of 580 ka, Undine Falls basalt erupted after the Lava Creek Tuff (Obradovich, 1992). These basalts will be used to determine if:

1. any of the basalts sampled can be geochemically derived from one another;

2. the mantle source of basalts in the Yellowstone Plateau volcanic field can be determined;

3. the basalts of the Norris-Mammoth corridor signify a new influx asthenosphere-derived partial melts into he overlying lithosphere or the waning stages of the Yellowstone caldera cycle.

Previous Work

The volcanic origin of Yellowstone was first recognized by F. V. Hayden and others (Hayden, 1872; 1873; Bradley, 1873; Peale, 1873) during the Geological and Geographical Survey of the Territories. Since its recognition as a volcanic field, Yellowstone's topographic and hydrothermal features have been attributed to large-scale, caldera-creating volcanism.

The distinction between the Tertiary Absaroka rhyolites and the Cenozoic ash-flow tuffs related to the present Pliocene and Pleistocene calderas was first made during an U.S. Geological Survey (USGS) study under the direction of Hague between 1883 and 1889 (Hague, 1912). In the early stages of this survey, Iddings (1888; 1889a,b) illustrated the apparent association of Yellowstone basalt and rhyolite. Later work focused on specialized problems such as the origin of the mixed basalt-rhyolite lavas of the Gardner River. Fenner (1938, 1944), Wilcox (1944), and Hawkes (1945) focused on the possible mechanisms producing the mixed lavas.

The most comprehensive mapping of the Yellowstone area was undertaken by the U.S. Geological Survey, more specifically by Christiansen (1974) and Christiansen and Blank (1974a, 1974b, 1975a, 1975b). Subsequently Christiansen and Blank (1972), Christiansen (1979, 2001) and Smith and Christiansen (1980) described the stratigraphic relationships and general geology. During this period of extensive mapping, Christiansen and others identified the eruptive products of at least three calderas within the Yellowstone Plateau volcanic field.

Doe et al. (1982) performed preliminary geochemical and isotope geochemistry of the basalts and rhyolites associated with the third caldera cycle. Specifically, they focused on Pb, Sr and Th/U isotopic systems. They noted that within the northern Rocky Mountains and the Snake River Plain, volcanic rocks characteristically have higher $^{87}Sr/^{86}Sr$ and lower $^{206}Pb/^{204}Pb$ than Oceanic Island Basalt (OIB). According to Doe et al. (1982) the relationships between $^{207}Pb/^{204}Pb$ and $^{206}Pb/^{204}Pb$ indicate the involvement of 1.5-3.0 Ga rocks in the source material (upper mantle keel?) and not contamination by crustal material. Hildreth et al. (1991) also suggested contributions of old lithospheric mantle to the melt source. Their evidence is substantiated by elevated baseline Nd and Sr isotope ratios.

However, Hildreth et al. (1991) suggested that the basaltic melt is also contaminated by crustal components, more specifically hydrothermal brines. In addition, Hildreth et al. (1991) provided evidence for crustal contamination including quartz xenocrysts and the enriched values of LIL (Large Ion Lithophile) elements relative to Mid-ocean Ridge Basalt (MORB). Christiansen (2001) organized his initial field observations, preliminary major and trace element data, petrographic descriptions, and stratigraphic relationships into a U.S. Geological Survey Professional Paper.
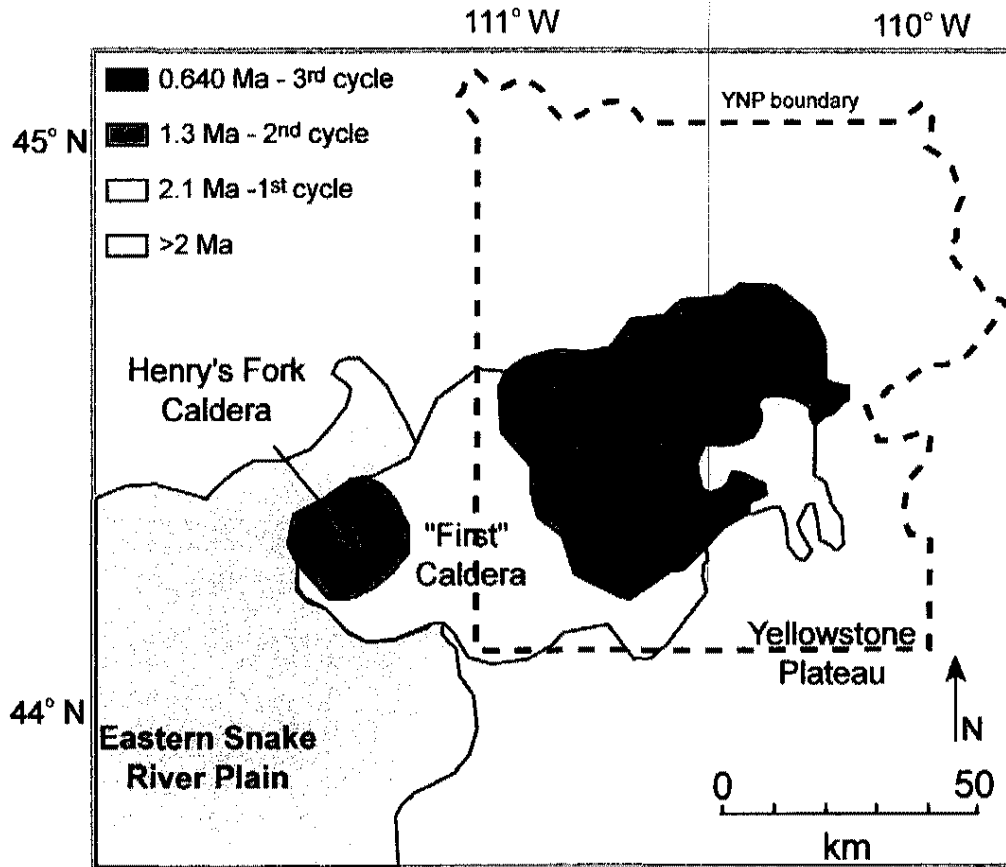
Figure 1: Depiction of the three caldera cycles within the Yellowstone Plateau volcanic field. The overlap of the basalts of the Eastern Snake River Plain is also shown west of the "First" and Henry's Fork Calderas. The boundary of Yellowstone National Park is shown with a dashed line.
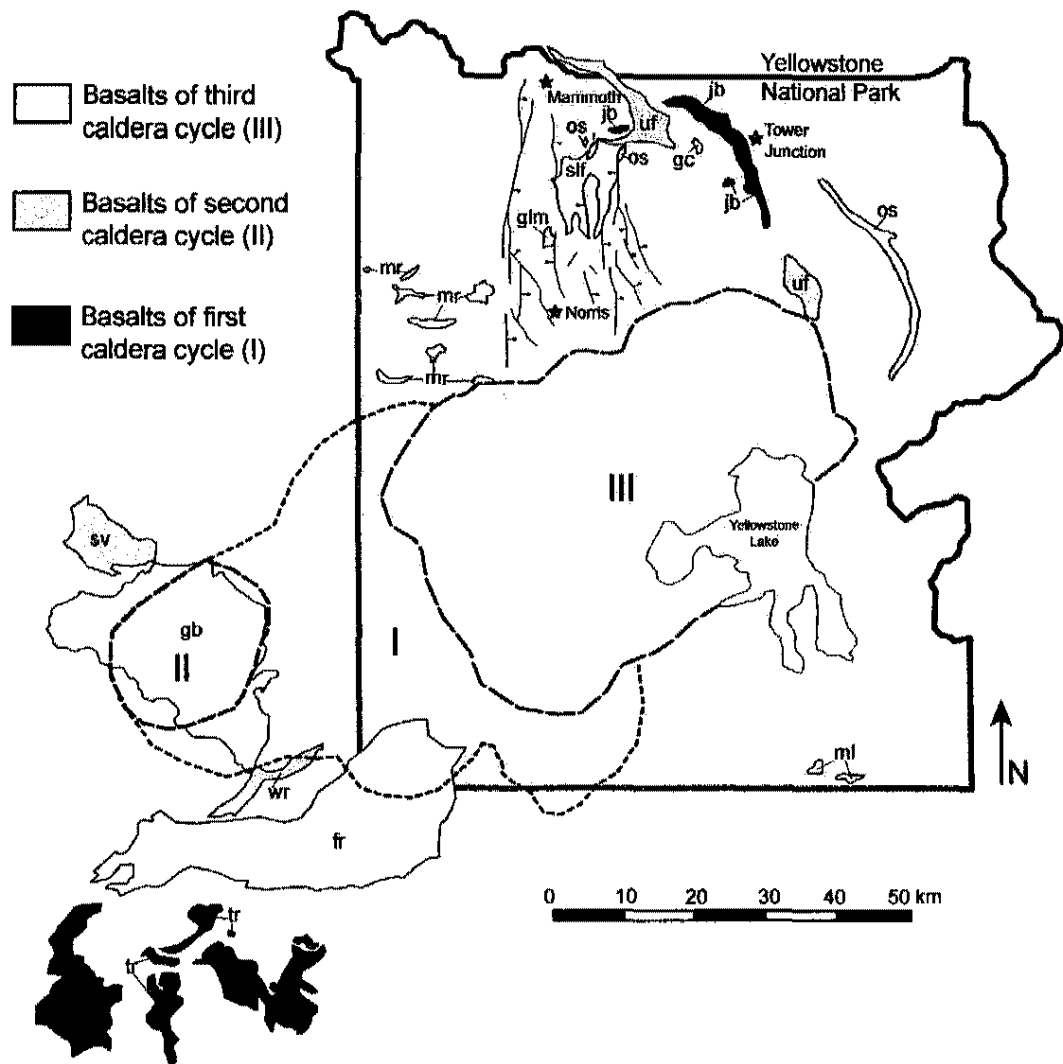
Figure 2: Exposures of basalts and their relationship to caldera cycles according to a figure modified from Hildreth et al. (1991). Basalts: jb=Junction Butte; tr=Teton River; sv=Shotgun Valley; wr=Warm River; fr=Falls River; uf=Undine Falls; mr=Madison River; slf=Swan Lake Flat; os=Osprey; gc=Geode Creek; ml=Mariposa Lake; and glm=Grizzly Lake mixed lavas. I, II, and III represent the calderas formed during each of the three caldera cycles.

CHAPTER 2

PHYSICAL VOLCANOLOGY

The information presented in this chapter is a compilation of stratigraphy, geochronology, and physical volcanology of lava flows and vent areas within the Norris-Mammoth corridor, the Madison Plateau, and north of the town of Gardiner, Montana. All basalts are considered as units within in the Yellowstone Plateau volcanic field.

The eruptive sequence of lava flows, shields, and cinder cone(s) is difficult to determine, because there is extensive cover of glacial till associated with pre-Pleistocene and Pleistocene glaciation events and/or alluvium. Regional volcanic stratigraphy, however, was established by Pierce (1979). Geologic mapping by Christiansen (1974) and Christiansen and Blank (1974a, 1974b, 1975a, 1975b) determined the regional stratigraphic relationships, but not the stratigraphy within each volcanic center. The ages of the basalts were determined by (1) previously published K/Ar dates by Obradovich (1992), (2) their stratigraphic relationship to other volcanic units of known age, and (3) by new $^{40}Ar/^{39}Ar$ ages as part of this thesis. Units were named by Christiansen (1974) and Christiansen and Blank (1974a, 1974b, 1975a, 1975b) during the mapping of the volcanic field. Names of vent areas vent areas were based upon the closest known geographic reference point.

Basalt flow thickness ranges from 3 to 14 meters. Any estimate of flow thickness within the Yellowstone Plateau volcanic field is a minimum estimate; it is impossible to determine the thickness of flow removed by glaciation. Additionally, most of the flows are covered by glacial drift and/or alluvium and cross-sectional views perpendicular to flow direction are extremely rare.

Units are described below from oldest to youngest and summarized on a stratigraphic section (See Figure 3). The petrography of each unit is discussed in Chapter 3.

Hepburn Mesa basalt

Hepburn Mesa basalt crops out approximately 10 km northwest of the town of Gardiner within the northern most portion of the Yellowstone Plateau volcanic field. First described by Bush (1967), the flows cover an area of 35.5 km^2 with no identified vent area, although numerous small basaltic dikes of unknown age crop out to the west of the main flow(s). The Hepburn Mesa basalt flow sampled for this project contains plagioclase and olivine phenocrysts. The flow is massive and the sparse vesicles (<1%) are partially filled with calcite. It overlies bedded Tertiary sedimentary rocks deposited within the Yellowstone River valley. Bush (1967) produced a K/Ar date of 8.4 Ma, but an ^{40}Ar/^{39}Ar date of 2.2 Ma is reported by Smith et al. (1997).

Basalt of Warm River and Shotgun Valley

The basalts of Warm River and Shotgun Valley crop out southeast of the Henry's Fork Caldera within the Warm River canyon and northeast of the Island Park reservoir. These outcrops collectively cover an area of 86 km^2. Flows erupted prior to the eruption of Member B of the Lava Creek tuff (0.640 Ma) and after the eruption of the Mesa Falls tuff (1.3 Ma).

Four vents for the Basalt of Warm River and Shotgun Valley were mapped by Hamilton (1965) and by Christiansen (2001). These include two fissure eruptions and two small Hawaiian-type shield volcanoes. These vents are to the northeast of the Island Park reservoir, a depression in the northern part of the Henry's Fork Caldera.

A K/Ar date of 0.759±0.052 Ma for the Warm River flows was produced by Obradovich (1992). The basalt of Shotgun Valley is presumed older by Christiansen (2001) with a probable age between 1.3 Ma and 0.78 Ma. Christiansen (2001) constrained these ages by the Mesa Falls tuff (1.3 Ma) and by the fact that the basalt of Warm River overlies the basalt of Shotgun Valley near the Island Park reservoir.

Undine Falls basalt

Undine Falls basalt crops out north and northeast of the Yellowstone Caldera within (1) the Yellowstone River canyon; (2) on the steep banks of Lava Creek; (3) north of Blacktail Deer plateau; and (4) in faulted remnants in the Mirror Plateau fault zone (See Plate 1). Christiansen and Blank (1974a; 1974b; 1975a; 1975b) also mapped the basalt flows above Gardner, Montana as Undine Falls basalt. The only vent location identified by Christiansen and Blank (1974a; 1974b; 1975a; 1975b) occurs within the normal-faulted Mirror Plateau outcrop.

Undine Falls basalt flows are light to dark gray and weather to olive gray. They are massive, vesicular, and holocrystalline. Large 1.5 to 3.0 mm vesicles are present in bands. Some vesicles exhibit diktytaxitic texture and may be partially filled with calcite, zeolites such as stilbite, or botryoidal hematite. Smaller vesicles occur in flows that exhibit a "frothy" texture. This frothy texture can be described as a 1 to 1 ratio of < 0.1 mm vesicles

to matrix. This flow has a K/Ar date of 0.588±0.032 Ma and covers an area of 8 km^2 (Obradovich, 1992).

Madison River basalt

There are at least twelve outcrops of basalt on the Madison Plateau northwest of the Yellowstone Caldera. These outcrops have a total area of 23 km^2. The Madison River basalt flows are light to medium gray, massive, and holocrystalline. Large, 1.5 to 3.0 cm vesicles are present within vesicle bands. Smaller vesicles occur in flows that exhibit a "frothy" texture.

Samples were collected from a small 0.5-km diameter shield volcano 1.3 km north of the Madison River and from a flow with no known vent area 1-km east of the western Yellowstone National Park boundary. The flows of the shield are medium to dark gray and contain only a few vesicles. Shield formation culminated with a Strombolian phase that produced lapilli to block-sized (2-8 cm) reddish-brown to black lapilli and scoria (See Figure 4).

A flow without a known vent, located 0.5 km southwest of the Madison River, is dense, medium gray basalt. In the bands of vesicles, bubbles are imbricated and suggest a flow direction of 110°. This flow is geochemically similar to Falls River and Warm River basalts and has an ^{40}Ar/^{39}Ar isochron age of 0.358±0.019 Ma. Based on geochemical data (Chapter 4), it is more likely that this flow is Falls River basalt and is not Madison River basalt.

Christiansen (2001) suggested that the Madison River basalt flows are <0.40 Ma but >0.13 Ma. The upper age of this basalt unit is constrained by the intruding Cougar Creek rhyolite dome (0.399±0.003 Ma) (Obradovich, 1992). During field reconnaissance, no contact was located between the Madison River basalt shield and the Cougar Creek rhyolite

dome. A dike of Madison River basalt cuts an outcrop of the Riverside rhyolite flow, thus the Madison River basalt must be younger than the Riverside flow. The relationship of the Riverside flow to the Cougar Creek dome is unknown. The age of the Riverside Flow has not been determined, therefore it can not be used as a stratigraphic check.

Swan Lake Flat basalt

Swan Lake Flat basalt is the least eroded and most voluminous of the basalt units in Yellowstone National Park and covers an area of 58 km^2. Multiple vents were identified by Christiansen (1974), Christiansen and Blank (1974a; 1974b; 1975a; 1975b), and Christiansen (2001) and all occur north of the Yellowstone Caldera in the Norris-Mammoth corridor. The ages of these flows are constrained by the Lava Creek tuff, which lies beneath the basalt (0.640+0.002 Ma), and by the Obsidian Cliff rhyolite flow (0.116$\pm$0.008 Ma) that intrudes the basalt. There are four source areas for the Swan Lake Flat basalt. These are the Panther Creek cinder cone, the Tower Road shield, and two Horseshoe Hill vents.

Horseshoe Hill vents

Flows from the Horseshoe Hill vents cover an area of 36 km^2. They produced the most voluminous flows of Swan Lake Flat basalt. The flows are light to medium gray and massive. Additionally, they are holocrystalline and slightly vesicular. The rounded vesicles range in size from 0.25 to 3.0 cm. The vesicles make up 2 to 3% of the rock by volume. Due to the inaccessibility of these vents (due to 1989 fire damage), only two samples were collected and the vent areas were not studied.

Tower Road shield

The silhouette of this broad shield volcano is visible from a hill near Swan Lake (See Figure 5). A gentle, Hawaiian-style eruption produced the 120-meter high, 16-km^2 shield.

Its eruption culminated with a Strombolian phase (see Madison River basalt for description of this type of shield eruption). The evidence for the Strombolian eruption is the presence of reddish gray to dark gray, lapilli to block-sized scoria at the summit of the shield.

The basalt flows are massive and medium to dark gray, but may weather to a dusky red purple along fractures. Additionally, they are holocrystalline and contain a small volume (~ 5%) of vesicles that vary in size from 0.5 to 2.0 cm. This shield is underlain by Lava Creek tuff.

Panther Creek vent

The Panther Creek vent was discovered during field mapping as part of this study. Its eruption style was primarily Strombolian and produced a cinder cone. Its geochemistry is also distinctly different from the other known Swan Lake Flat basalt vents. The Panther Creek vent is described in detail in Chapter 3.

Osprey basalt

Outcrops of Osprey basalt occur within the Yellowstone River Canyon south of Mt. Everts and 18 kilometers northeast of the Yellowstone Caldera within the Lamar River Canyon in YNP. Christiansen (1974), Christiansen and Blank (1974a, 1974b, 1975a, 1975b) identified the only known vent for this basalt within the Lamar River canyon. The vent for the flow within the Yellowstone River canyon has not been identified. The outcrop area of this unit is 5.25 km^2.

The basalt flows are massive and dark gray to black. They are holocrystalline and slightly vesicular. The vesicles may be partially filled with calcite. The flow in the Yellowstone River Canyon overlies the Undine Falls basalt in some locations and overlies

Lava Creek tuff in other locations within the canyon. A K/Ar date of 0.220±0.041 Ma suggests that this basalt flow is the youngest in the Yellowstone Plateau (Obradovich, 1992).

Falls River basalt

Falls River basalt crops out within the Henry's Fork Caldera and covers a total area of 316 km^2. One part of the unit crops out south of the Henry's Fork Caldera, near Ashton, Idaho and covers an area of 96 km^2. The larger outcrop area (220 km^2) occurs southeast of the Henry's Fork Caldera and infringes upon the southwestern corner of Yellowstone National Park. Christiansen (2001) mapped one vent for Falls River basalt; the nature of this vent is unknown. This unit overlies the Mesa Falls and Lava Creek tuffs (0.640 Ma). It is also partially covered by Pleistocene glacial drift and by the Pitchstone member of the Yellowstone Central Plateau rhyolite that has a K/Ar age of 0.110±0.001 Ma. Based on this information, Christiansen (2001) determined a probable age for Fall River basalt of >0.11 but <0.64 Ma.

Gerrit basalt

Gerrit basalt crops out within the structural depression of the Henry's Fork Caldera in the southwestern portion of the Yellowstone Plateau volcanic field. Hamilton (1969) petrographically described the pahoehoe flows as "gabboric" due to their porphyritic appearance and identified at least three vent areas. Porphyritic flows cover most the caldera floor and their total outcrop area is 528 km^2. All of the Gerrit basalt sampled in this study is dark gray to black and massive to slightly vesicular.

Later mapping by Christiansen (1974) and Christiansen and Blank (1974a; 1974b; 1975a; 1975b), located at least 13 vent areas for the Gerrit basalt, although the nature of these vents (i.e. whether they are shields of cinder cones) was not determined. Gerrit basalt locally

overlies the B Member of the Lava Creek tuff, which erupted from the Yellowstone Caldera at 0.640 ± 0.002 Ma (Obradovich, 1992) (See Figure 3).

In the northwest portion of the Henry's Fork Caldera, Gerrit basalt overlies the Mesa Falls tuff produced by the eruption of the Henry's Fork Caldera. On the southwestern rim of the caldera, Snake River Plain basalts overlap the Henry's Fork Caldera and the Gerrit basalt. The Gerrit basalts also flowed around numerous rhyolitic flows and domes (i.e. Bishop Mountain flow, Osbourne Butte dome, Elk Butte dome, Silver Lake dome) of the Snake River Group. Obradovich (1992) produced a K/Ar date for one dome within the Snake River Group at 0.198 ± 0.008 Ma and a date of 0.199 ± 0.009 Ma for the Hatchery Butte flow of the Gerrit Basalt. Because the Gerrit basalt flowed around a dome within this group, its probable age is <0.198 Ma.

Discussion

Two types of basalt volcanoes (shields and cinder cones) were documented. The Madison River and Tower Road shields are smaller in volume than typical Hawaiian-type shields like Mauna Loa and have steeper slope angles than Hawaiian shields (Williams, 1932). Small volume, monogenetic shields, like those described in Yellowstone National Park, have been documented within the Snake River Plain and within Lassen Volcanic National Park (Hughes et al., 2004; Sakimoto et al., 2003; Williams, 1932). These small shields, like the shield on the Madison Plateau and south of the Tower Road, are composed almost entirely of massive basaltic flows, except for the scoria and lapilli found within their summit craters.

The shield volcanoes in Lassen Volcanic National Park are similar to those in Yellowstone National Park. They are approximately 4 to 5-km in diameter at their base and

have well formed cinder cones at their summits. Williams (1932) suggested that these cinder cones represented the gas-charged, upper portions of the volcanic conduit. Hughes et al. (2004) noted that many of the shield volcanoes on the Snake River Plain have shallow angle slopes at their base with steeper angle, dome-like summits. The lavas at the base have fewer vesicles and fewer phenocrysts that the lavas erupted near the summit crater. The lavas near the summit "dome" have diktytaxitic networks of larger phenocrysts (25 vol %). Hughes et al. (2004) suggest that the lavas found near the steep-summit region are more fractionated than those found at the base. The increased phenocryst size and content due to fractionation causes the magma viscosity to increase thereby increasing the steepness of the slope angles of the shield. If the viscosity increase is coupled with an increase in volatile content, the eruption style of the shield could change from Hawaiian to Strombolian, producing a cinder cone within the summit crater of the shield.
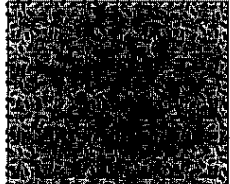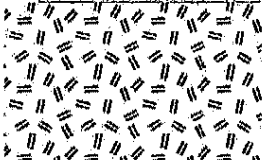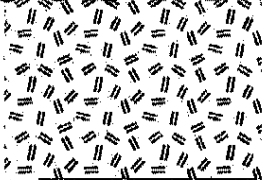
Probable or Analytical Age (in Ma)	Rock Unit Name	Rock Unit Type
<0.20	Gerrit basalt	
0.220+0.041	Osprey basalt	
>0.32, <0.64 *0.590+0.065* *0.174+0.046*	Swan Lake Flat basalt	
	Gardner River mixed lavas (basalt and rhyolite)	
>0.11, <0.64	Falls River basalt	
>0.13, <0.40 *0.530+0.06*	Madison River basalt	
0.588+0.026	Undine Falls basalt	
0.640+0.002	Lava Creek tuff (Yellowstone caldera cycle)	
0.759+0.052	Warm River basalt	
1.292+0.005	Mesa Falls tuff (Henry's Fork caldera cycle)	
2.053+0.006	Huckleberry Ridge tuff ("First" caldera cycle)	
2.2+0.0	Hepburn Mesa basalt	

Figure 3: Stratigraphic section depicting the relative and absolute ages of basalts sampled during this study. Ages were complied from Christiansen (2001) and Obradovich (1992); ages determined during this study are in italics. The ages of the ash-flow tuffs and mixed lava units are inserted to provide chronostratigraphic constraints on the ages of the basaltic units.

Figure 4: Strombolian phase products (lapilli and cinders) in the summit crater of Madison River shield. Lense cap is 5.7 centimeters in diameter.

0   5   10 cm

Figure 5: Tower Road shield within the Swan Lake Flat basalt unit. View to south. Shield is approximately 120 meters high and 1330 meters in diameter.

CHAPTER 3

DESCRIPTION OF THE PANTHER CREEK VENT

The Panther Creek vent is 1.8 km southwest of Swan Lake and 1.5 km northwest of the

Yellowstone National Park Sheepeater Cliff roadside exhibit (See Figure 6). This vent area

was discovered during this study. It is significant because it represents the first cinder cone

formed by a Strombolian eruption in Yellowstone National Park.

This cinder cone is 0.75 km in diameter at its base. The cone and its associated flows

cover an area of approximately 6 km^2. Pleistocene glaciation has eroded the cone; therefore

it is impossible to determine its original height. The present height of the cone is 75 meters.

At least three eruptive stages were identified (See Figure 7). During the first eruptive

phase, partially molten, reddish brown scoria and bombs produced a broad agglutinate cone

with a summit crater. Some bombs are cored with partially melted "granitic" xenoliths (See

Figure 8). The amount of melt (visible obsidian) present in the xenoliths varies from <1% to

90%. The xenoliths with <1% to 10% melt have a light pink groundmass with 20%

phenocrysts of feldspar (15%) and quartz (5%). The xenoliths that are visibly melted (10 to

80% melt) consist of a black obsidian groundmass with up to 15% phenocrysts of 0.5 to 1-

mm-sanidine.

The second eruptive phase produced a lava lake within the summit crater. A 1-meter

thick exposure of lava lake basalt crops out near the summit of the cone (See Figure 10).

The lava lake basalt has subtle banding identified by alternating light and dark gray streaks (See Figure 9). Besides differing in color, these light and dark streaks differ in phenocryst abundance and composition. The light gray bands contain large (0.5-mm) plagioclase laths (95%) and rare, miniscule (<10 μm) iron oxides grains (<5%) in a holocrystalline groundmass. The dark gray bands contain fewer, and smaller (<0.2 mm), plagioclase laths (80%) and larger and more abundant iron oxides grains (20%).

At the culmination of the second eruptive phase, the lava lake overflowed producing flows to the northeast (towards Sheepeater Cliff) and to the south (toward Indian Creek campground). The flow near the Indian Creek campground is approximately 3.5 meters thick, while the flow exposed at Sheepeater Cliff is 8 meters thick. The total volume of the flows produced during this stage is approximately 0.03 km^3.

In thin section, the flows closest to the central vent area have a "swirly" appearance. The visible swirls appear to be the same light and dark gray bands visible in lava lake basalt. The "swirly" appearance of the lava flows was created as the lava lake spilled over the rim of the summit crater and flowed down the slopes of the broad cone. The "swirly" textured lava flows are found as far as Indian Creek to the south and 0.5 km southwest of Swan Lake to the north (See Figure 6).

During the third phase, welded scoria erupted again. This reddish-brown agglutinated scoria does not contain any of the partially melted felsic xenoliths visible in the products of the first eruptive stage. The scoria of this stage crop out on top of the remnants of the lava lake and flows (See Figure 11). The quantity of the erupted material is unknown.

A 2.5-m wide composite dike crops out on the northeastern side of the cone (See Figure 12). This composite dike represents the conduit of this cinder cone. The presence of this dike

was critical to the recognition of the Panther Creek cone. The outer portion of the composite dike is massive and contains few plagioclase phenocrysts. This portion of the dike is cut by the inner dike and is 0.5 meters thick. The outer part of the dike contains 4 to 25 cm diameter partially-melted granitic xenoliths similar in appearance to the xenoliths described in the first stage agglutinated material. Therefore, this portion of dike probably erupted the agglutinated scoria of the first eruptive stage. The inner portion of the dike is 2 meters thick and is similar in texture and mineralogy to the outer dike, but does not contain any xenoliths. Near the top of the inner dike, it appears to "turn over" to become a lava flow that flowed to the north (See Figure 13).

Lava Creek tuff is exposed in gullies below Panther Creek lava flows to the northeast of the cone. At the terminus of basalt flows near Sheepeater Cliff, Panther Creek basalt lies stratigraphically above the Gardner River mixed basalt and rhyolite lavas.

Additionally, the lava lake within the Panther Creek cone may have served as a resistant layer within the cinder cone that allowed for the preservation of most of the cone during the numerous Pleistocene glacial episodes.

Discussion

Small volume lava lakes that erupt within the summit craters of cinder cones have been documented by many, but the processes involved during their infilling have not been described in great detail (Kuntz et al., 1982; Wolfgang et al., 1987). The most studied lava lake (and most cited in the literature) is the lava lake that formed on the flanks of Kilauea at Kilauea Iki. This lava lake formed during the 1959-1960 eruptive phase and accumulated during a period of lava fountaining (Richter and Moore, 1966). Ultimately, the creation of the Kilauea Iki lava lake caused the lava fountaining to cease. The formation of the lava lake

within the Panther Creek cone may have accomplished the same feat, by stifling the Strombolian eruption that formed the cinder cone. The Strombolian eruption did not end entirely. The eruption of scoria most likely continued after the lava lake overflowed its crater "basin" because agglutinated scoria overlies the lava lake exposure.

Also, convection within the 111-meter thick Kilauea Iki lava lake was presumed to have thoroughly mixed the repeated injections of basalt into one chemically homogeneous unit. This appears to have not been the case within the Panther Creek lava lake, as discrete bands divided by vesicle layering have preserved a record of the infilling of this lava lake. One light (Fe-oxide poor and plagioclase rich) and one dark (Fe-oxide rich, plagioclase poor) may represent one period of magma injection into the lake. Alternatively, the alternating colors and mineral contents could have been produced by flow banding within one flow.

Legend:

☐	Massive basalt (flows)	■	Massive basalt (Inner dike)
☐	Massive basalt (lava lake)	▨	Massive basalt (Outer dike)
■	Agglutinated scoria	⌐●	Inferred Fault, ball on thrown down side
▨	Blocks of massive basalt and agglutinated scoria	∥	Paved or gravel access road

APPROXIMATE MEAN DECLINATION, 2000
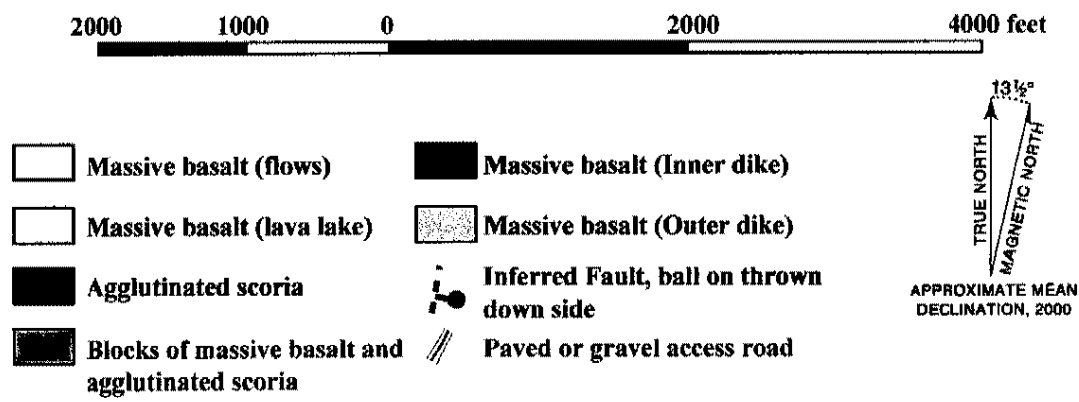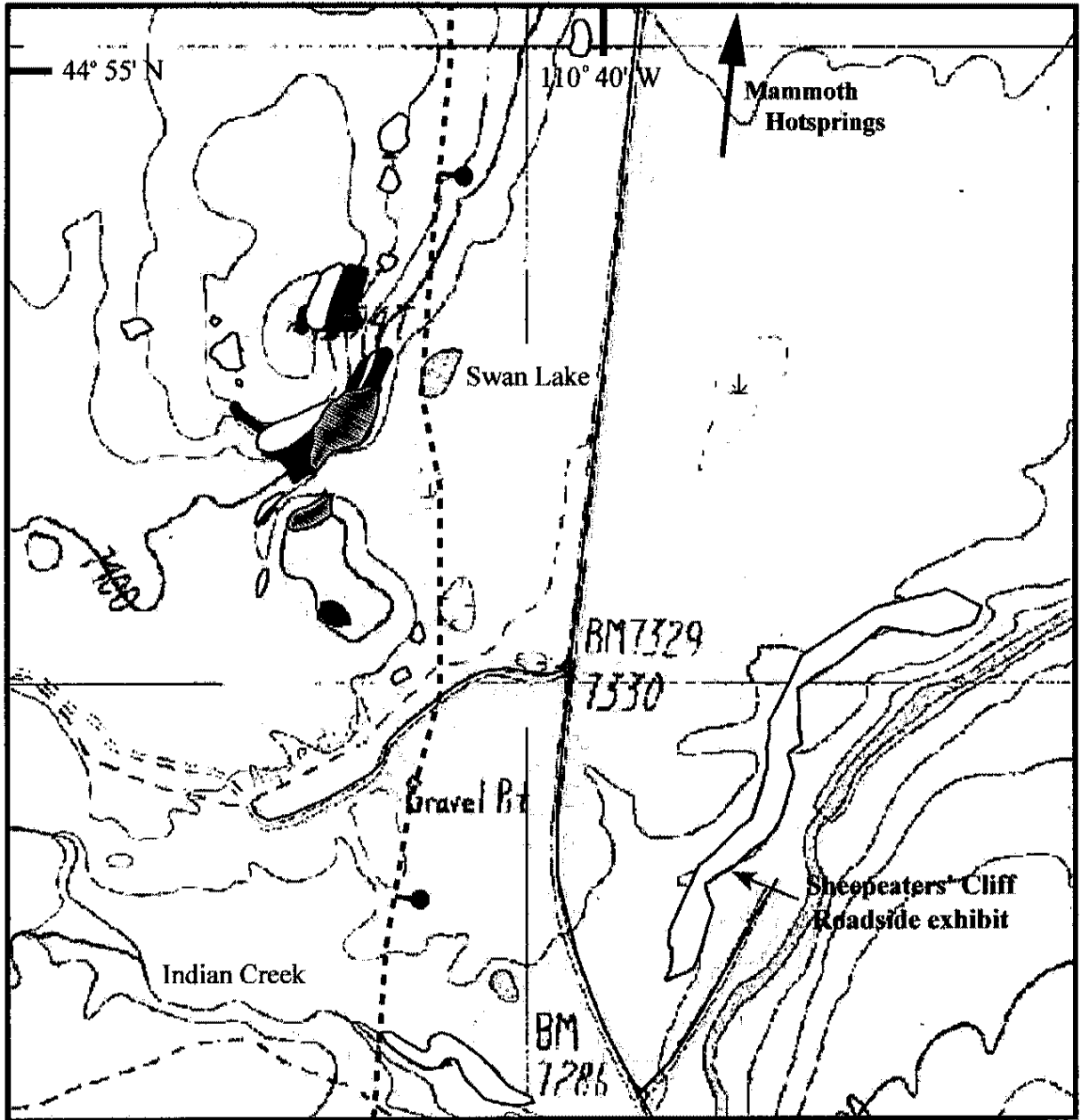
Figure 6: Field map of the newly identified Panther Creek vent within the Swan Lake Flat basalt unit.

Phase 1

Phase 2

Phase 3 cone

Phase 1 cone

Phase 3

Phase 1 and 3 scoria cones

Outer part of dike

Lava-lake basalt, lava flows and inner part of dike
related to phase 2 and 3 activity
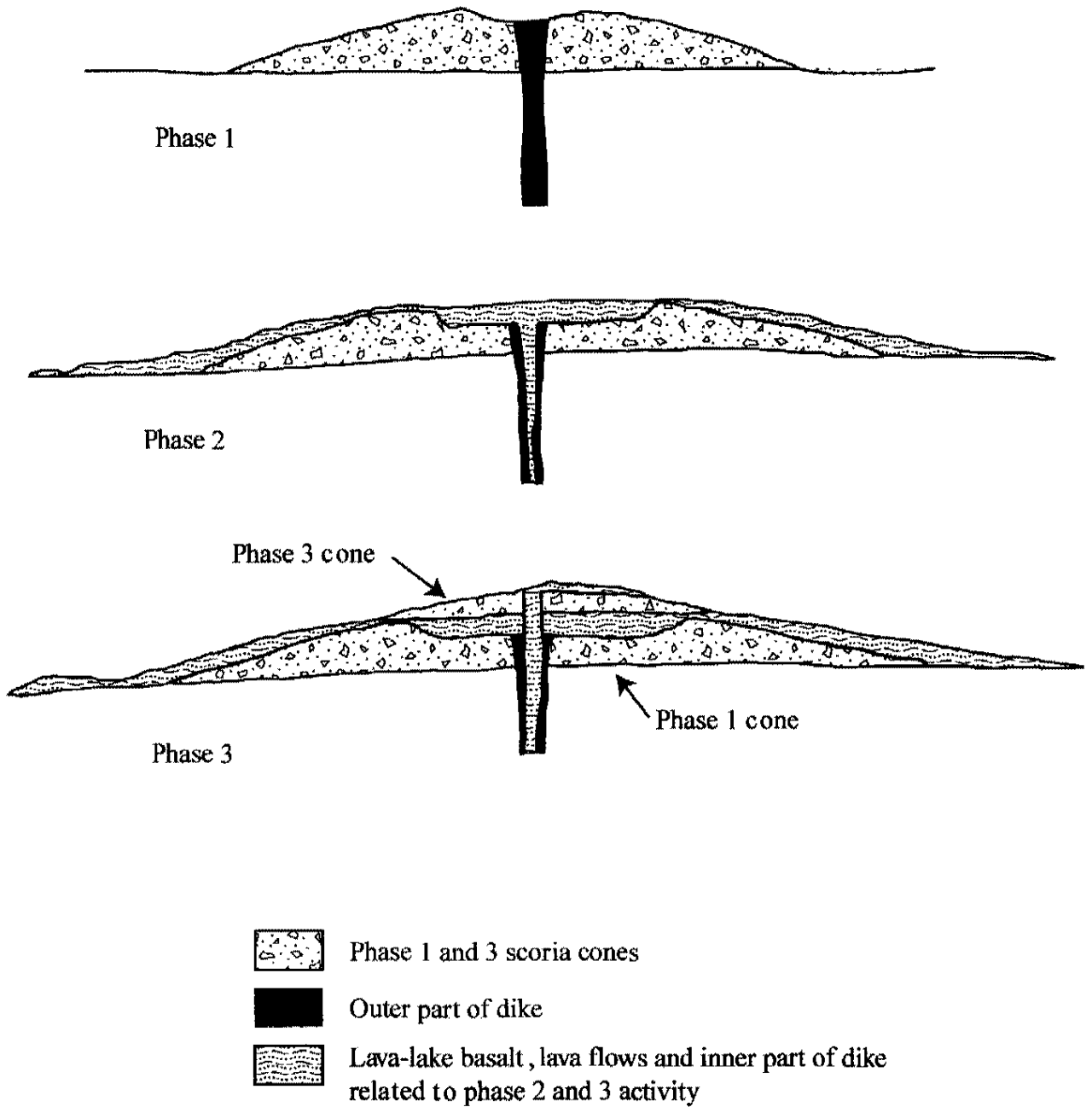
Figure 7: Stages of development of the newly discovered Panther Creek cinder cone in the Swan Lake Flat basalt unit.

Figure 8: Reddish-brown to gray agglutinated scoria produced by the first eruptive stage of the Panther Creek vent. Volcanic bomb is composed of a partially melted granite block that is 35 cm across.

0   10   20   30   40 cm
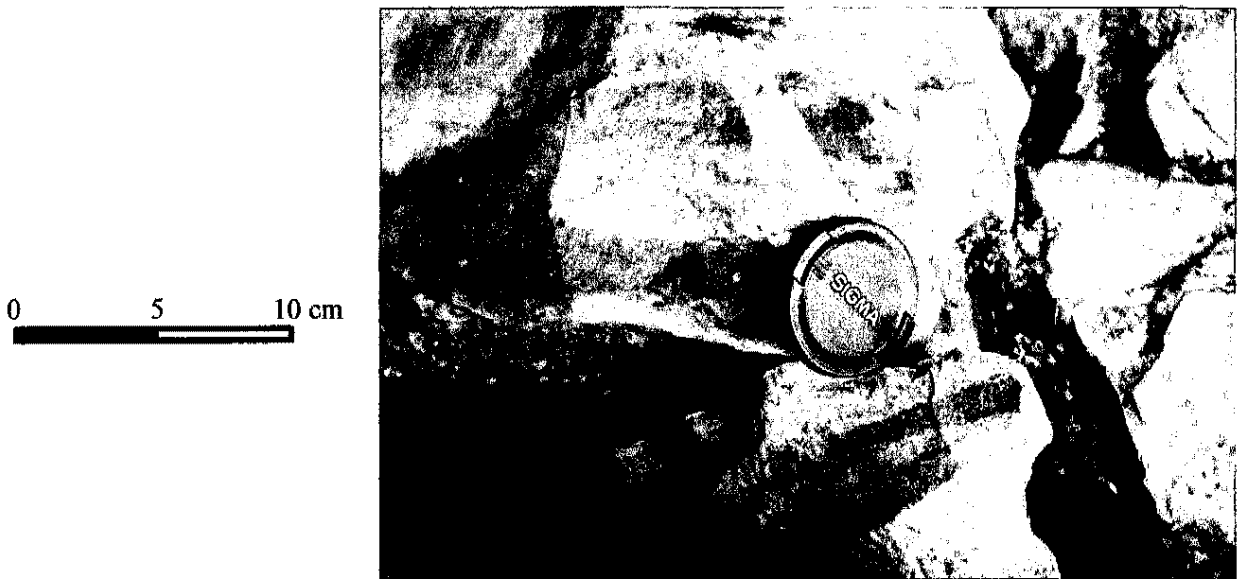
0   5   10 cm

Figure 9: Banded lava found within summit crater of Panther Creek vent. The banded lava formed within a lava lake. Lens cap is 5.7 centimeters in diameter.
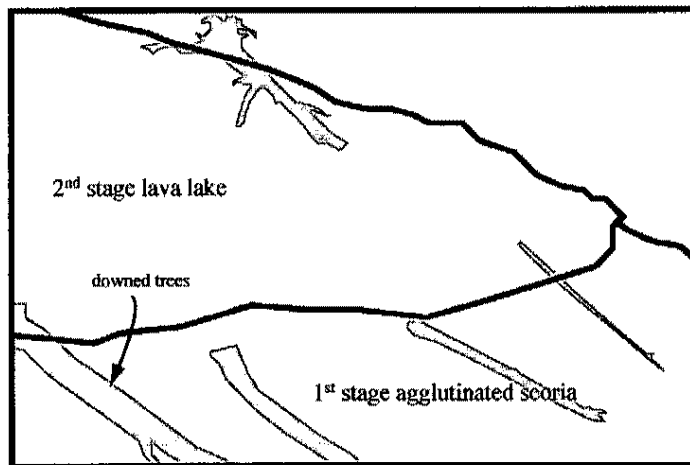
Figure 10: Outcrop of lava lake in the Panther Creek summit crater.

Figure 11: Reddish-brown agglutinated scoria produced during the third eruptive stage of the Panther Creek vent. Agglutinated scoria does not contain any of the partially melted felsic xenoliths of the first eruptive stage.
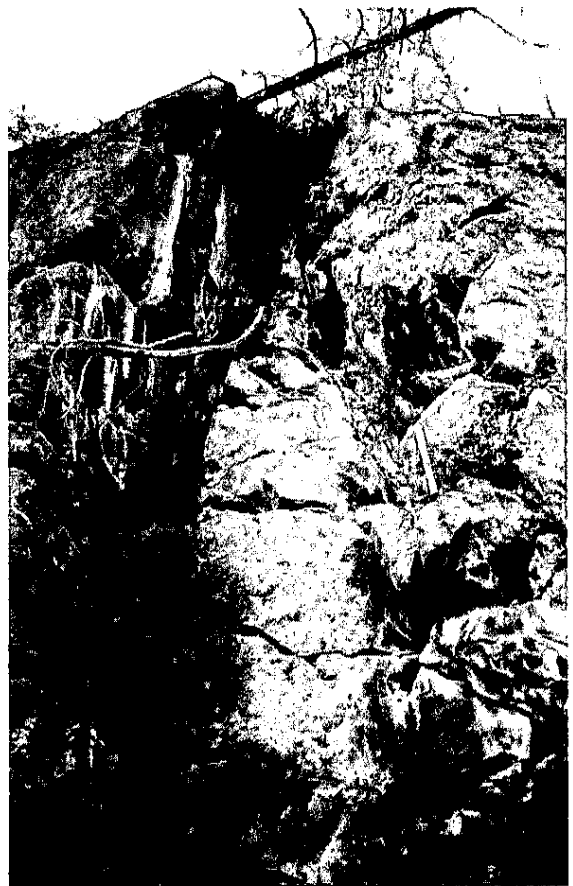
Figure 12: Composite dike found on northeast side of the Panther Creek cone. This dike represents the feeder dike for the Panther Creek vent. Hammer handle is 35 centimeters long.

0   30   60   90   120 cm
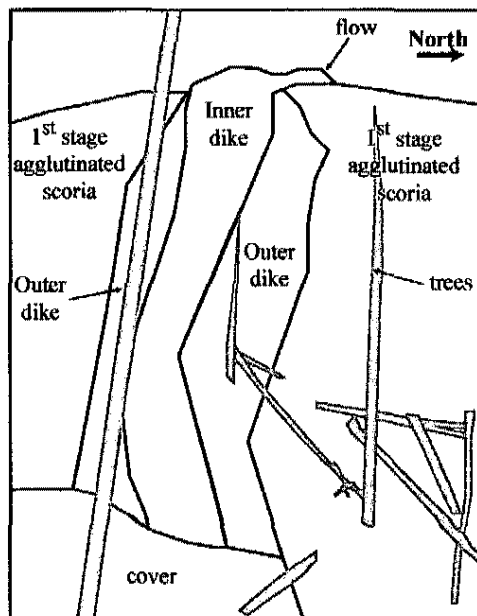
Figure 13: The inner part of the composite dike turns over into a flow towards the north. The outer dike is in contact with the agglutinated scoria of the first eruptive stage.

CHAPTER 4

GEOCHEMISTRY

Analytical Techniques

Thirty-four basalt samples were collected north of the Yellowstone Caldera within the

Norris-Mammoth corridor. Basalts associated with the Henry's Fork (Gerrit, Fall River, and

Warm River basalts) and first caldera (Hepburn Mesa basalt) cycles were also collected.

Each sample was bagged and labeled and consists of fresh pebble to cobble-sized rock

pieces. Samples were crushed to pea size in a Bico chipmunk crusher. The chipmunk

crusher is equipped with tungsten-carbide jaws. The pea size pieces were handpicked to

identify those samples that contained vesicle fillings. The clean pieces were then placed in a

shatterbox that uses a tungsten-carbide ring inside a tungsten-carbide lined stainless steel

bowl.

Major, and trace element (Ni, Cr, Sc, V, Ba, Rb, Sr, Zr, Y, Nb, Ga, Cu, Zn, Pb, La, Ce,

and Th) analyses were done using a Rigaku automated X-ray fluorescence spectrometer

(XRF) at the GeoAnalytical laboratory at Washington State University. Additional trace

element and rare-earth element (REE) analyses (La, Ce, Pr, Nd, Sm, Eu, Gd, Tb, Dy, Ho, Er,

Tm, Yb, Lu, Ba, Th, Nb, Y, Hf, Ta, U, Pb, Rb, Cs, Sr, Sc, Zr, and W) were completed using

a Hewlett-Packard inductively coupled plasma mass spectrometer (ICP-MS) at the

GeoAnalytical laboratory at Washington State University. Precision and accuracy for XRF and ICP-MS analyses are reported in Appendix A.

Sr, Nd, and Pb isotopes were analyzed by the Isotope Geochemistry Laboratory at the University of Kansas. Feuerbach et al. (1993) provides a detailed description of the methods of isotope analysis. Precision and accuracy are reported in Appendix B.

Geochemistry of Basalts in the Yellowstone Plateau

Volcanic Field and the Snake River Plain

The basalts of the Yellowstone Plateau volcanic field and Snake River Plain are subalkaline tholeiites (See Figures 14-16) with SiO_2 ranging from 45.5 to 51%. Basalts in the SRP (46.6-50%) and those associated with the Henry's Fork Caldera (45.7-49.83%) are lower in silica than those associated with the Yellowstone Caldera (48.3-51.2%) (See Figure 17). Previous authors have suggested that this increase in silica content is due to crustal contamination (Hildreth et al., 1991). Magnesium numbers (Mg#) vary from 46 to 59 in those basalts associated with the Yellowstone Caldera (See Figure 18). This suggests that they are somewhat evolved compared to Mg # of 68-75 for those basalts that are in equilibrium with mantle olivine compositions (Wilson, 1989). The Gerrit basalts associated with the Henry's Fork Caldera are less evolved with Mg # of 49 to 69. Snake River Plain basalts have a broader range of Mg# from 35 to 68.

CaO ranges from 8.61 to 11.42 wt%. For basalts of the Yellowstone Plateau volcanic field, K_2O, CaO, TiO_2, and MnO increase with increasing SiO_2, while Al_2O_3, FeO, MgO, and P_2O_5 decrease with increasing SiO_2 (Figure 17). Basalts of the Snake River Plain have slightly different trends; FeO, MgO, Na_2O, K_2O, P_2O_5, and MnO decrease with increasing SiO_2.

A chondrite-normalized spider diagram shows that the tholeiitic basalts within the Yellowstone Plateau volcanic field are similar to continental flood basalts (See Figure 19). An OIB-normalized spider diagram indicates that the basalts are also similar to ocean island basalts, but are slightly depleted in large ion lithophile elements (LIL), light rare earth elements (LREE), and high field strength elements (HFSE) and are slightly enriched in heavy rare earth elements (HREE) compared to OIB (See Figure 20). On an EMORB-normalized spider diagram (Figure 19), the Yellowstone Plateau volcanic field basalts are equal to slightly enriched in LILE, HFSE, and LREE and have similar to HREE abundances. The significance of this figure will be discussed in Chapter 7.

Major and Trace Element Geochemistry of Basalts

in the Norris-Mammoth Corridor

Major Elements

Magnesium numbers (Mg#) for basalts of the Norris-Mammoth corridor vary from 46 to 59 indicating that these basalts are somewhat evolved compared to mantle peridotite with Mg# of 68 to 75 (Wilson, 1989). SiO_2 contents range from 47 to 52.9-wt%. Al_2O_3, MgO, CaO, Na_2O, TiO_2, P_2O_5, and MnO decrease with increasing SiO_2 (See Figure 21). K_2O increases with increasing SiO_2.

Trace Elements

A plot of Cr versus Sr defines several volcanic centers within the Norris-Mammoth corridor. Undine Falls basalt has the highest Sr and lowest Cr in the volcanic field. Cr increases and Sr decreases in successively younger Swan Lake Flat basalts. A similar trend of increasing Cr and decreasing Sr is seen in the Osprey basalt (Figure 22).

A plot of Sr versus Zr/Nb was used to discriminate between the vent areas within the Swan Lake Flat basalt (See Figure 23). This plot was also used to determine if the basalts with no known vent areas were geochemically related to other basalts within the volcanic field. The basalts associated with the Panther Creek vent have intermediate Sr (325 to 370 ppm) and low Zr/Nb (7.6 to 8.4). The basalts associated with the Tower Road vent have high Sr (425 to 440 ppm) and low Zr/Nb (7.9 to 8.1). Last of all, the basalts associated with the Horseshoe Hill vent areas have moderate to high Sr (380 to 420) and moderate to high Zr/Nb (9.8 to 10.2).

On a plot of Ni vs. Cr, basalts associated with the Panther Creek cone have higher Cr (253 to 330 ppm) but have intermediate Ni (83 to 93 ppm) compared to the other Swan Lake Flat vents (See Figure 24). The Horseshoe Hill vents have low Cr (106 to 124 ppm) and intermediate Ni (91 to 94 ppm). Tower Road shield vent basalts also have low Cr (132 to 135 ppm) and intermediate Ni (87 to 91 ppm).

Isotopic geochemistry of Basalts

in the Norris-Mammoth Corridor

Basalts associated with the Panther Creek vent have the lowest $^{87}Sr/^{86}Sr$ (0.7052 to 0.7054) and the lowest ε_{Nd} (0.20 to -0.18) compared to the other basalts within the Norris-Mammoth corridor (See Figure 25). Basalts associated with the Horseshoe Hill vents have intermediate $^{87}Sr/^{86}Sr$ (0.7060) and low to intermediate ε_{Nd} (-2.53) compared to the other basalts within the Norris-Mammoth corridor. These basalts also have the highest $^{87}Sr/^{86}Sr$ and ε_{Nd} of all the Swan Lake Flat basalts. The basalts associated with the Tower Road vent have low $^{87}Sr/^{86}Sr$ (0.7056) and low ε_{Nd} (-2.38). The Osprey basalts also have low $^{87}Sr/^{86}Sr$ (0.7054) and one of the lowest ε_{Nd} (0.14) in the Norris-Mammoth corridor. Undine Falls

basalt also has low to intermediate $^{87}Sr/^{86}Sr$ (0.7052 to 0.7059) and low to intermediate ε_{Nd} (-3.15 to -8.43). Finally, the Madison River basalt has higher $^{87}Sr/^{86}Sr$ (0.7065) and higher ε_{Nd} (-5.46) compared to the other basalts in the Norris-Mammoth corridor.

Norris-Mammoth corridor basalts cluster into three groups above the Northern Hemisphere Reference Line (NHRL) of Hart (1984) (See Figure 26). The Panther Creek vent and the Osprey basalts have the highest $^{206}Pb/^{204}Pb$ (15.49-15.54) and moderate $^{207}Pb/^{204}Pb$ (17.77-17.89) compared to the other basalts in the field. The Swan Lake Flat basalts associated with the Tower Road shield and Horseshoe Hill vents and the upper flow of Undine Falls all lay along a trend line towards higher $^{207}Pb/^{204}Pb$ (15.46-15.54) and lower $^{206}Pb/^{204}Pb$ (17.09-17.34). The lower flow of Undine Falls and Madison River basalts follow a trend line towards lower $^{206}Pb/^{204}Pb$ (16.62-16.82) and lower $^{207}Pb/^{204}Pb$ (15.37-15.42).
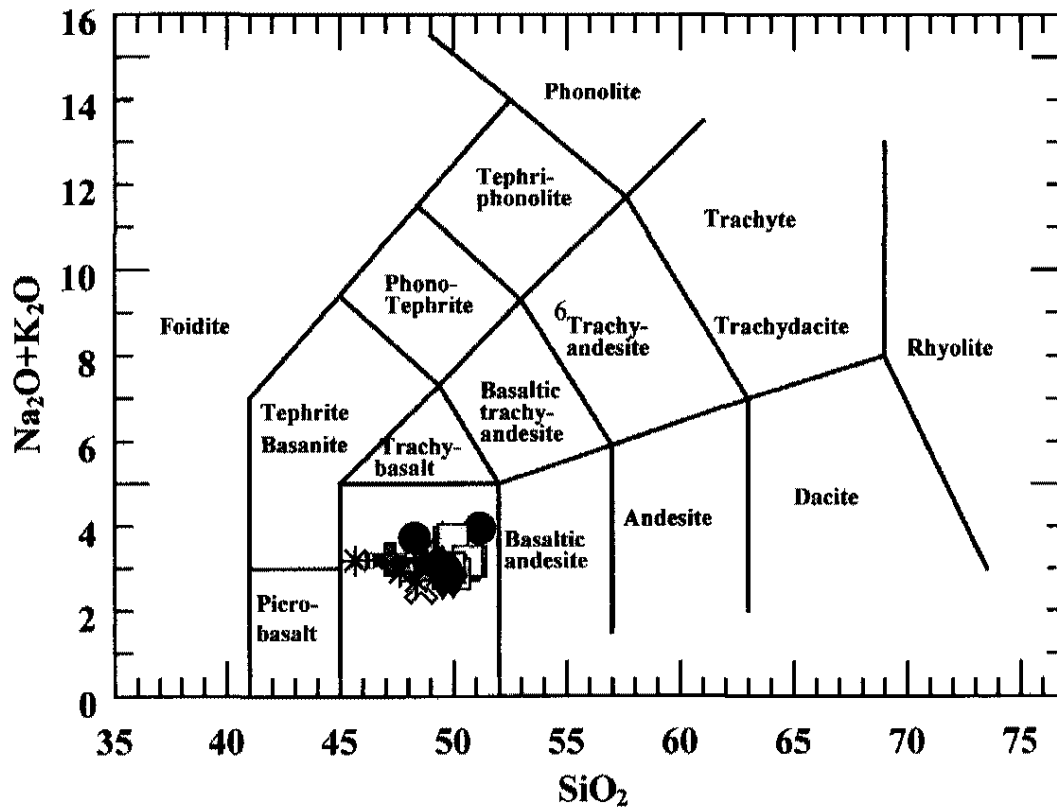
Figure 14: Selected volcanic rocks of the Yellowstone Plateau volcanic field are basalts according to the classification of LeBas et al. (1986).
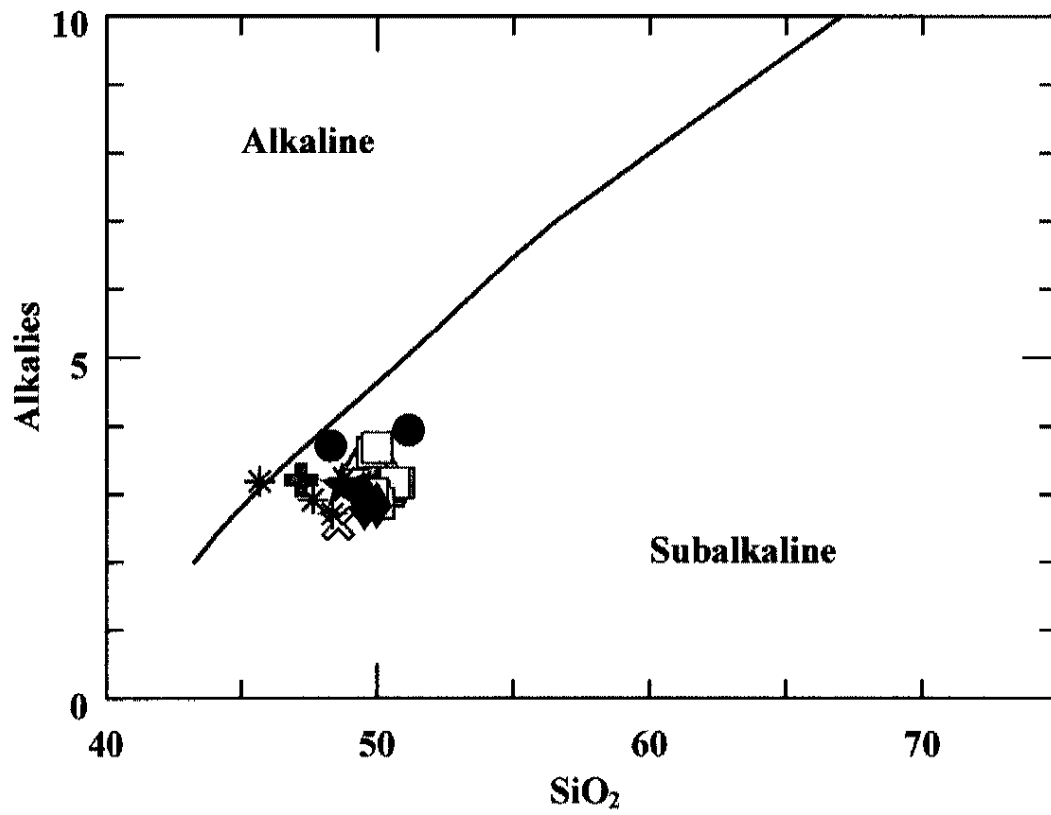
Figure 15: With the exception of Gerrit basalt (HFGE-02), Yellowstone Plateau volcanic field basalts are subalkalic.
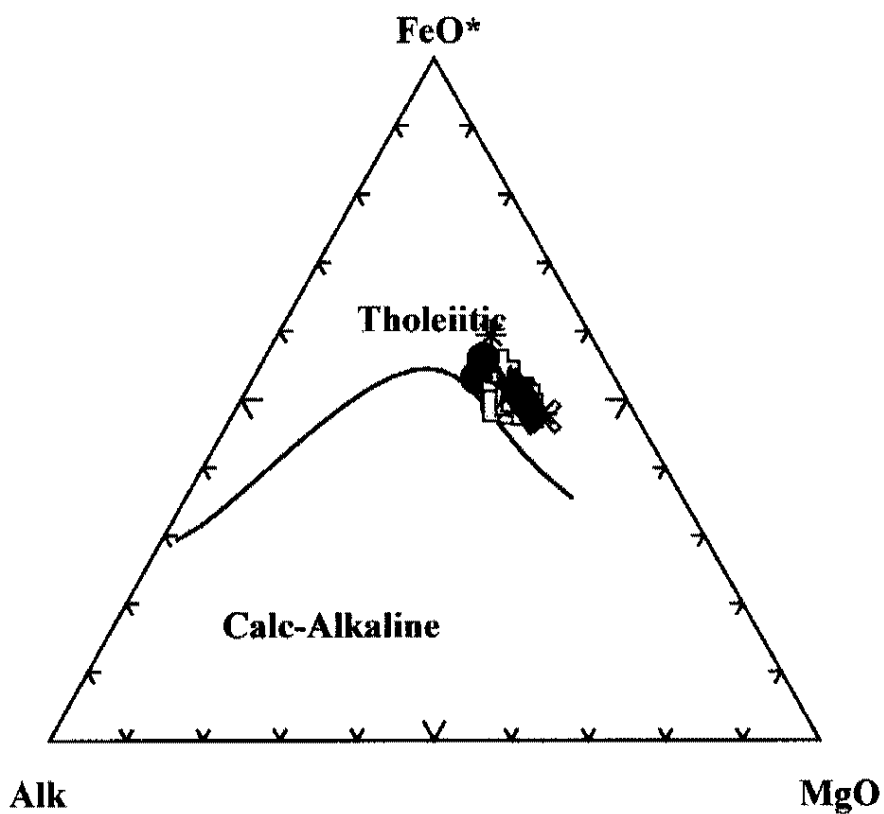
Figure 16: On an AMF diagram, Yellowstone Plateau volcanic field basalts are tholeiitic.
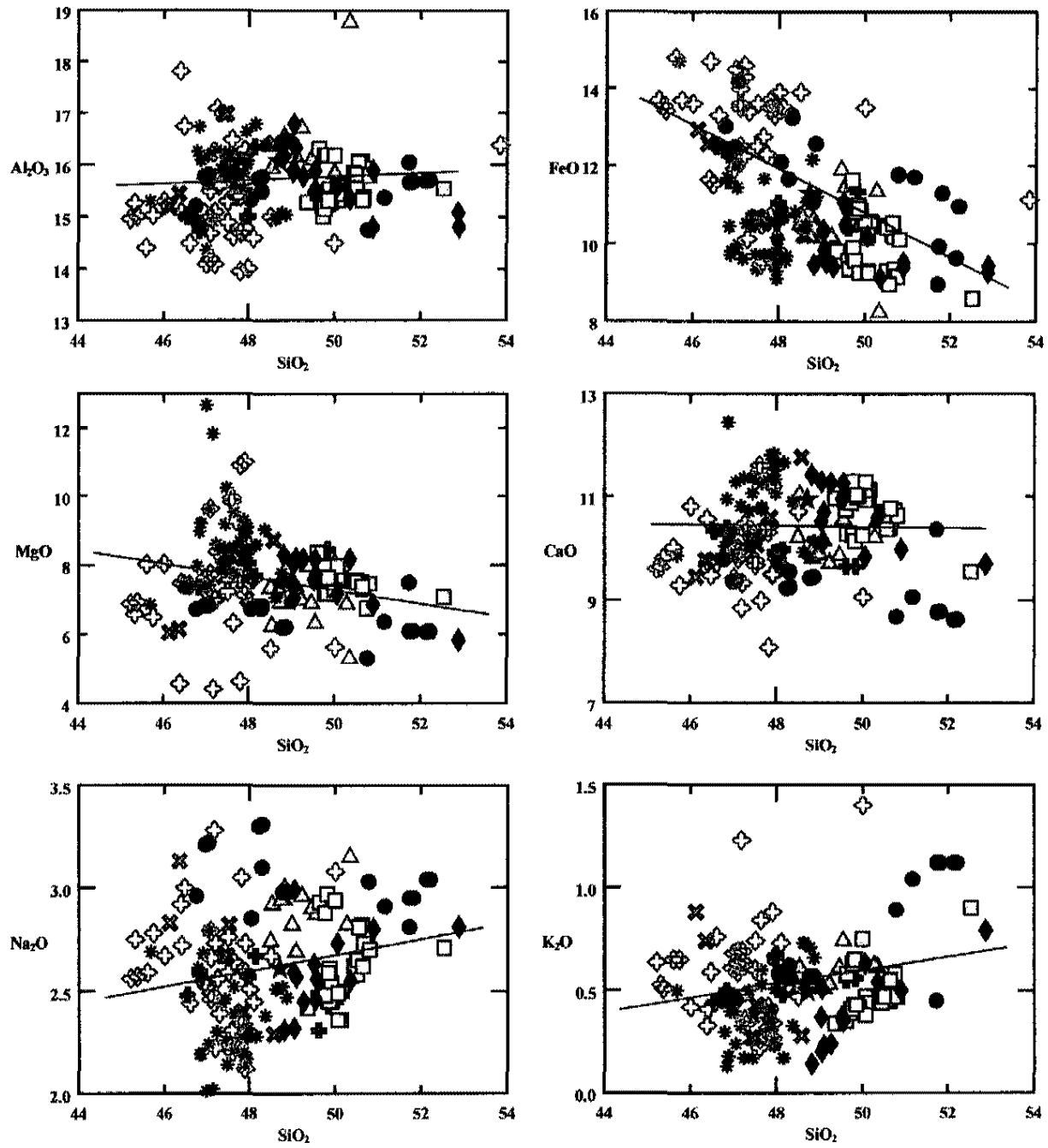
Figure 17: Harker variation diagrams for selected Snake River Plain, Henry's Fork, and Yellowstone Plateau basalts. K_2O, Na_2O, and CaO increase with increasing SiO_2, while Al_2O_3, FeO, and MgO decrease with increasing SiO_2. ◇ =Snake River Plain; ✳ =Gerrit; ✚ =Warm River; ✖ =Falls River; ● =Madison River; □ =Swan Lake Flat; △ =Undine Falls; ◆ =Osprey; ★ =Hepburn Mesa. Gray trend lines includes all YPVF data, but excludes SRP basalt data. Additional data from Doe et al. (1982), Lehman et al. (1982), Smith and Braile (1984), Hildreth et al. (1991), and Christiansen (2002).

37
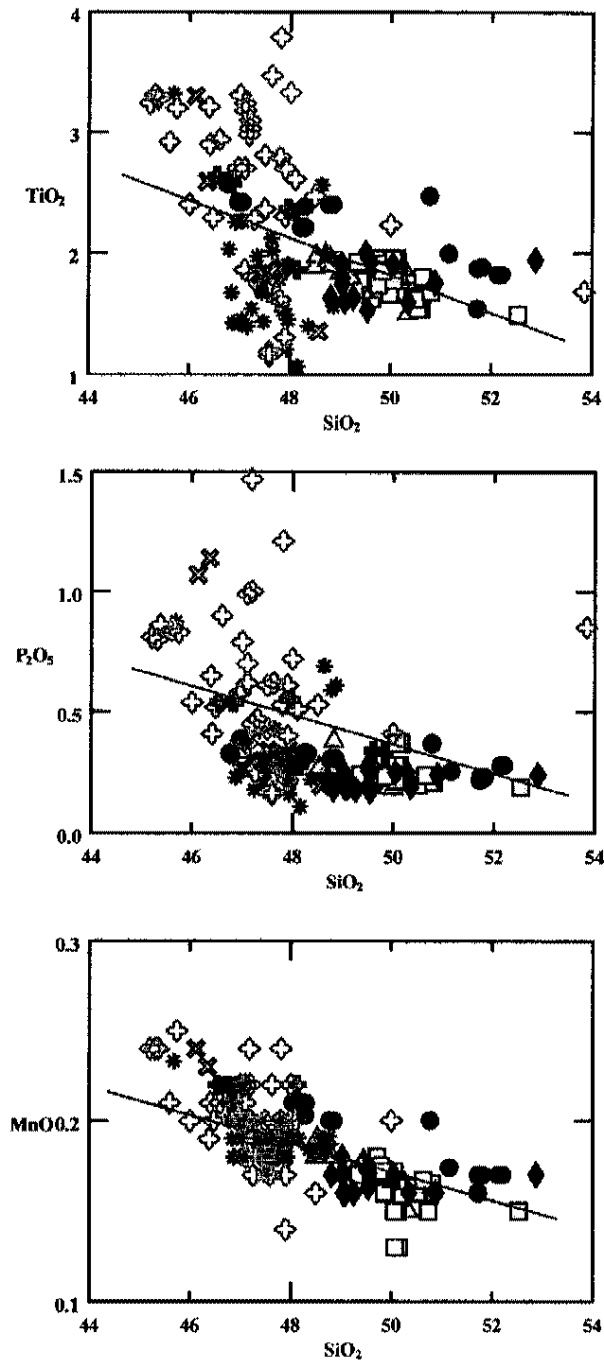
Figure 18: Harker variation diagrams for selected Snake River Plain, Henry's Fork, and Yellowstone Plateau basalts. Al_2O_3, FeO, and MgO decrease with increasing SiO_2. ◇ =Snake River Plain; ✱ =Gerrit; ✚ =Warm River; ✖ =Falls River; ● =Madison River; □ =Swan Lake Flat; △ =Undine Falls; ◆ =Osprey; ★ =Hepburn Mesa. Gray trend lines includes all YPVF data, but excludes SRP basalt data. Additional data from Doe et al. (1982), Lehman et al. (1982), Smith and Braile (1984), Hildreth et al. (1991), Chrisitansen (2002).
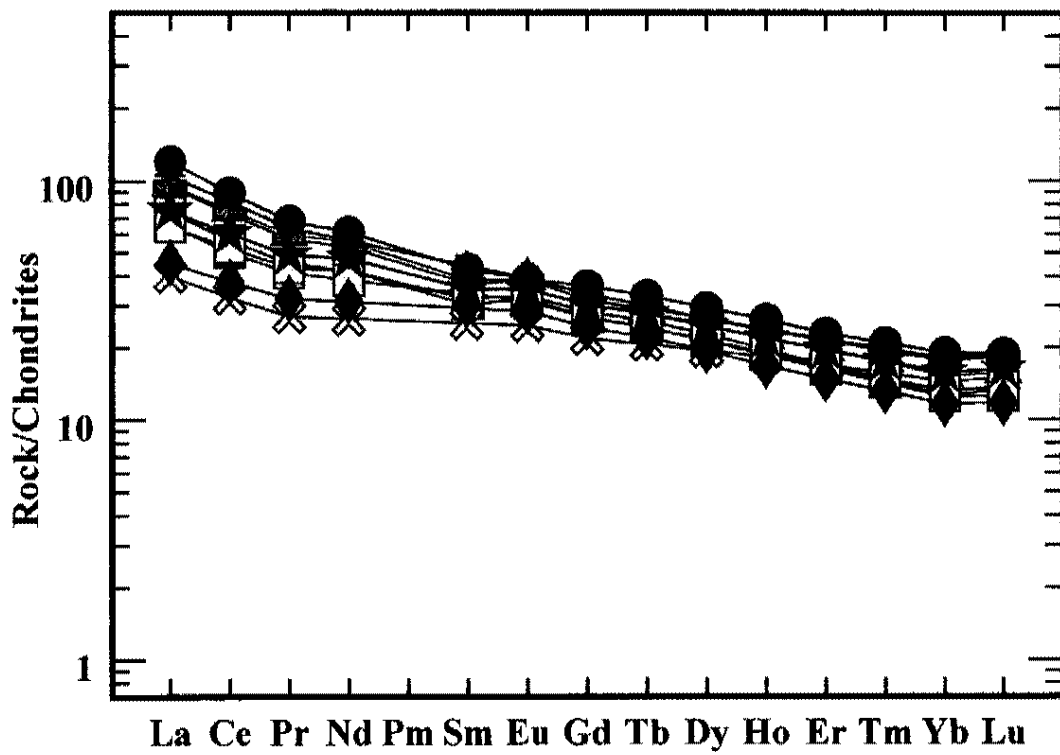
Figure 19: Chondrite-normalized spider diagram of Yellowstone Plateau volcanic field basalts. Normalized to chondrite compositions (Sun and McDonnell, 1989).
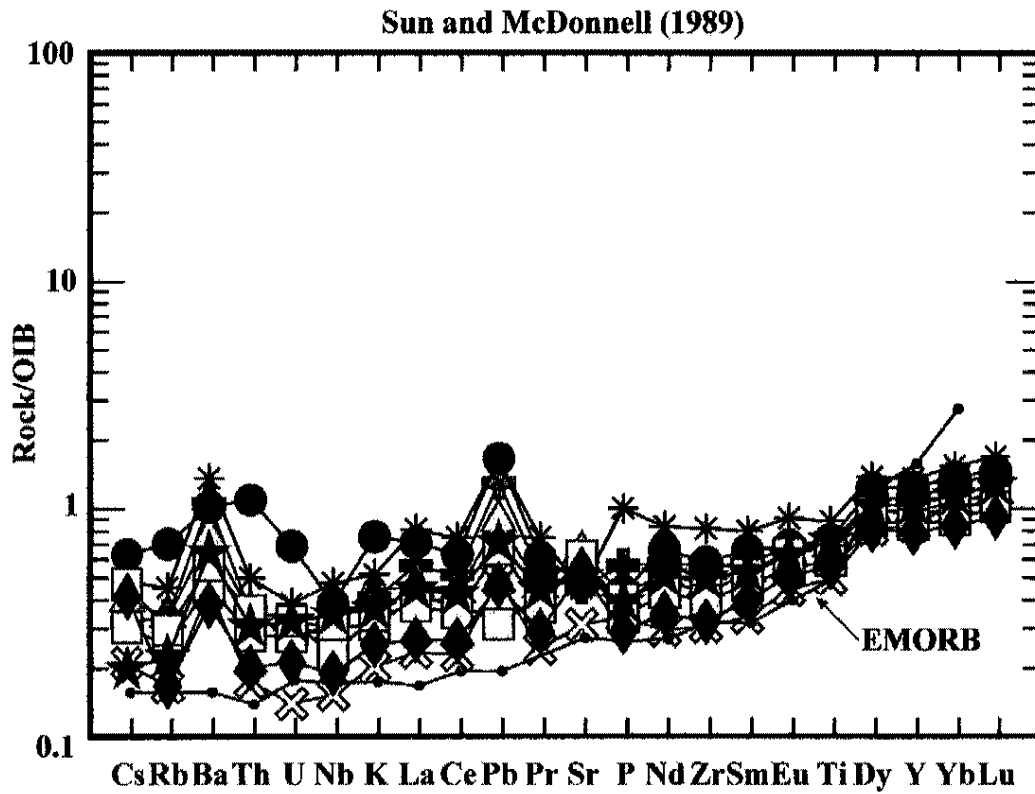
Figure 20: OIB-normalized spider diagram of selected Yellowstone basalts. EMORB is plotted for comparison. EMORB and OIB compostions from Sun and McDonnell (1989).
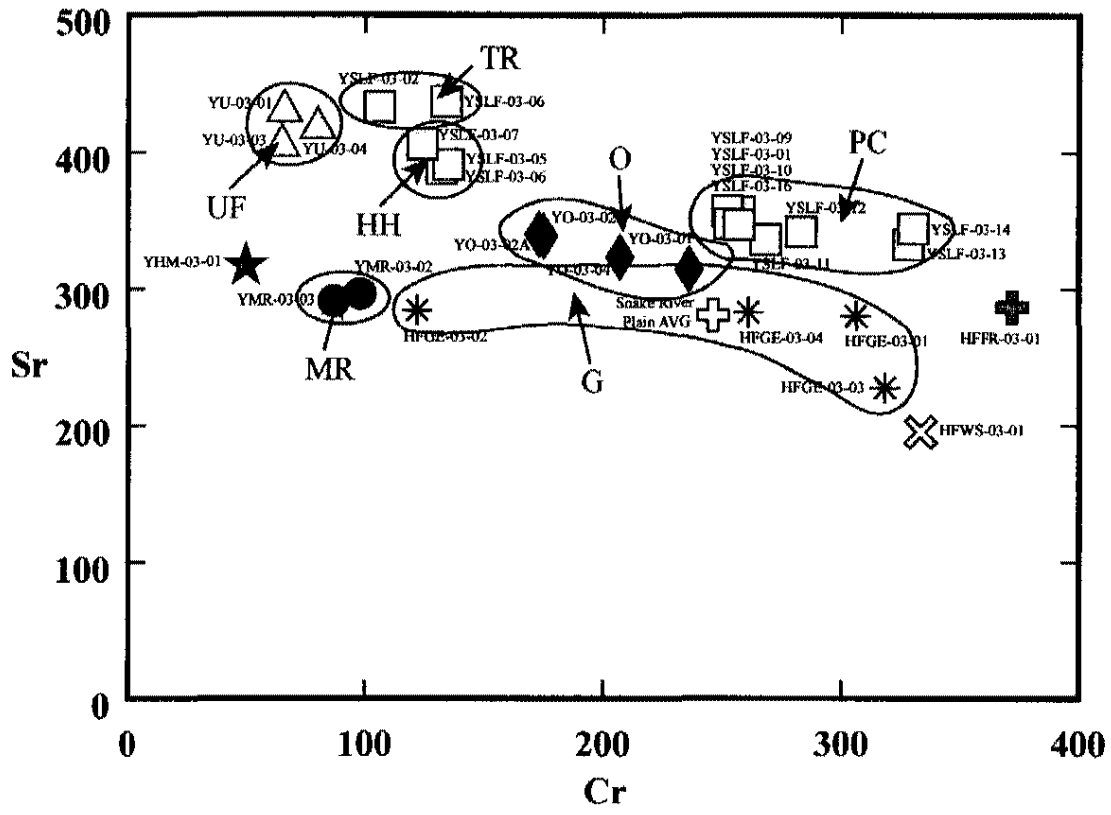
Figure 21: Cr versus Sr define groups which correspond to individual vents or flow units. Vents identified are as follows: TR=Tower Road, HH=Horseshoe Hill, O=Osprey, PC=Panther Creek, MR=Madison River, UF=Undine Falls, and G=Gerrit.

41
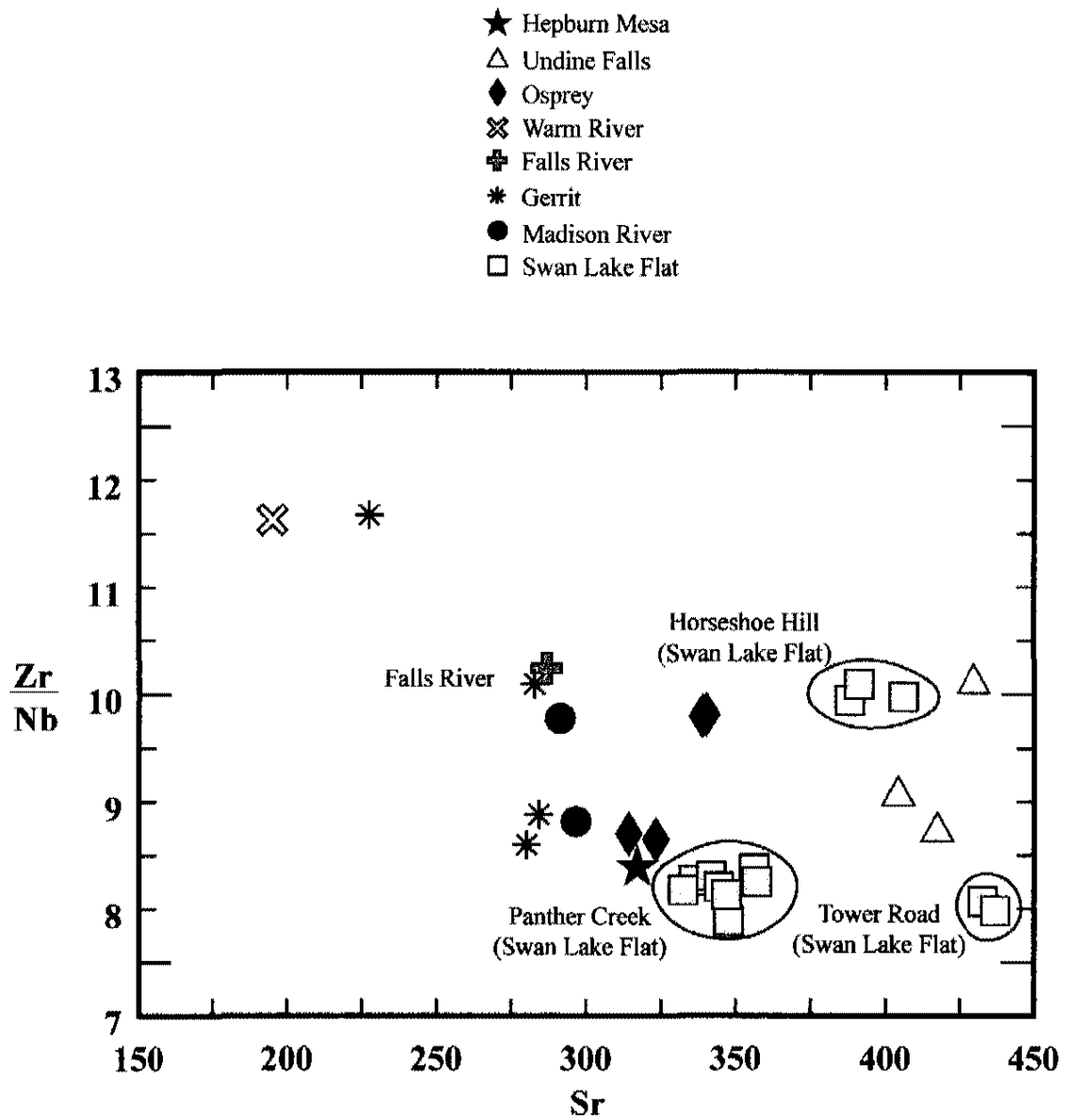
Figure 22: Sr versus Zr/Nb was used to discriminate between the vent areas within the Swan Lake Flat basalt and separate lava flows and vents within the Yellowstone Plateau volcanic field.
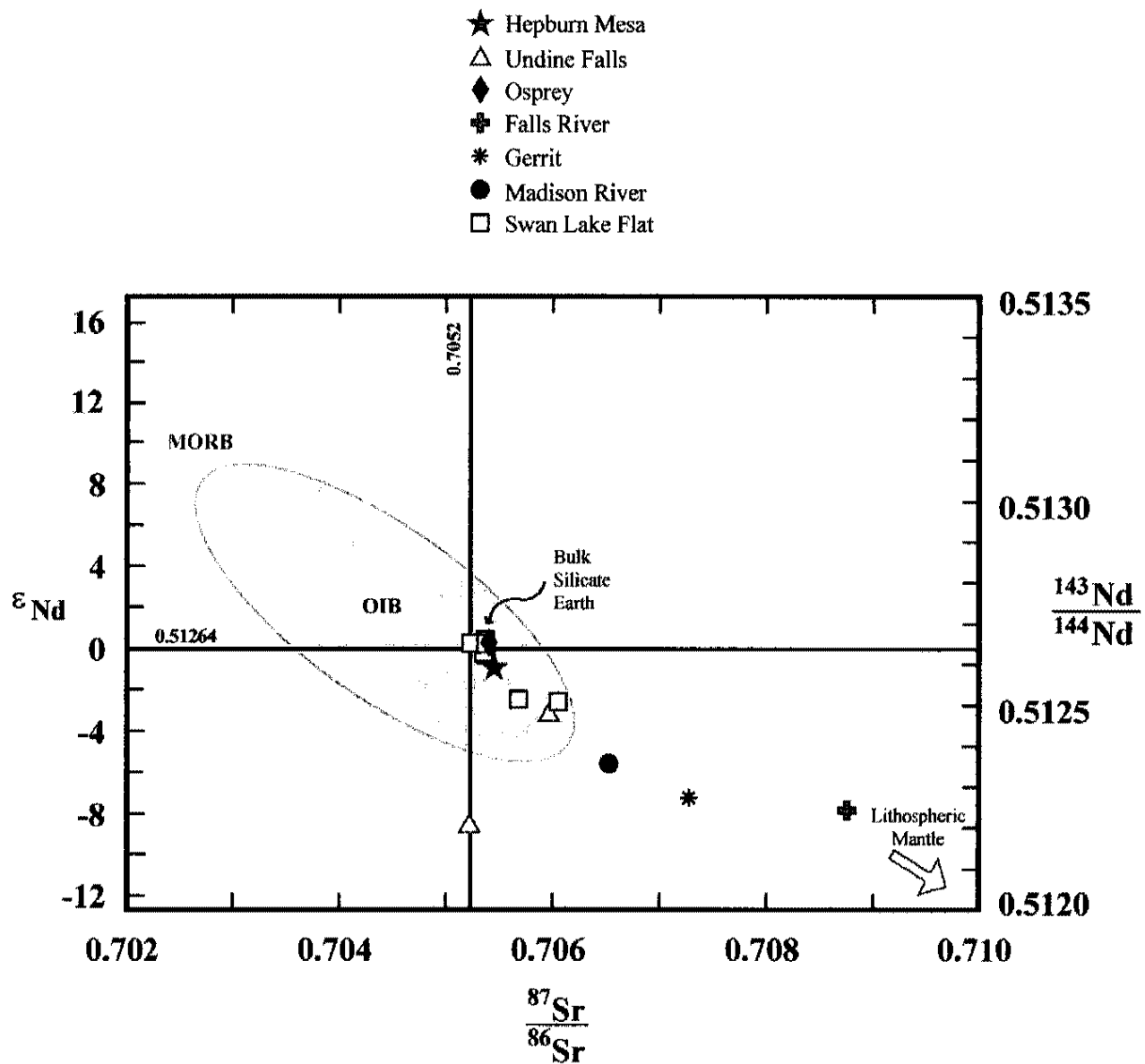
Figure 23: $^{87}Sr/^{86}Sr$ versus epsilon Nd for tholeiitic basalts in YPVF. Hepburn Mesa, Swan Lake Flat, Undine Falls, and Osprey basalt samples fall within the field of ocean island basalts while Falls River, Gerrit and Madison River basalts trend towards lithospheric isotopic values. OIB and mid-ocean ridge basalts (MORB) fields defined by Rollinson (1993). Diagram modified from Rollinson (1993).
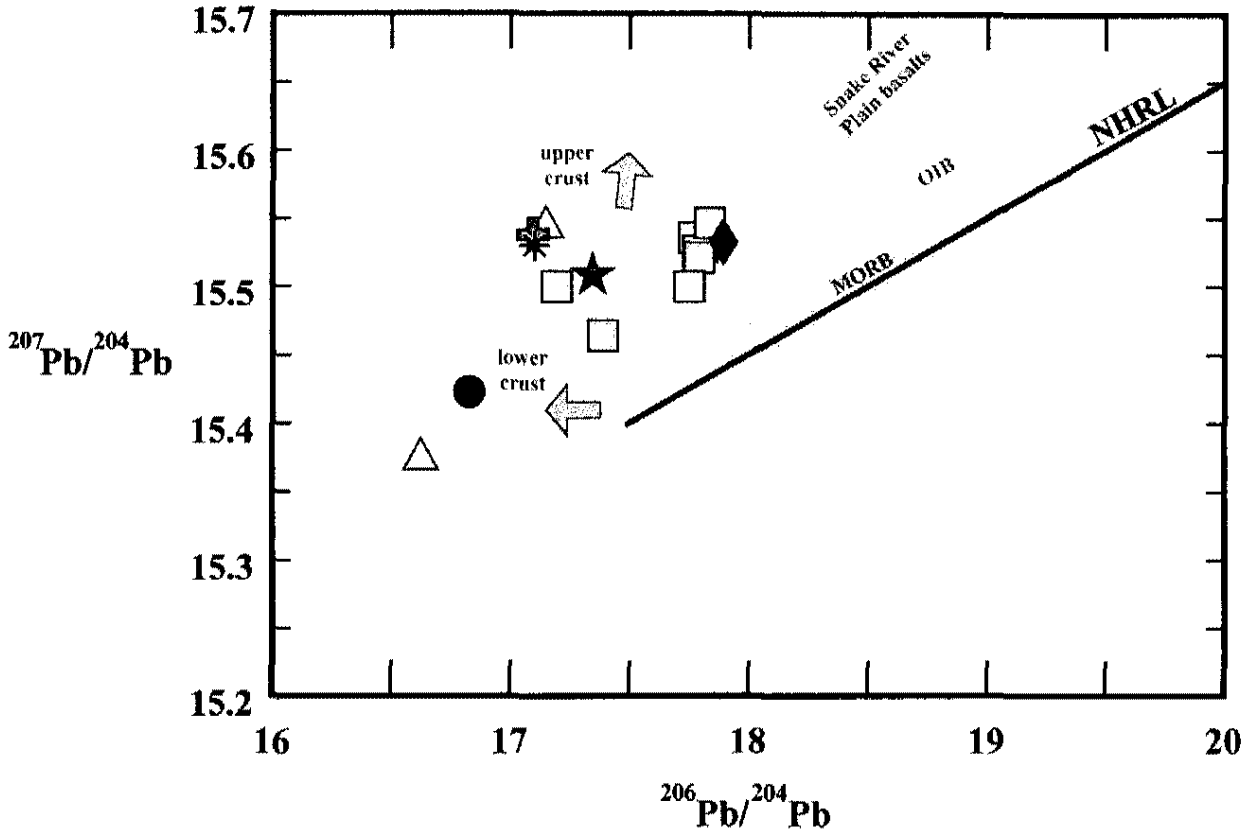
Figure 24: $^{206}Pb/^{204}Pb$ and $^{207}Pb/^{204}Pb$ of basalt (solid symbols) sampled in the Yellowstone Plateau volcanic field. MORB, OIB, and Snake River Plain basalt fields from Wilson (1989). NHRL is the Northern Hemisphere Reference Line of Hart (1984).

CHAPTER 5

GEOCHRONOLOGY

Besides the new dates reported in this thesis, other Pleistocene basalts within the
Yellowstone plateau volcanic field were previously dated using the K-Ar method
(Obradovich, 1992). A summary of the dates of the sampled basalts for this study is
presented in Table 1. A description of the new $^{40}Ar/^{39}Ar$ dates is presented below.

Madison River basalt from known

Madison River shield (YMR2)

Sample YMR2 (YMR-03-02) was collected from the summit of the shield 2.0 km north
of the Madison River. The age spectrum shows a consistent release of ^{39}Ar during all the
incremental heating events (See Figure 25). The first seven steps were used and a reasonable
isochron was produced giving a date of 0.530±0.06 Ma. Additionally, the isochron diagram
illustrates that the initial $^{40}Ar/^{36}Ar$ ratio of 295.8±0.7 is within analytical error of the accepted
atmospheric $^{40}Ar/^{36}Ar$ ratio of 295.5. This indicates no excess or deficiency of ^{40}Ar within
this sample and that most or all of the ^{40}Ar is radiogenic. Based on the field data, this date is
geologically realistic.

Isolated flow of Madison River basalt (YMR3)

Sample YMR3 (YMR-03-03) was collected from an exposure 0.2 km southwest of
Madison River and 0.5 km from the West Yellowstone park entrance. The age spectra
provided by the plateau diagram shows a consistent release of ^{39}Ar during all the incremental
heating events (See Figure 26). Steps 2 through 5 were used and a reasonable isochron was
produced giving a date of 0.358±0.019 Ma. Additionally, the isochron diagram illustrates

that the initial $^{40}Ar/^{36}Ar$ ratio of 299.5±0.9 is greater than the accepted atmospheric value of 295.5. If the $^{40}Ar/^{36}Ar$ ratio of the initial argon is greater than 295.5, there is "extraneous" argon present. The extraneous argon may be incorporated into the groundmass by a process other than the insitu decay of ^{40}K. Based on the field data and the geochemical evidence presented in Chapter 4, this date is geologically realistic.

Swan Lake Flat basalt from the Tower

Road shield (YSLF2)

Sample YSLF2 (YSLF-03-02) was collected from 1.7 km north of the summit crater of the Tower Road shield. The age spectrum shows a consistent release of ^{39}Ar during all the incremental heating events (See Figure 27). Steps 4 through 7 were used and an isochron was produced giving a date of 0.590±0.065 Ma. Additionally, the isochron diagram illustrates that the initial $^{40}Ar/^{36}Ar$ ratio of 293±2.6 is within analytical error of the accepted atmospheric $^{40}Ar/^{36}Ar$ ratio of 295.5. An $^{40}Ar/^{36}Ar$ of less than 295.5, suggests that there may be a deficiency in radiogenic argon. This deficiency may be attributed to a partial loss in ^{40}Ar after cooling of the basalt flow. This may or may not be the case for this particular sample.

Swan Lake Flat basalt from the Panther

Creek vent (YSLF12)

Sample YSLF12 (YSLF-03-12) was collected from the inner dike of the Panther Creek vent. The age spectrum shows a consistent release of ^{39}Ar during all the incremental heating events (See Figure 28). Steps 2 through 5 were used to produce an isochron, but the age produced was within the analytical error of the method thus was not statistically reasonable. Additionally, the isochron diagram illustrates that the initial $^{40}Ar/^{36}Ar$ ratio of 301.7±2.5 is greater than the accepted atmospheric value of 295.5. Ultimately, steps 2 through 5 were

used to produce a plateau date of 0.174±0.046 Ma. At the 2σ confidence level, this lava flow is no older than 220 ka. Even considering this date, this basalt is still the youngest sampled in the Norris-Mammoth corridor.

Swan Lake Flat basalt from Sheepeaters' Cliff exposure (YSLF1)

Sample YSLF1 (YSLF-03-01) was collected from 0.5 km northeast of Sheepeaters' Cliff roadside exhibit along the Norris-Mammoth road. The plateau diagram shows that approximately 66% of the ^{39}Ar present was released during the first three, lower temperature (600-690 °C) step heating events (See Figure 29). No isochron could be produced from the discontinuous plateau data, thus a date could not be determined.

Upper flow of Undine Falls basalt (YU4)

Sample YU4 (YU-03-04) was collected upstream of Undine Falls 0.5 km north of the Tower Road. A statistically significant date could not be obtained from this sample. The age spectra shows that approximately 57% of the ^{39}Ar present was released during the first three, lower temperature (600-690 °C) step heating events (See Figure 30). Additionally, the three-point isochron diagram, which includes steps 1 through 3, illustrates that the initial ^{40}Ar/^{36}Ar ratio of 291±11 is less than the accepted atmospheric value of 295.5. If the ^{40}Ar/^{36}Ar ratio of the initial argon is less than 295.5, there is an apparent deficiency in the radiogenic argon, which may be attributed to a partial loss in ^{40}Ar after cooling of the basalt flow.

Isolated flow of Osprey basalt (YO1)

Sample YO1 (YO-03-01) was collected from an exposure of Osprey basalt 0.2 km northwest of Tower Road approximately 1.5 km from the Tower Road bridge. A geologically realistic date could not be obtained from this sample. The age spectrum shows a consistent release of ^{39}Ar during all the incremental heating events (See Figure 31). While eight steps were used to determine a reasonable isochron, the date derived from the isochron

of 3.7±0.8 Ma does not agree with field data. This basaltic unit must be younger than the 640 k.y. Lava Creek tuff onto which it flowed. Excess ^{40}Ar must be present throughout the groundmass to produce a plateau with this unusually old date.

Isolated flow of Osprey basalt (YO4)

Sample YO4 (YO-03-04) was collected from an exposure near the trailhead of Wraith Falls 0.2 km southeast of the Tower Road. A geologically realistic date could not be obtained from this sample. The age spectra shows that approximately 69% of the ^{39}Ar present was released during the first four lower temperature (600-730 °C) step heating events (See Figure 32). Although four steps were used to determine a reasonable isochron, the date derived from the isochron of 0.770±0.22 Ma does not agree with field data. This basaltic unit must be younger than the 640 k.y. Lava Creek tuff onto which it flowed. Excess ^{40}Ar must be present throughout the entire groundmass to produce a plateau with this unusually old date.

Table 1: Summary of Basalt Dates Sampled During this Study

Basaltic Unit	Age (Ma)	Technique	Reference
Snake River Group (Henry's Fork Caldera)	0.198±0.008	K-Ar	1
Gerrit Basalt	*<0.20*	Estimate	2
Osprey Basalt			
Lamar River flow	*0.220±0.041*	K-Ar	1
Madison River Basalt	>0.13, <0.40	Estimate	2
Madison River Basalt shield (YMR2)	***0.530±0.060***	^{40}Ar/^{36}Ar	3
Falls River Basalt	>0.11, <0.64	Estimate	2
Madison River Basalt (YMR3)			
(may be flow of Falls River Basalt)	***0.358±0.016***	^{40}Ar/^{36}Ar	3
Swan Lake Flat Basalt	>0.32, <0.64	Estimate	2
Tower Road shield (YSLF2)	***0.590±0.065***	^{40}Ar/^{36}Ar	3
Panther Creek vent (YSLF12)	***0.174±0.046***	^{40}Ar/^{36}Ar	3
Undine Falls Basalt, upper flow	0.588±0.026	K-Ar	1
Basalt of Warm River	0.759±0.052	K-Ar	1

References:
1: Obradovich (1992); 2: Christiansen (2001); 3: Bennett (2005)

YMR2 - basalt groundmass

YMR2 - basalt groundmass

Plateau age = 565 ± 63 ka
85% of the 39Ar released
Steps 1 through 7 out of 9

Isochron age = 530 ± 60 ka
40/36 = 295.8 ± 0.7
MSWD = 0.54
Steps 1 through 7 out of 9
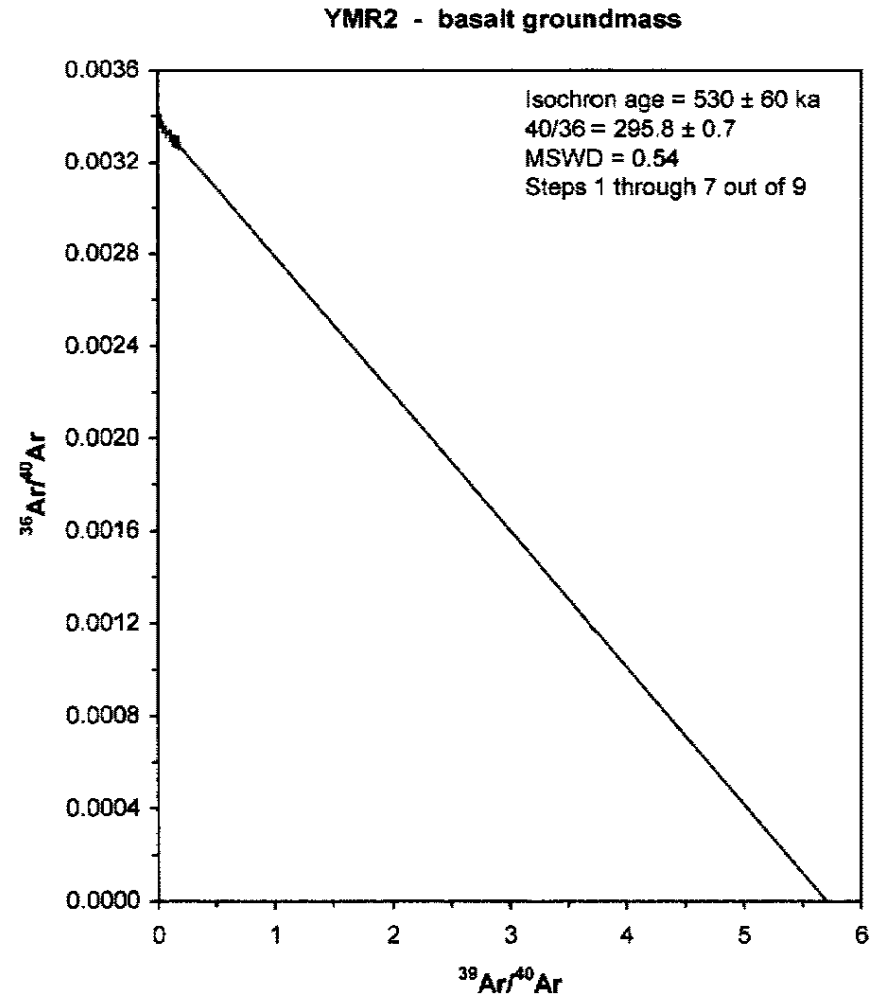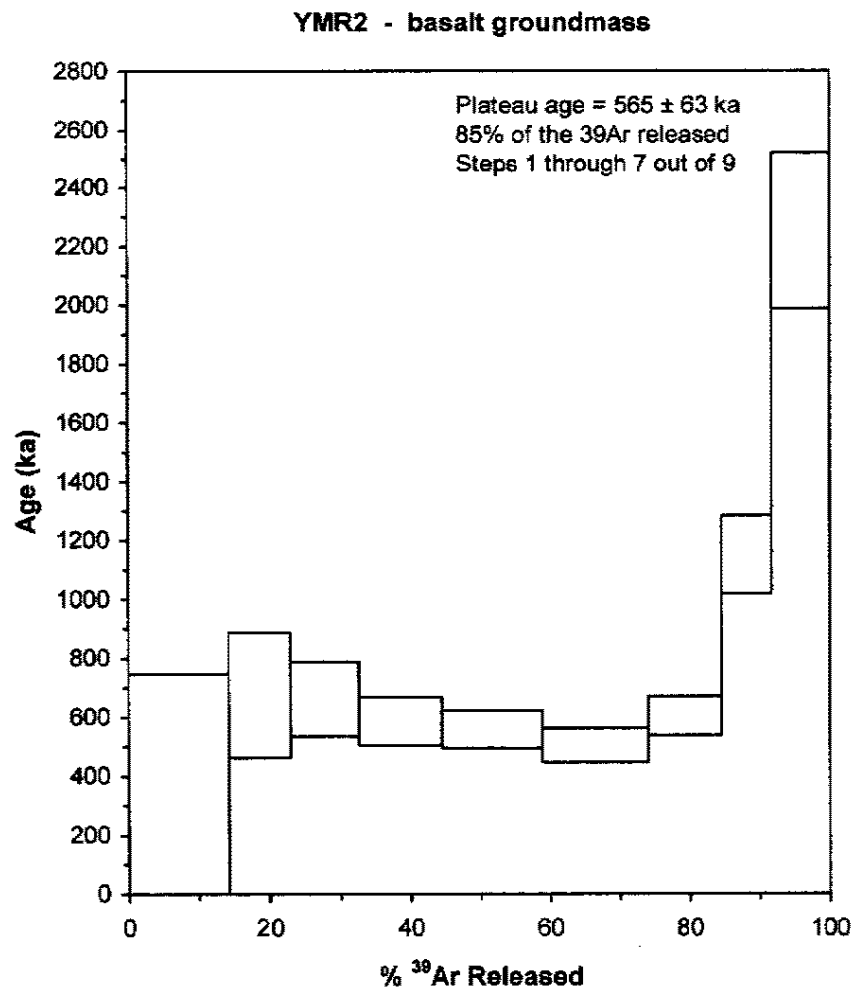
Figure 25: Age spectrum and isochron diagrams for Madison River basalt from the Madison River shield (YMR2).
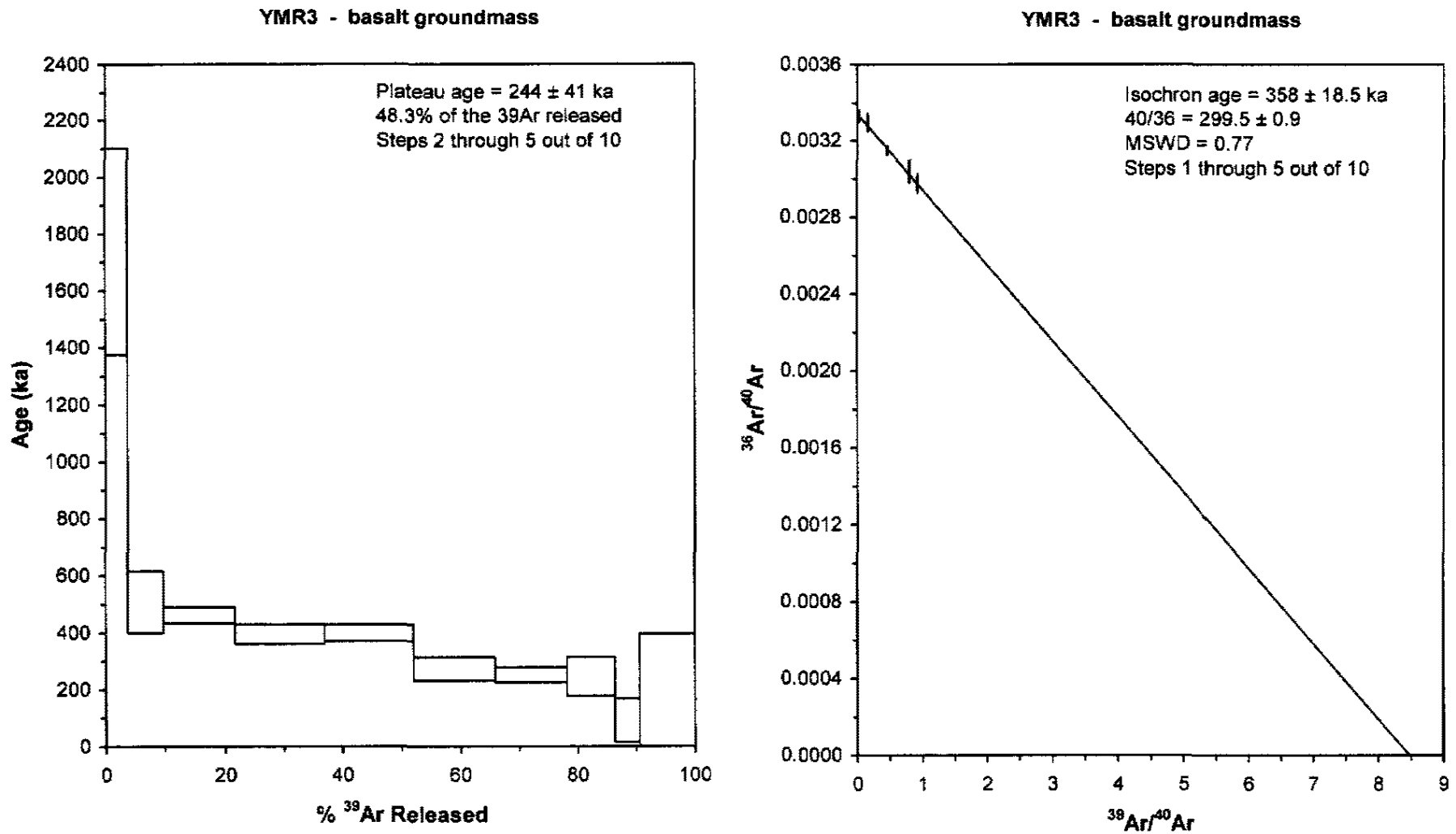
Figure 26: Age spectrum and isochron diagram for an isolated flow of the Madison River basalt (YMR3).

YSLF2 - basalt groundmass

Plateau age = 547 ± 29 ka
60% of the 39Ar released
Steps 4 through 7 out of 9

YSLF2 - basalt groundmass

Isochron age = 590 ± 65 ka
40/36 = 293 ± 2.6
MSWD = 2.7
Steps 5 through 8 out of 9
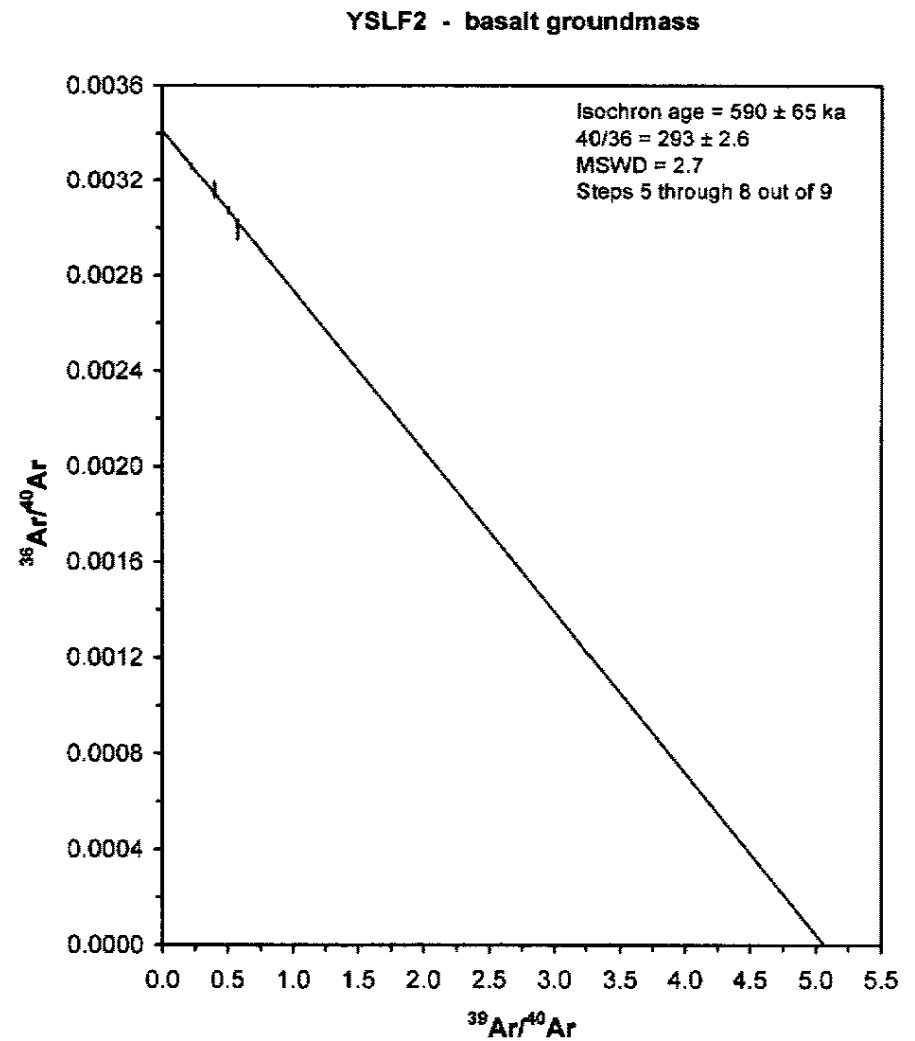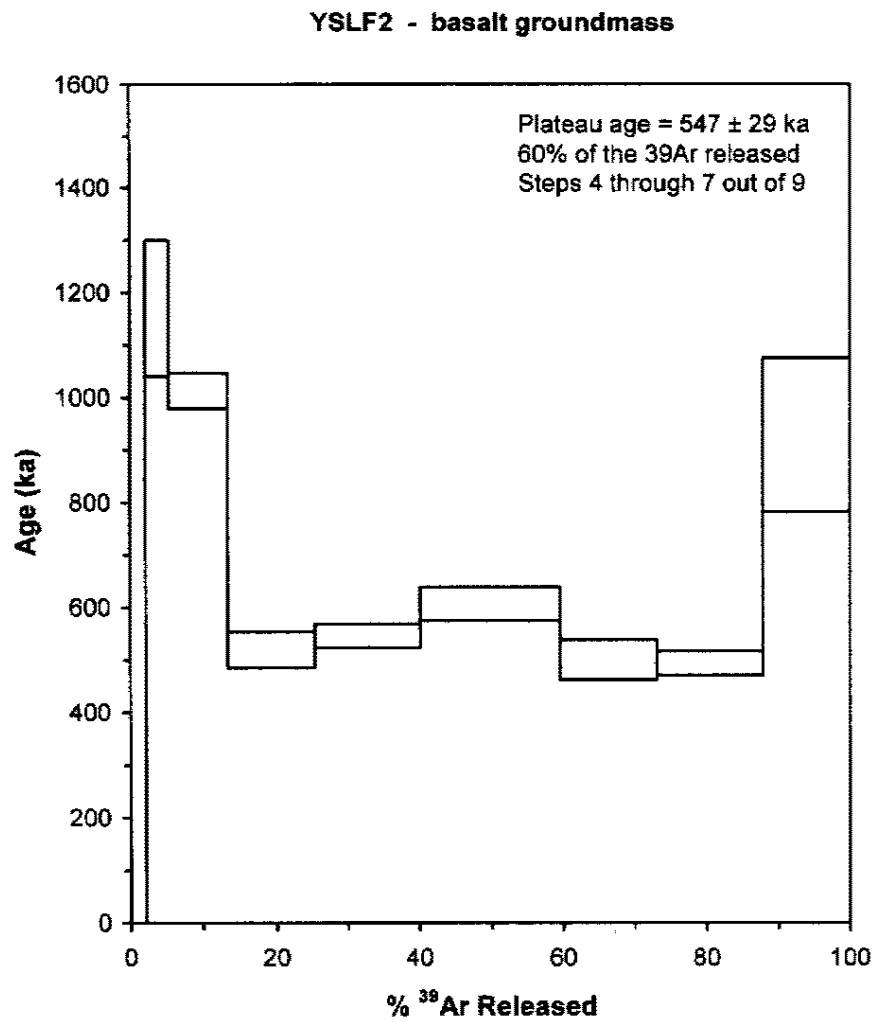
Figure 27: Age spectrum and isochron diagrams for a flow of Swan Lake Flat basalt that outcropped near the summit of the Tower Road shield (YSLF2).
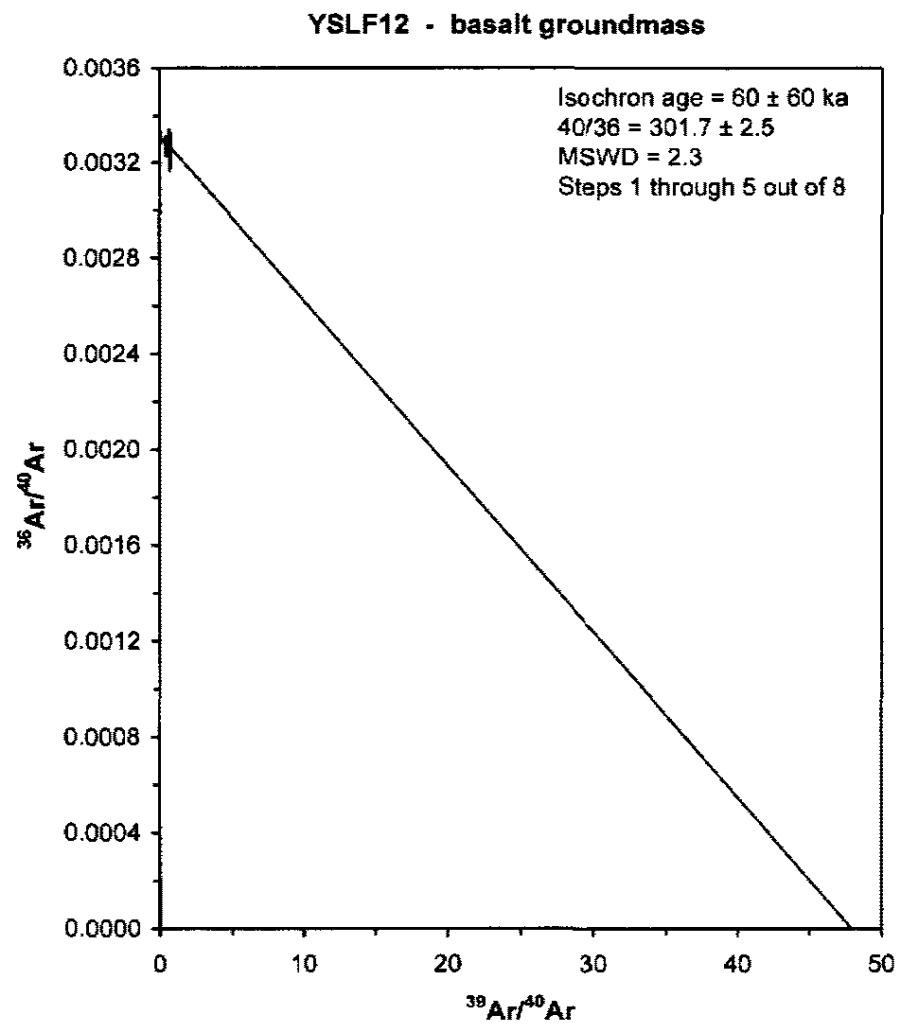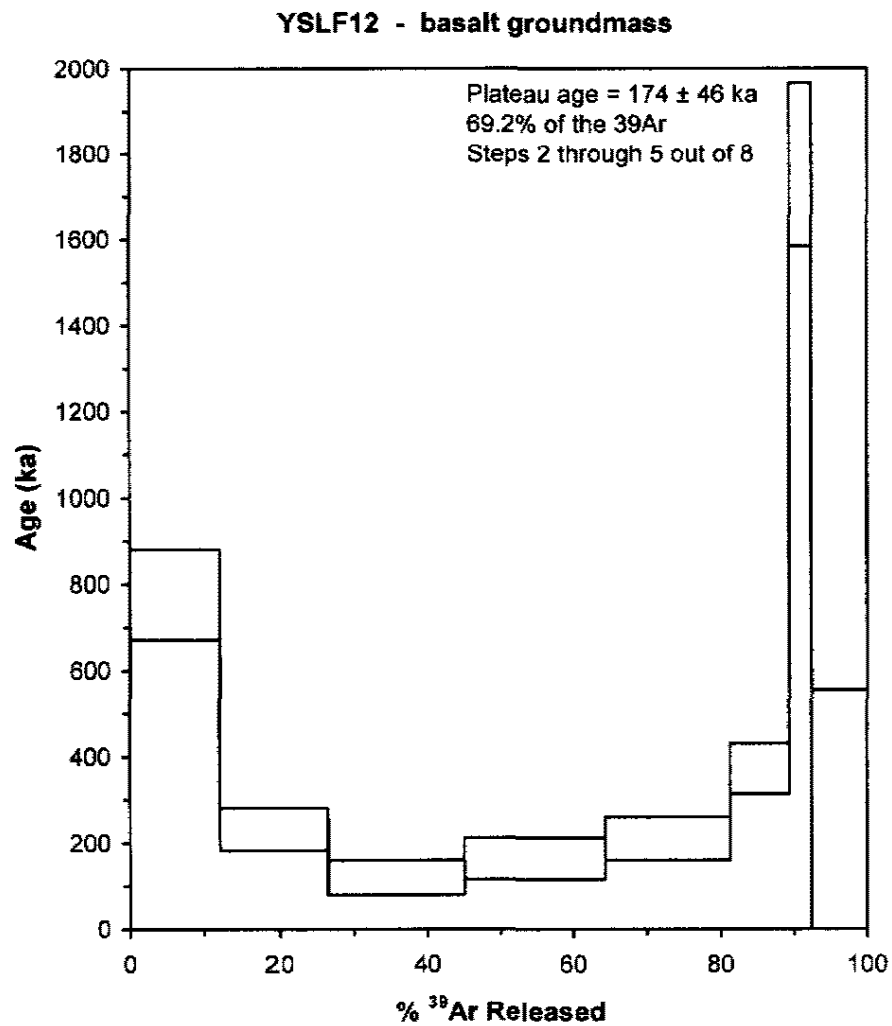
Figure 28: Age spectrum and isochron diagrams for a sample of Swan Lake Flat basalt collected form the inner dike of the Panther Creek vent (YSLF12).

YSLF-1 - basalt groundmass
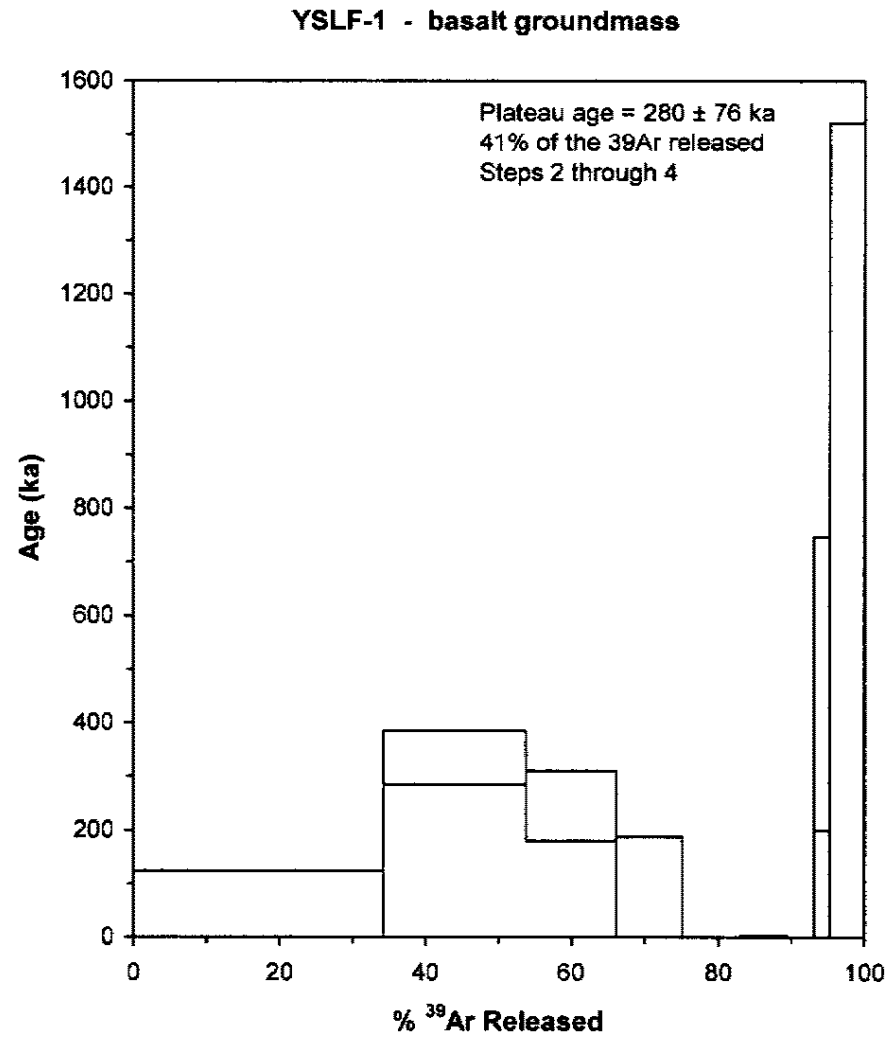
Figure 29: Age spectrum for Swan Lake basalt exposure at Sheepeaters' Cliff (YSLF1). An isochron could not be produced from the discontinuous data.
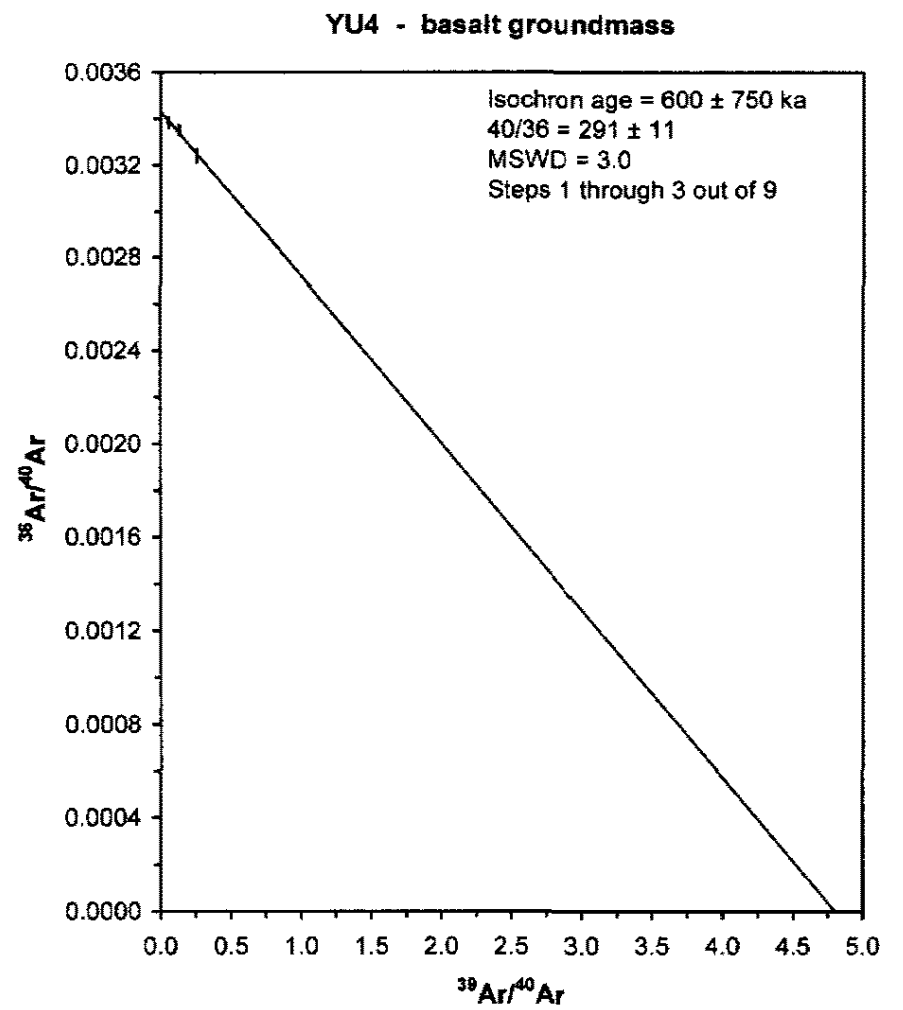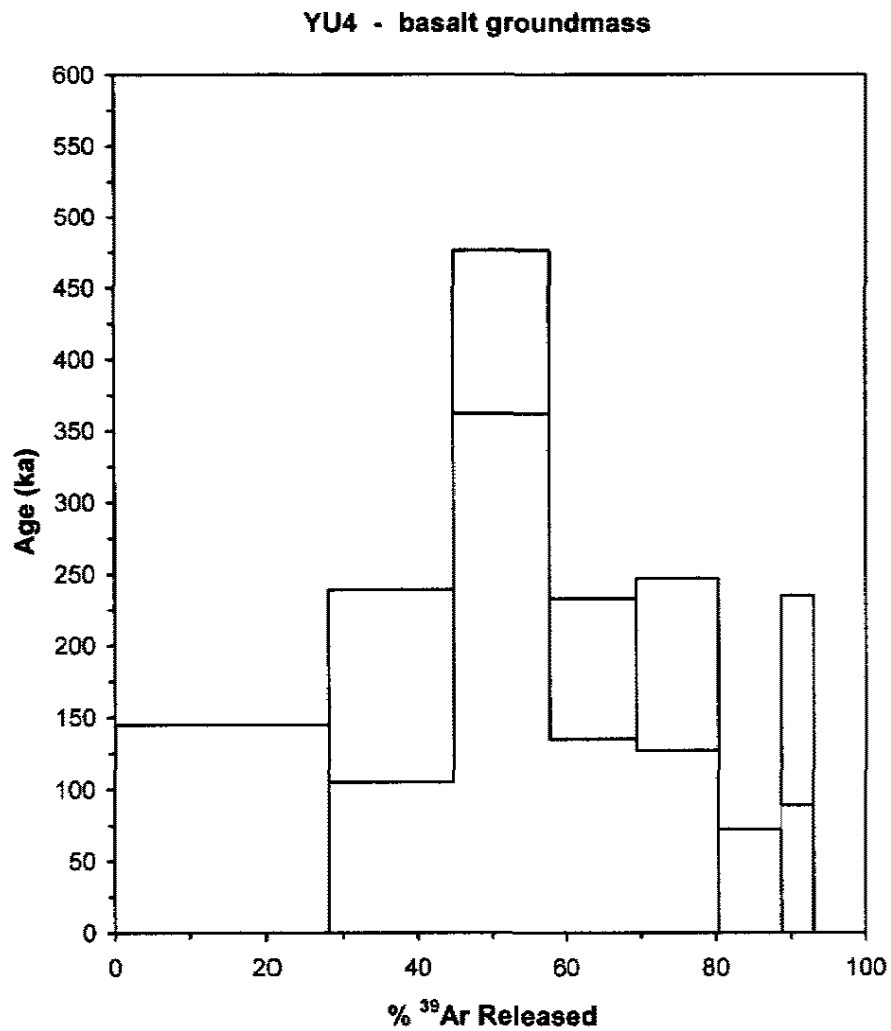
Figure 30: Age spectrum and isochron diagrams for an isolated flow of Undine Falls basalt (YU4).
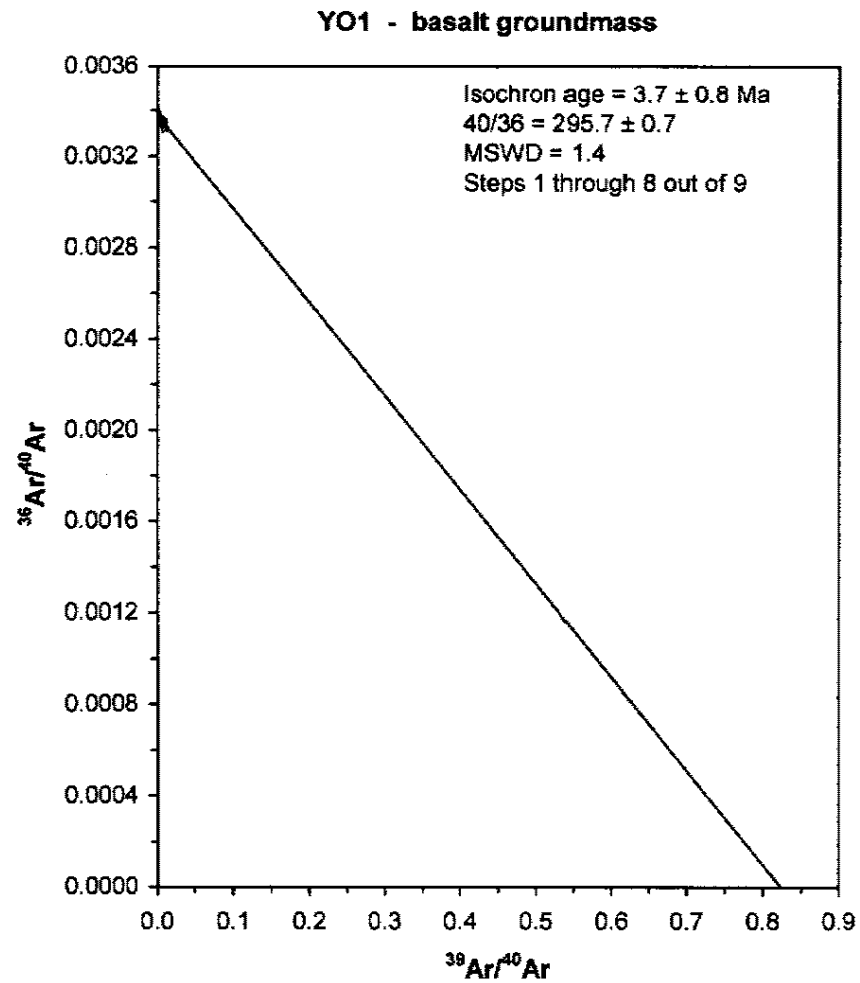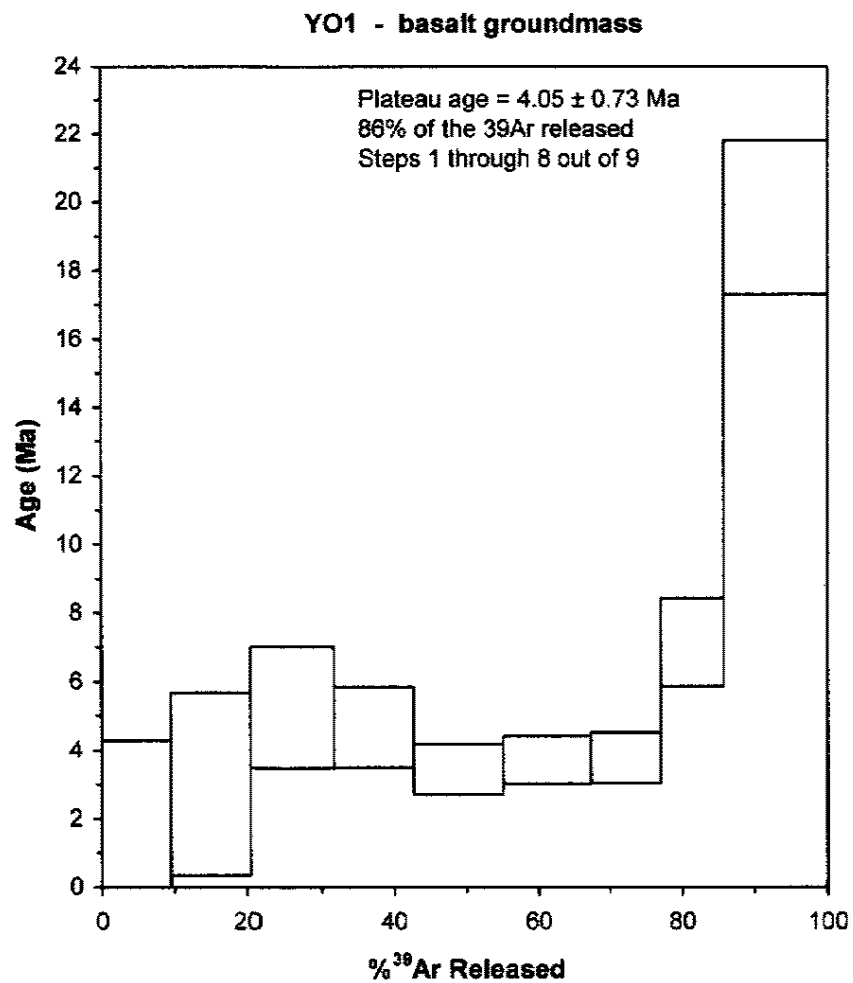
Figure 31: Age spectrum and isochron diagram for an isolated flow of Osprey basalt (YO1).
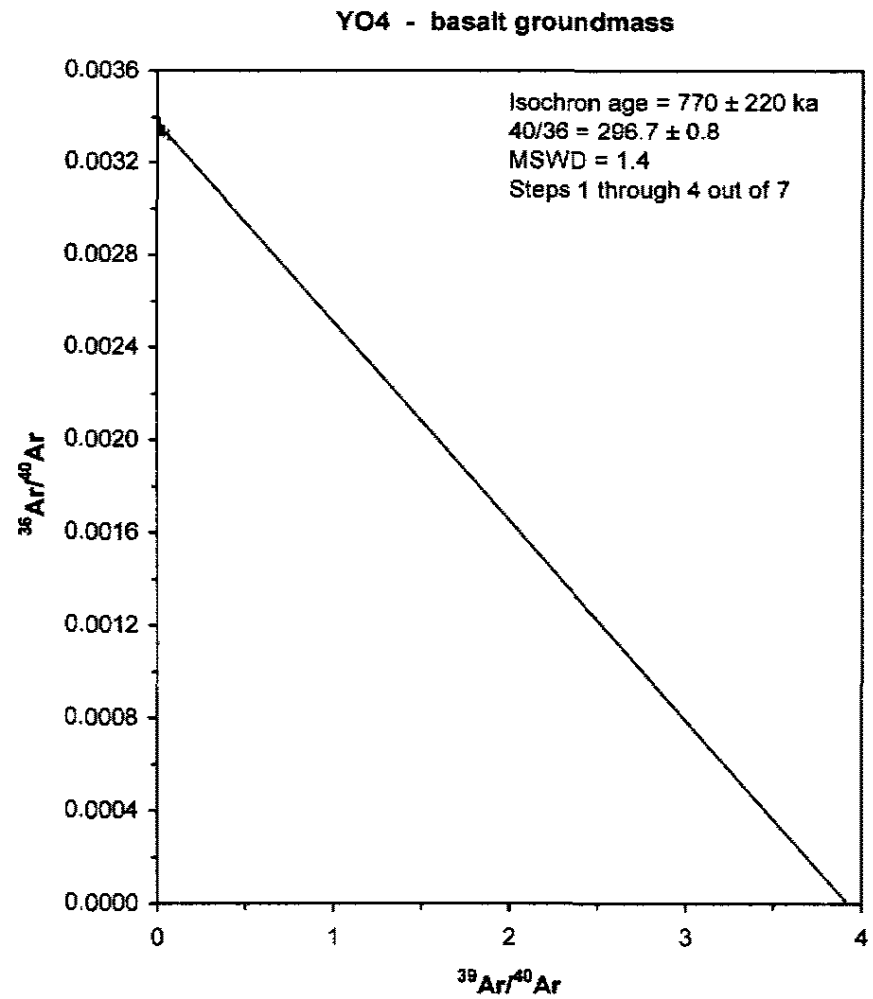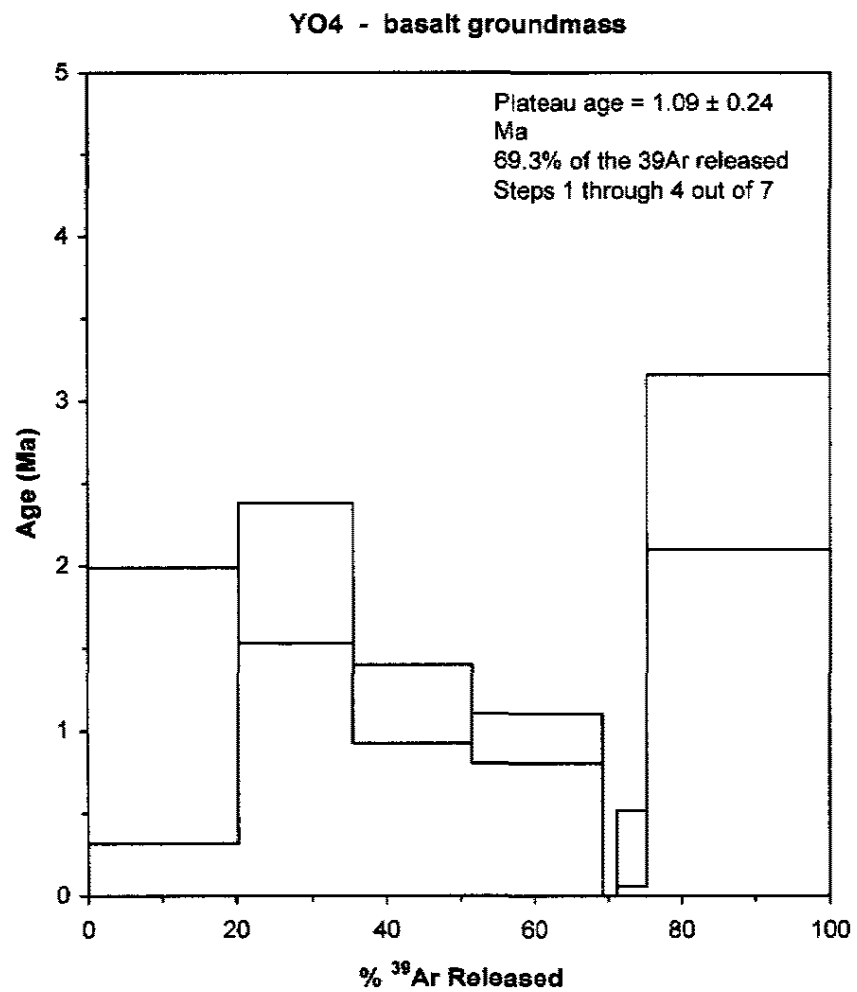
Figure 32: Age spectrum and isochron diagrams for an isolated flow of Osprey basalt (YO4).

CHAPTER 6

INTERPRETATION

Petrogenesis of Norris-Mammoth Corridor Basalts

The models discussed in this chapter pertain to the petrogenesis of basalts within the Norris-Mammoth corridor. Modeling indicates that independent partial melting of compositional variable mantle produced the basaltic magma within the Norris-Mammoth corridor. Other models discussed include: (1) open and closed system processes, such as fractional crystallization (FC), assimilation-fractional crystallization (AFC), and/or magma mixing/commingling; (2) partial melting of heterogeneous mantle; (3) and contamination of asthenospheric partial melts by lithospheric mantle and/or crustal components. Furthermore, modeling also provided preliminary evidence of the nature of the mantle source below the Norris-Mammoth corridor.

FC, AFC, and/or Magma Mixing/Commingling

FC, AFC, and magma mixing/commingling models were tested to explain chemical variation between magma groups and among individual magmas within these groups. In theory, the geochemical models must be numerically realistic and agree with isotopic source characteristics. The models test whether the basalts were derived from the same parent magma (comagmatic) and/or melted from the same (or similar) mantle sources (cogenetic).

Modeling was done using Igpet for Windows (Carr, 2000). Distribution coefficients of Cenozoic basalts from the western United States were compiled by the Center for Volcanic and Tectonic Studies (CVTS) using data from Budahn et al. (1985), Lemarchand et al. (1987), Liotard et al. (1988), and Bradshaw, (1991). Calculation of bulk distribution coefficients, to reflect phenocryst percentages in the basalts, was done by using a Microsoft Excel spreadsheet written by Tim Bradshaw and later modified by Eugene Smith.

Observations

Geochemical models must honor the following field and geochemical observations.

1. Olivine and plagioclase are common phenocrysts in all lavas.

2. Basalts contain zoned and/or sieved plagioclase phenocrysts. No reaction rims are present.

3. Trace element plots (See Figure 20 or 21) demonstrate that each basalt unit has a distinct signature.

4. The Swan Lake Flat basalt from the Panther Creek vent is the most primitive basalt in the Norris-Mammoth corridor. It has $^{87}Sr/^{86}Sr$ of 0.7053 and ε_{Nd} of 0.18. This basalt lies between the OIB and EMORB fields on a $^{87}Sr/^{86}Sr$ vs. ε_{Nd} plot.

5. Swan Lake Flat basalt from the Tower Road shield and the Horseshoe Hill vents, Undine Falls, Osprey, and Madison River basalts form a linear array on a $^{87}Sr/^{86}Sr$ vs. ε_{Nd} plot that extends from the Swan Lake Flat Panther Creek basalt to higher $^{87}Sr/^{86}Sr$ and lower ε_{Nd} values (See Figure 22).

6. Magmas related to individual vents display different trends on Sr vs. Cr plots (See Figure 20).

7. Basement rocks in the Norris-Mammoth corridor include: (1) the Lava Creek and Huckleberry Ridge tuffs; (2) the Eocene Absaroka Volcanic Supergroup, which include trachybasaltic, shoshonitic, and silicic rocks; (3) Cambrian to Cretaceous sedimentary rocks that are mostly marine clastics and carbonates; (4), and Precambrian basement that consists of late Archean granitic gneiss and smaller amounts of metasedimentary and metavolcanic rocks.

Assumptions

1. Basalt magma related to volcanoes in the Norris-Mammoth corridor is cogenetic. In other words, the magmas erupted within the Norris-Mammoth corridor are similar in chemistry, were produced by partial melting of a similar mantle source over a short period of time (less than 600 ka). Most likely, these magmas did not share the same magma chamber.

2. Small volumes of basaltic magma erupted over short periods of time from individual cinder cones are most likely comagmatic.

3. Considering the small volume of magma erupted over the 2.2 million year eruptive history of basaltic magma in the Norris-Mammoth corridor, it is highly unlikely that a single magma chamber could persist for the entire time span of the volcanic field. Therefore, simple FC and AFC models involving a single magma body are not suitable for explaining chemical variations between magma groups. Production of similar parental magmas from similar mantle sources by multiple partial melting events over the life span of the volcanic field is more likely.

Basalt Models

Osprey

Osprey basalt is geochemically distinct in trace element concentrations, but is isotopically similar to the basalts erupted from the Panther Creek vent. The most evolved Osprey basalt can be produced by fractional crystallization (FC) of more primitive samples. Using Sr and Cr, samples YO-03-02, YO-03-01, and YO-03-04 can be produced from YO-03-02A by 2%, 18%, and 29% fractionation, respectively, of 69% plagioclase and 31% olivine (See Figure 39A). Alternatively, using Ce and Zr, samples YO-03-02A, YO-03-01, and YO-03-04 can be produced from YO-03-02 by 8%, 32%, and 35% fractionation, respectively, of 78% plagioclase and 22% olivine (See Figure 39B).

Table 2: Summary of FC Models to produce Evolved Osprey Samples (01-02 and 04) from Primitive Osprey Sample (02A)

Model (from YO-03-02A)	YO-03-01	YO-03-02	YO-03-04
Model 1 (Cr vs. Sr) *Figure 36A*	2% FC of 69% Plagioclase, 31% Olivine	18% FC of 69% Plagioclase, 31% Olivine	29% FC of 69% Plagioclase, 31% Olivine
Model 1 (Ce vs. Zr) *Figure 36B*	8% FC of 78% Plagioclase, 22% Olivine	32% FC of 69% Plagioclase, 31% Olivine	35% FC of 69% Plagioclase, 31% Olivine

Swan Lake Flat

Assimilation-fractional crystallization, fractional crystallization, and/or mixing models do not work to relate any of the basalts within the Swan Lake Flat basalt unit. Each vent erupted basalts that were from a distinct partial melting event. This conclusion is confirmed by: (1) the variation in incompatible element composition and (2) isotopic heterogeneity (See Figure 33).

As stated previously, the basalts that erupted from the Panther Creek vent are the most isotopically primitive of all the basalts in the Norris-Mammoth corridor. Therefore, if the Norris-Mammoth corridor basalts are cogenetic, FC or AFC models using samples of this basalt as the parent rock should produce most, or all, of these basalts. Using Sr and Cr, and

the most isotopically primitive Panther Creek basalt (YSLF-03-14), fractionation of the phenocryst assemblage present in YSLF-03-14 (75% plagioclase and 25% olivine) ought to approximate concentration of Sr and Cr in the Norris-Mammoth corridor basalt (See Figure 36). However, the model produces magmas with higher Cr and lower Sr, or the opposite of what is required to match the composition of Norris-Mammoth corridor magmas. Therefore, fractional crystallization could not produce the observed compositional variation.

Partial Melting of Heterogeneous Mantle

Lateral compositional variation

Partial melting of mantle with lateral compositional variation would produce magmas with varying isotopic ratios within a single volcanic field. Melting of laterally variable mantle assumes that melting is occurring at similar depths, but that mantle isotopic compositions vary on the kilometer, or smaller, scale. If this model is correct, patterns of isotopic variation should be random with no geographic or age correlation. However, there is a correlation of chemistry with geographic position; magmas become more isotopically enriched from west to east (See Figure 37).

In detail, there is an age and the isotopic composition correlation between basalts. Older Madison River and Undine Falls magmas are more isotopically enriched and are distributed along a broad arc north of the Yellowstone Caldera (Plate 1). Younger Swan Lake Flat and Osprey magmas are more isotopically depleted and are located in the Norris-Mammoth corridor. The trends of isotopic composition suggest that random lateral compositional variability in the mantle is not the cause of the isotopic variations observed in these magmas. Based on these arguments, lateral heterogeneity can be ruled out as the sole cause of compositional variations in these magmas groups.

<u>Changes in the depth of melting (or vertically heterogeneous mantle)</u>

Partial melting of mantle at varying depths may also result in lavas with varying isotopic ratios. If lithospheric mantle is melted, an isotopically-enriched (high $^{87}Sr/^{86}Sr$ and low ε_{Nd}) and incompatible element enriched (i.e. light REE) basaltic magma would be created. If basalt is produced from an EMORB-like, upper asthenospheric mantle, the magma would be low in $^{87}Sr/^{86}Sr$, high in ε_{Nd}, and depleted in incompatible elements. If basalt is produced from and OIB-like, lower asthenospheric mantle, the magma would have intermediate $^{87}Sr/^{86}Sr$ and ε_{Nd} and would be enriched in incompatible elements.

Undine Falls, Swan Lake Flat, and Osprey basalts all erupted in the same locality over the last ~600 ka. While, trace element abundances are similar, isotopic ratios vary as a single trend from the isotopically depleted Swan Lake Flat and Osprey cluster to the more isotopically enriched Undine Falls magmas (See Figure 22). If progressively deeper mantle was melted over time, the basalts produced would become more isotopically depleted with time. This isotopic trend (from high $^{87}Sr/^{86}Sr$ and low ε_{Nd} to low $^{87}Sr/^{86}Sr$ and high ε_{Nd} with time) is observed in Undine Falls, Swan Lake Flat, and Osprey samples. Changing the depth of melting with time can generate the observed isotopic trend in the northern section of the Norris-Mammoth corridor.

In general, magmas in the Norris-Mammoth corridor become more EMORB-like from west to east, therefore, changes in geochemistry is more likely related to geography and the age of the magma. Based on the observations presented above, lateral mantle variability can be discounted. Vertical mantle heterogeneity may control basalt compositions in the northern portion of the Norris-Mammoth corridor, but cannot explain the chemical variability in all the basalts of the Norris-Mammoth corridor.

Contamination of asthenospheric mantle partial melts

Contamination models discussed in this section involve lithospheric mantle assimilation and contamination of asthenospheric partial melts with crust that is present in the Norris-Mammoth corridor and Yellowstone Plateau volcanic field.

Lithospheric Mantle Contamination

Evidence of lithospheric mantle contamination is noticeably apparent when Sr and Nd isotopes are compared to known mantle provinces in the Yellowstone Plateau volcanic field (see Figure 33). With the exception of one Undine Falls sample, the remainder of the sampled basalts trend toward the field of lithospheric mantle; higher Sr ratios and lower epsilon Nd. The lower flow of Undine Falls basalt plots near the field of other Wyoming Province Archean volcanic rocks.

Crustal Contamination

Variations in basalt geochemistry in relation to the individual magma groups may be related to contamination by different composition crustal materials. Possible contaminants in the Yellowstone Plateau volcanic field include, but are not limited to:

1. Precambrian crustal xenoliths found in basalts erupted in the vicinity of Island Park;

2. Precambrian crustal rocks in the Gallatin Range and north of Gardiner, Montana;

3. Paleozoic clastic sedimentary rocks and limestones;

4. Eocene Absaroka volcanic rocks; and/or

5. Tertiary and Quaternary volcanic rocks (rhyolite domes, flows and ash-flow tuffs).

Field evidence of crustal contamination occurs in the Panther Creek feeder dike (See Chapter 2). Partially melted granitic xenoliths were incorporated in the outer portion of the feeder dike and are present in bombs within the first stage agglutinated scoria. In thin

section, the partially melted xenoliths are surrounded by basaltic glass. No other evidence of mixing or commingling was present in thin-section.

Late Archean rocks have the greatest likelihood of contaminating the basaltic magmas during their ascent and storage within mid-level crust. Archean rocks outcrops are present throughout the Wyoming Province. In general, Archean lower crust has lower ε_{Nd}, $^{87}Sr/^{86}Sr$ and $^{206}Pb/^{204}Pb$ and higher $^{207}Pb/^{204}Pb$ compared to Proterozoic and younger basement rocks (Taylor and McLennan, 1985).

Proterozoic intermediate to felsic rocks crop out approximately 12 km north of the Norris-Mammoth corridor within the Beartooth Mountains of Montana (Hildreth et al., 1991). These rocks range in composition from granite and granodiorite to amphibolite in composition and have high $^{87}Sr/^{86}Sr$, low ε_{Nd}, and high $^{206}Pb/^{204}Pb$. (Wooden et al., 1988).

Minor amounts of assimilation of these silica-rich rocks would produce a volcanic suite with varying SiO_2 contents. SiO_2 content, however, varies little in selected basalt samples from the Yellowstone Plateau volcanic field (See Figure 35). Small variations in SiO_2 may imply that the crustal assimilates may have been mafic or ultramafic in composition, such as lower crustal granulites or mantle rocks (O'Brien et al., 1995).

Leeman et al. (1985) identified mafic xenoliths in Spencer-Kilgore area approximately 100 kilometers southwest of the Yellowstone Plateau volcanic field. They used Sr, Nd, and Pb isotopic analyses to "evaluate the nature and age of the basement beneath the Snake River Province (Leeeman et al., 1985)." The xenoliths range from charnockite to norite and have low $^{206}Pb/^{204}Pb$ and medium $^{207}Pb/^{204}Pb$ compared to Norris-Mammoth corridor basalts. Although the mafic xenoliths may be considered a potential contaminant, the Pb isotope

ratios are too depleted to generate the isotopic ratios seen in the Norris-Mammoth corridor basalts (See Figure 34).

Other potential crustal contaminants may have the proper isotopic ratio, but can be eliminated because their major or trace element abundances may be unsuitable. For example, a high SiO_2 contaminant would create a magma that is no longer basaltic in composition. Also, the lead isotopic ratios of some of the potential crustal contaminants relative to the lead ratios of the sampled Norris-Mammoth corridor basalts also exclude crustal contamination (See Figure 34). For example, the $^{207}Pb/^{204}Pb$ of Paleozoic limestone and Mesozoic clastic rocks is considerably higher than any of the basalts in the Norris-Mammoth corridor. These examples, alone, discount most of the Precambrian crustal rocks, Paleozoic clastic sedimentary rocks, Eocene Absaroka, and Tertiary and Quaternary volcanic rocks (See Figure 34). Also, many of the xenoliths (i.e. Crazy Mountain xenoliths) have values that are similar to those of the Norris-Mammoth corridor basalts. Assimilation of these xenoliths would result in little variation.

Additionally, the Paleozoic and Mesozoic sedimentary rocks and the Eocene Absaroka volcanic rocks are not likely to be significant sources of crustal contamination in the Norris-Mammoth corridor because of their stratigraphic thickness. In the Yellowstone region, the maximum thickness of the Cambrian to Cretaceous marine section is approximately 2.5 km, while the thickness of the Eocene Absaroka volcanic section is estimated at 1.5 km (Hildreth et al., 1991). The Precambrian to Eocene stratigraphic section is not a likely contaminant because the section lies above the "rhyolitic density barrier" that may be beneath the Yellowstone Plateau (Spell et al., 2004; Lehman et al., 1982; Smith and Braile, 1984). Detailed active-seismic experiments show the top of a rhyolitic magma body (that may still

be molten) larger in area than the Yellowstone Caldera at approximately 5-6 km beneath the surface (Lehman et al., 1982; Smith and Braile, 1984). This batholith-sized body may act as a density barrier to ascending basaltic magma at depth. Based upon the hypothesis by Spell, et al. (2004), a similar "density barrier" may be forming in the Norris-Mammoth corridor. If this is the case, this density barrier lies beneath the Paleozoic and Mesozoic units, therefore it is highly unlikely that basaltic magma would have accumulated in a chamber large enough to incorporate crustal assimilates above this density barrier.

In conclusion, limited crustal contamination did occur in the Panther Creek basalts of Swan Lake Flat. Petrologic and geochemical evidence suggests that these xenoliths were not mixed within the basaltic magma. Other potential crustal contaminants either do not have comparable major and trace element contents (like SiO_2 or Pb) or Sr, Nd, or Pb isotopic ratios to produce the geochemical trends within the Norris-Mammoth corridor.

Independent mantle partial melts

The argument for the formation of Norris-Mammoth corridor basalts by independent partial melting of heterogeneous mantle is supported by the following data:

1. Clustering of data from each volcanic center on several different trace element diagrams;

2. Lack of continuous chemical variation between volcanic centers;

3. Simple fractional crystallization (FC) cannot produce the necessary trace element compositions; and

4. The fact that lavas associated with each volcanic unit have different isotopic ratios.

A Sr vs. Cr plot was originally used to define groups of basalts that erupted from separate vents (See Figure 20). This diagram shows grouping of Swan Lake Flat basalts, which

initially appeared to be two separate vents, and discrete clustering of Undine Falls, Madison River, and Osprey basalts. Further analysis of Sr vs. Zr/Nb diagram demonstrates that the Swan Lake Flat basalt actually clusters into three groups that are consistent with the three identified vent areas (Tower Road, Horseshoe Hill, and Panther Creek) in the Norris-Mammoth corridor. The lack of continuous variation between the clustered volcanic centers on the above mentioned diagrams is evidence in support of independent partial melting. The Swan Lake Flat basalt, from the Panther Creek vent, and the Osprey basalt, are the most isotopically primitive of all the basalts within the Norris-Mammoth corridor, therefore, they should be an end member composition in all modeling for petrogenesis in the Norris-Mammoth corridor. When these end members are used in FC or AFC geochemical modeling, they cannot produce any of the more evolved basaltic magmas (See Figure 36).

Isotopic dissimilarity is another indication of independent partial melts. As stated previously, the Panther Creek vent and Osprey are the most isotopically primitive basalts in the Norris-Mammoth corridor and plot in the OIB field, close to the Bulk Silicate Earth composition (See Figure 33). The remainder of the basalts sampled in the Norris-Mammoth corridor trend towards the lithospheric mantle domain, or are depleted in $^{87}Sr/^{86}Sr$ and enriched in Nd.

<div align="center">Nature of the Mantle Source beneath the Yellowstone</div>

<div align="center">Plateau Volcanic field</div>

The youngest Yellowstone Plateau volcanic field basalts should retain a "chemical fingerprint" of the source of the basalts that have continually erupted throughout the eastern Snake River Plain during the last 14 Ma. This fingerprint may be best revealed in a simple mixing model using Gerrit basalt and EMORB to produce the Sheepeaters' Cliff flow from

the Panther Creek vent (See Figure 40). Both the Gerrit basalt and the Sheepeaters' Cliff flow most likely erupted within the same 50,000 time interval (Chapter 5 *and* Christiansen, 2001). During the initial process, the closest analog (in the Yellowstone Plateau volcanic field) to the average eastern Snake River Plain basalts was chosen to represent a portion of the "fingerprint." Sample HFGE-03-04 was used to represent the basalts that have continually erupted throughout the Snake River Plain in the last 14 Ma (See Figure 39). Also, this basalt was chosen because it is likely the youngest flow of the Gerrit basalt as evidenced by its glassy groundmass.

When 45% of the youngest Gerrit flow (HFGE-03-04) was mixed with 55% EMORB-like component, it produced basalt strikingly similar to the basalt flow from Sheepeaters' Cliff near Swan Lake Flat (YSLF-03-01). Mapping and geochemistry have indicated that the Sheepeaters' Cliff flow erupted from the Panther Creek vent, one of the youngest vents within the Norris-Mammoth corridor (See Figure 37). This simple model demonstrates that the source of the Swan Lake Flat basalt is probably in the upper mantle. This EMORB component may represent basalt produced by the upper mantle thermal anomaly referenced by Smith et al. (2004).

Summary

- Modest volumes of erupted material, isotopic diversity, 2 m.y. span of ages, vent distribution scattered over a 140 km^2, and the apparent lack of a consistent time-compositional patterns are factors, considered cumulatively, indicate independent partial melting episodes, ascent and storage within the lithosphere of each basaltic magma unit.

- Sr and Nd isotopes provide evidence of lithospheric mantle contamination when compared to known mantle provinces in the Yellowstone Plateau volcanic field (see

Figure 33). With the exception of one Undine Falls sample, the remainder of the sampled basalts trend toward the field of lithospheric mantle; higher Sr ratios and lower epsilon Nd. The lower flow of Undine Falls basalt plots near the field of other Wyoming Province Archean volcanic rocks.

- Limited crustal contamination may have occurred at the Panther Creek vent of the Swan Lake Flat basalt; this is evident by out partially melted felsic xenoliths. Significant crustal contamination within the NMC can be eliminated based upon the lack of suitable major and trace element abundances and isotopic ratios of the possible contaminants.

- Changes in the lateral extent of the partially melted mantle can be ruled out because the ND, Sr, and Pb isotopic systems do not change from enriched to depleted with time in the Norris-Mammoth corridor. Changes in the depth of partial melting can produce local isotopic variation (i.e. the northern portion of the Norris-Mammoth corridor) but cannot account for variation in the entire Norris-Mammoth corridor.

- Fractional crystallization and assimilation-fractional crystallization models cannot explain the geochemical differences between magma groups. The Osprey basalt is the only basaltic unit whose flows can be explained by fractional crystallization.
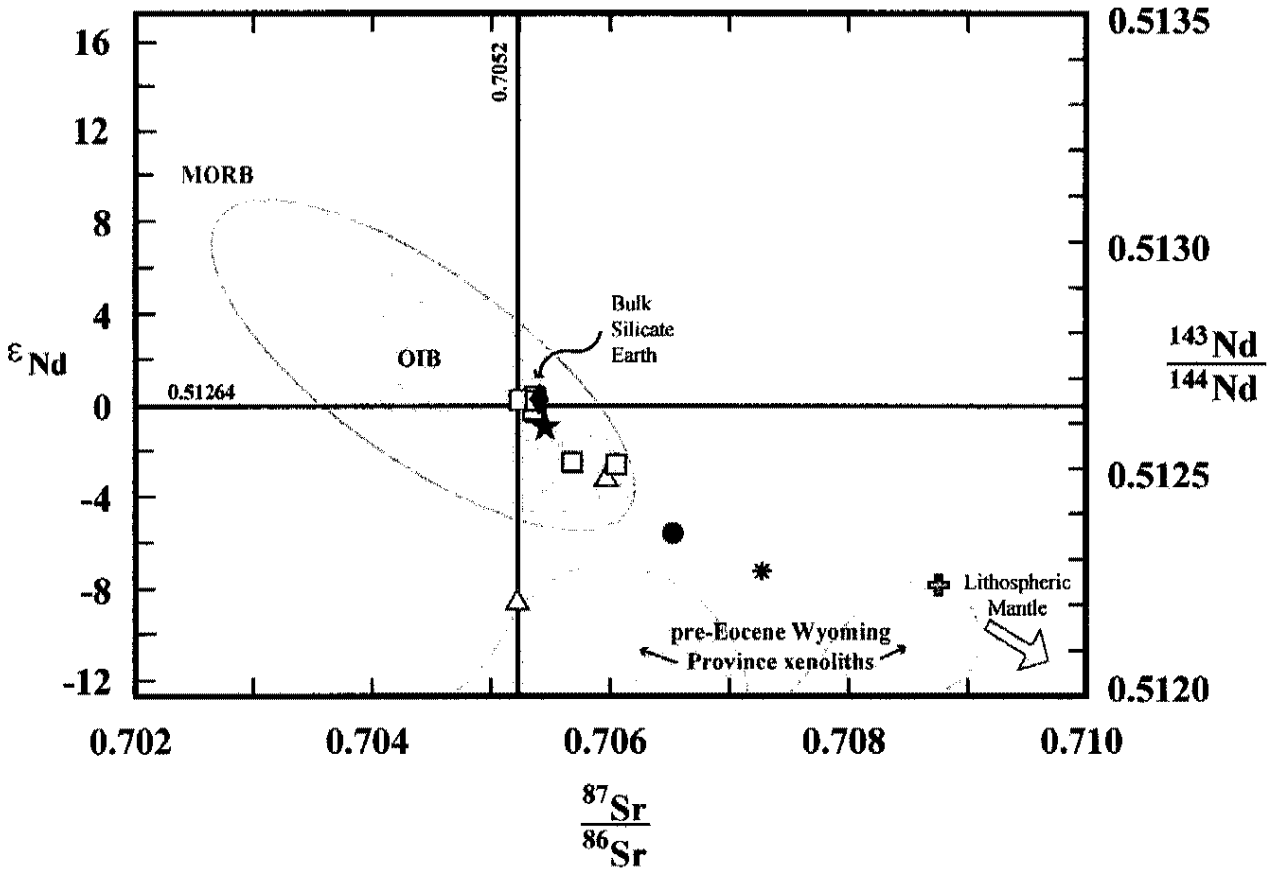
Figure 33: Sr and Nd isotopic ratios for tholeiitic basalts in Yellowstone Plateau volcanic field. Hepburn Mesa, Swan Lake Flat, Undine Falls, and Osprey basalt samples fall within the field of ocean island basalts while Falls River, Gerrit and Madison River basalts trend towards lithospheric isotopic values. OIB and mid-ocean ridge basalt (MORB) fields defined by Rollinson (1993) and pre-Eocene Wyoming Province xenoliths from Feeley et al. (2003) after Dudás et al. (1987) and Joswiak (1992). Diagram modified from Rollinson (1993).

Figure 34: $^{206}Pb/^{204}Pb$ and $^{207}Pb/^{204}Pb$ ratios of basalts (solid symbols) sampled within the Norris-Mammoth corridor. Ratios of possible contaminants (open symbols) of varying age from the surrounding area. NHRL is the Northern Hemisphere Reference Line of Hart (1984). Data from Doe et al. (1982); Leeman et al. (1985); Wooden et al. (1988); Hildreth et al. (1991); and O'Brien et al. (1995).
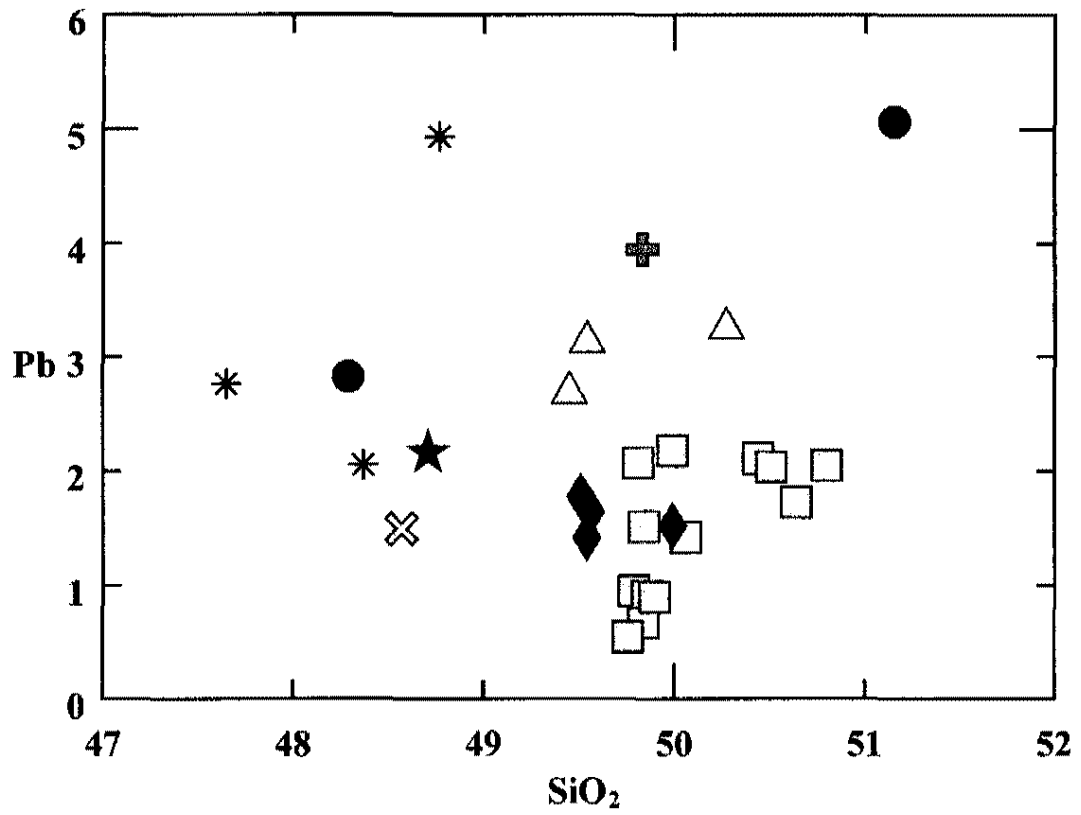
Figure 35: SiO$_2$ versus Pb of basalts to demonstrate the small and insignificant variation in silica with Pb content.
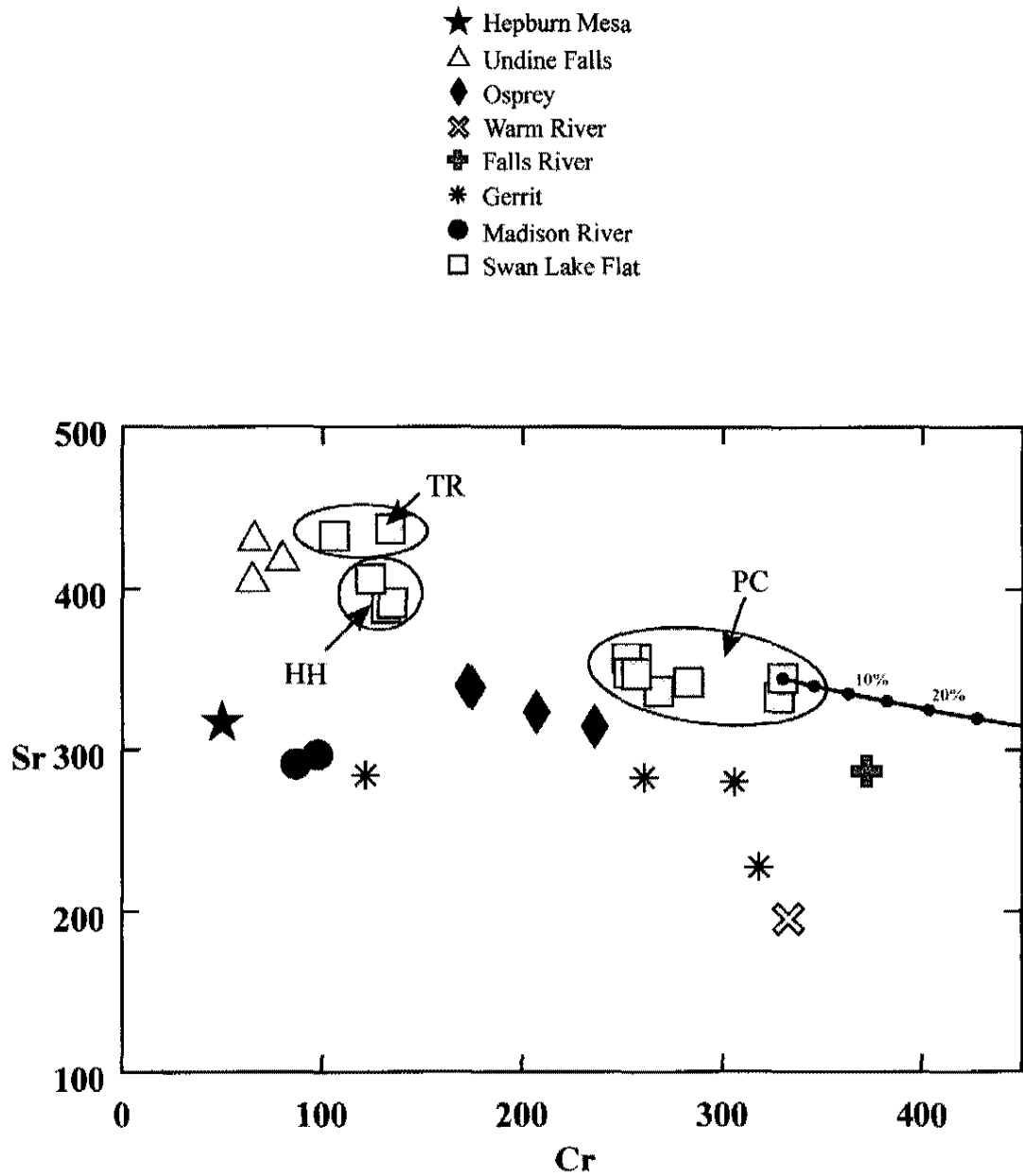
Figure 36: Fractional crystallization (FC) model of most geochemically and istotopically primitive basalt (YSLF-03-13) of Swan Lake Flat basalts. The lack of correlation between the model and evolved samples in the model suggests that FC could not produce remaining Swan Lake Flat basalts, or any other basalts in the volcanic field. PC=Panther Creek; HH=Horseshoe Hill; and TR=Tower Road.
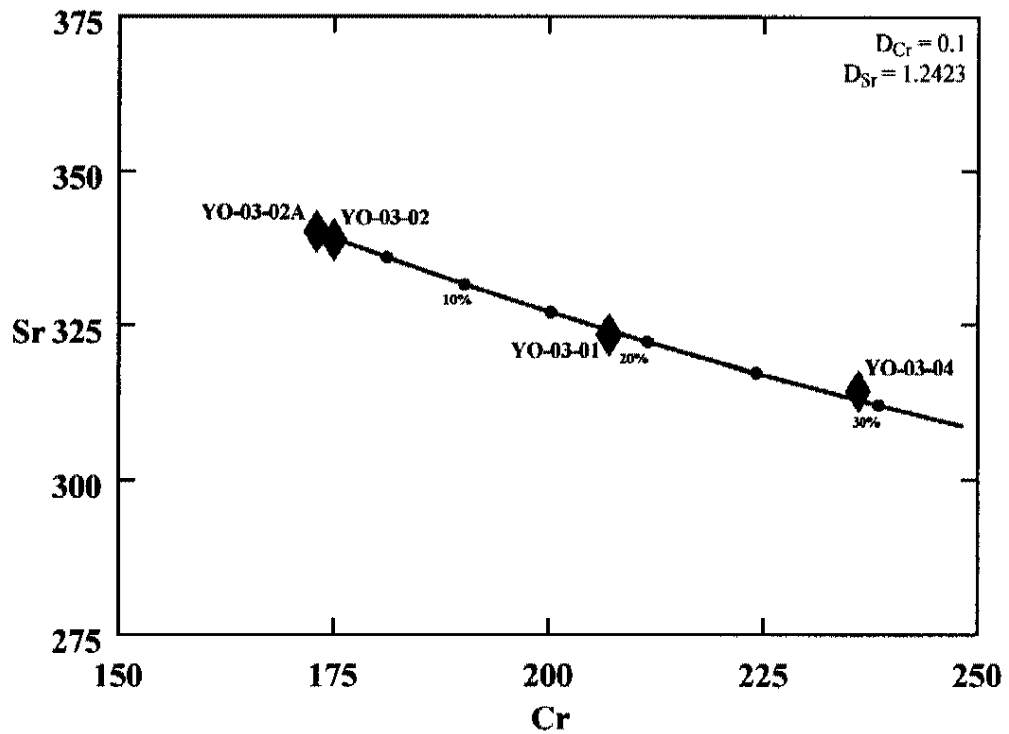
Figure 37A: Fractional crystallization model for Osprey basalt. Samples YO-03-02, YO-03-01, and YO-03-04 can be produced from YO-03-02A by 2%, 18%, and 29% fractionation, respectively, of 69% plagioclase and 31% olivine.
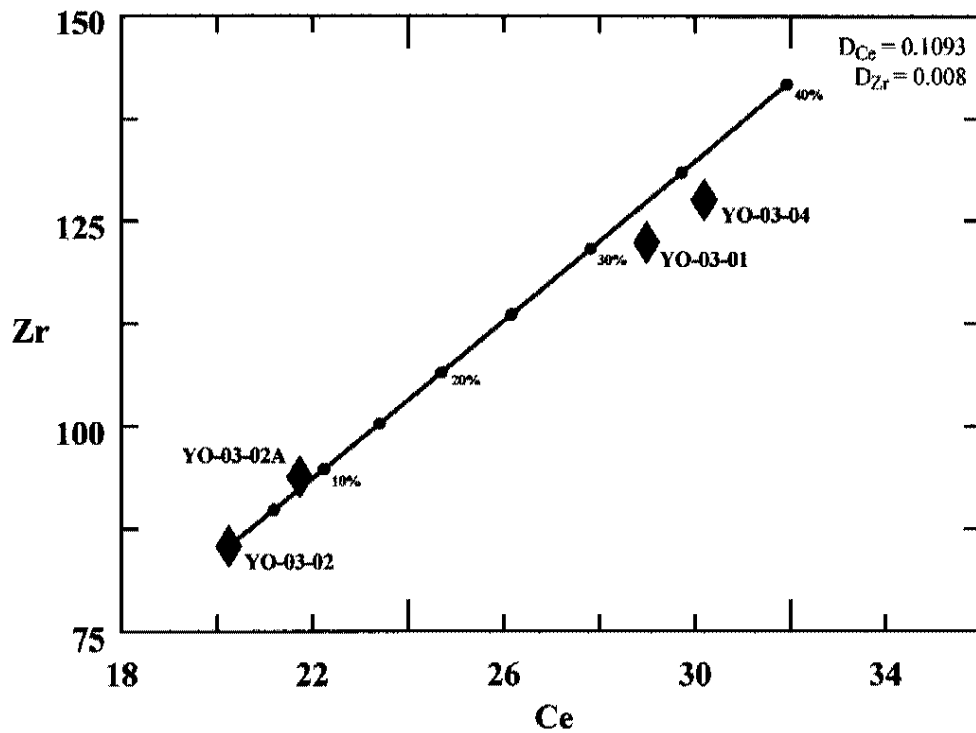
Figure 37B: Fractional crystallization model for Osprey basalt flows. Samples YO-03-02A, YO-03-01, and YO-03-04 can be produced from YO-03-02 by 8%, 32%, and 35% fractionation, respectively, of 78% plagioclase and 22% olivine.
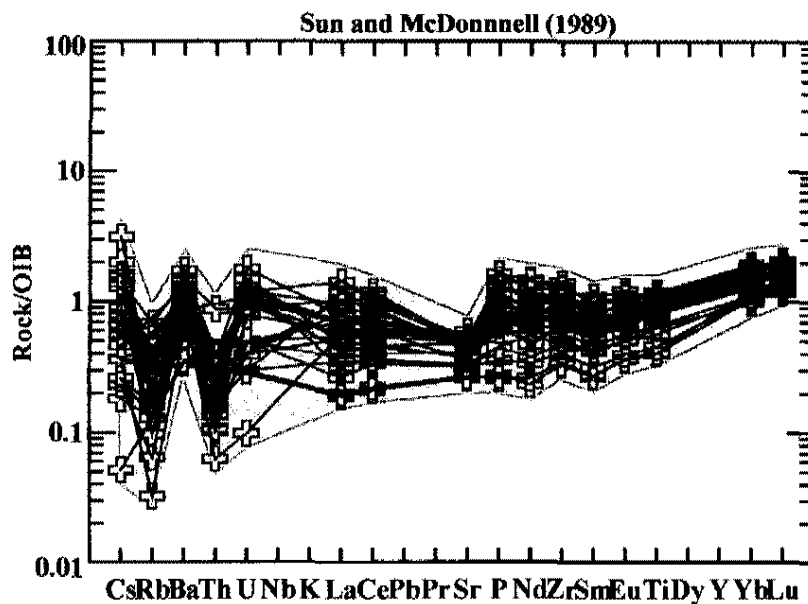
Figure 39A: Compilation of eastern Snake River Plain basalts (⊕) from White et al. (2002) and Hughes et al. (2004) to produce a Snake River Plain basalt field (shaded area).

Sun and McDonnnell (1989)
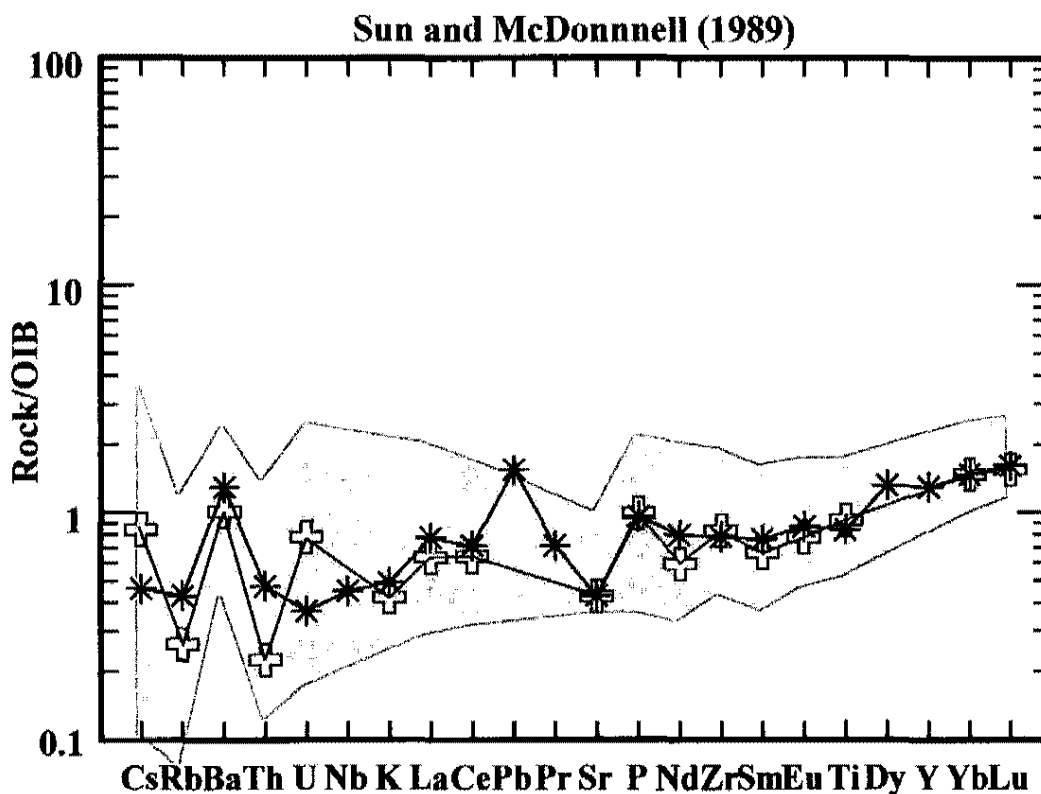
Figure 39B: The youngest flow of Gerrit basalt (HFGE-03-04) (✳) is similar to an average Snake River Plain basalt composition (⊕) and falls within the Sanke RIver Plain basalt field (White et al., 2002; Hughes, et al., 2004).

Sun and McDonnell (1989)
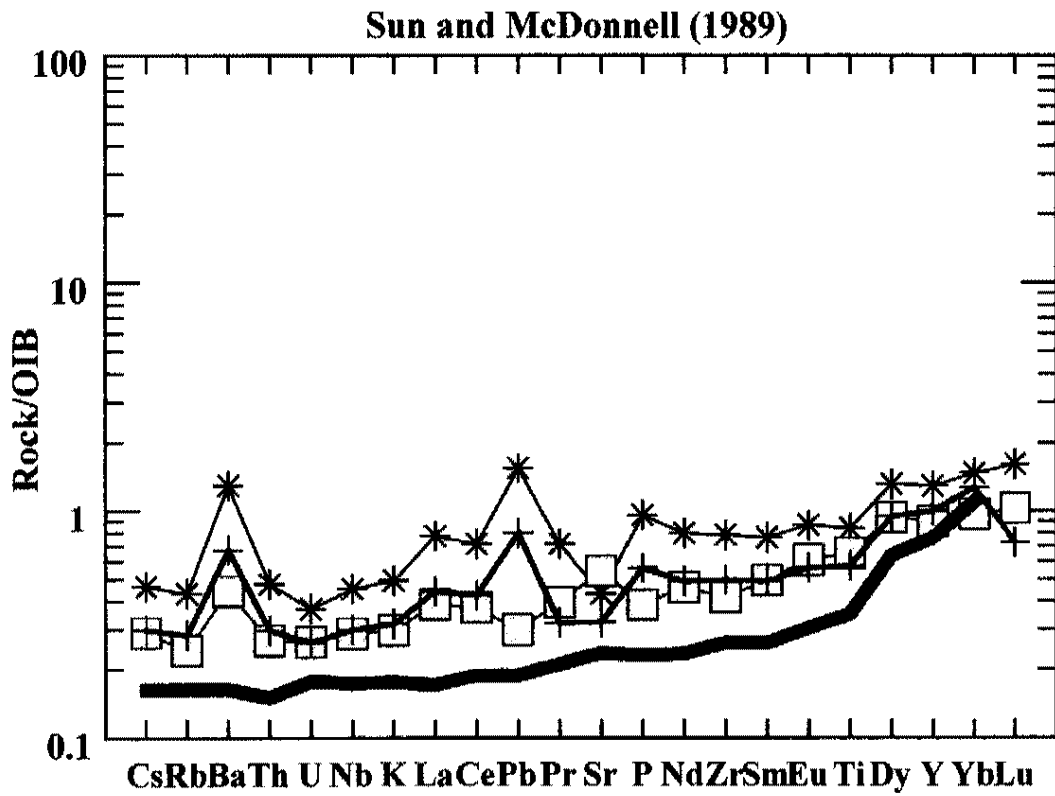
Figure 40: A mixing model (+) of 55% EMORB (━) and 45% Gerrit basalt (HFGE-03-04) (✳) can produce a composition remarkably similar to the Sheepeaters' Cliff flow of Swan Lake Flat basalt (YSLF-03-01) (☐).

CHAPTER 7

DISCUSSION

Implications for the "Deep Plume" model

Traditionally, the "hotspot" mantle plume hypothesis has been applied to the Yellowstone

Plateau volcanic field to explain the path of rhyolite and basaltic volcanism that trends to the

southwest to merge with the eastern Snake River Plain. Initially, the hotspot model was

developed by Wilson (1963) to explain the large volumes of basaltic lava erupting from the

Hawaiian volcanic chain. Hotspots are interpreted as large-scale thermal plumes derived

from the core-mantle boundary (Wilson, 1963).

Hotspots provide localized sources of exceptional heat energy that may sustain volcanism for

long periods of geologic time. Over time, these mantle plumes create a time-transgressive

linear chain of volcanism at the earth's surface (i.e. the Hawaiian-Emperor seamount chain).

Thus, the "hotspot" hypothesis was applied to the eastern Snake River Plain, and the

Yellowstone Plateau volcanic field, to explain the trend of rhyolitic volcanic centers

becoming younger to the northeast.

The northwest trending, backward-propagating "hotspot" track of the Newberry melting

anomaly and recent seismic tomography has challenged the idea of a deep-seated mantle

plume (or hotspot) beneath the Yellowstone Plateau volcanic field (Humphreys et al., 2000;

Christiansen et al., 2002). The Newberry melting anomaly is a bimodal basalt-rhyolite

system in central Oregon that has the same rate of propagation as the Snake River Plain-Yellowstone anomaly.

Christiansen (2002) arguments against the application of deep-seated mantle plume model to the Yellowstone Plateau volcanic field are as follows:

1. The deep mantle model does not explain the coeval volcanism along the eastern and western branches of the Snake River Plain.

2. The Yellowstone "melting anomaly" seems to have developed at the same time as the Newberry melting anomaly in southeast Oregon. The symmetry and rate of propagation suggests a link between the two systems.

3. The Basin and Range tectonic province south of the Yellowstone and Newberry areas has undergone large amounts of extension, whereas, the areas to the north have undergone significantly less extension.

4. The melting anomaly began to propagate at the western edge of the Archean continental crust of Wyoming (Reed, 1993). Eaton et al. (1975) and Mabey et al. (1978) show a regional aeromagnetic anomaly along the axis of the eastern Snake River Plain that continues southwestward into Nevada and northeastward across Montana and into Canada. This anomaly cuts across Laramide structures in a region practically undeformed during the Cenozoic but parallels the principal Precambrian structural trend.

Seismic tomography models generated by Humphreys et al. (2000), Dueker et al. (2001), and Christiansen (2002) suggest the possibility that the "hotspot" beneath the Yellowstone Plateau is rootless and may only extend 300 km into the mantle. Most recently, Smith (2004) proposed a mantle plume that projected NW into the mantle. Smith could not image

this thermal feature any deeper than the 660-km discontinuity. He suggested that a mantle plume does exist, but is primarily an upper mantle feature and does not extend to the core-mantle boundary. If these models are correct, then melting may be attributed to a shallow mantle source rather than a deeper, asthenospheric source, as the original "hotspot" hypothesis suggests.

If these recent seismic tomography images are accurate, and the Yellowstone Plateau volcanic field basalts do record the nature of their mantle source (as indicated by this thesis), this source would be in the upper mantle. The mixing model presented in Chapter 6, utilized the upper mantle, EMORB composition of Sun and McDonnell (1989) and the trace element composition of Gerrit basalt to produce Swan Lake Flat basalt. This model provides additional geochemical evidence that a shallow mantle thermal anomaly (EMORB composition) may be responsible for the basalt production in the Yellowstone Plateau volcanic field.

Relationship of the Snake River Plain to the

Norris-Mammoth corridor and source of basalts

Yellowstone Plateau volcanic field basalts are slightly depleted in LIL, HFSE, and in LREE elements relative to OIB (See Figure 19). The eastern Snake River Plain basalts are also depleted in LIL elements and HFSE compared to other OIB basalts but are not as enriched in LREE and HREE as are the Yellowstone Plateau volcanic field basalts. Basalts in the Yellowstone Plateau and Snake River Plain are enriched in Ba compared to OIB (See Figure 20). Fitton et al. (1991) also noted this Ba enrichment within the Snake River Plain and suggested that high Ba is typical of many late Cenozoic Cordilleran basalts.

A trend of incompatible element depletion compared to OIB, as well as lower ε_{Nd}, occurs from west to east, from the Henry's Fork area to the Norris-Mammoth corridor. Starting with Gerrit basalt in the west followed by Madison River, the Swan Lake Flat and Osprey basalts to the east, the LIL, HFSE, and LREE become more depleted relative to OIB and become chemically more like EMORB (Figure 40).

Although the Snake River Plain and Yellowstone Plateau basalts are similar to EMORB (and OIB) basalts in trace element composition, their Sr and Nd isotopic ratios are not. For example, the Gerrit basalt, although more comparable to OIB, has higher $^{87}Sr/^{86}Sr$ than the basalts of the Norris-Mammoth corridor. Lum et al. (1989) explained the elevated Sr isotopic ratios in the SRP (which are similar to the Gerrit basalt) by contamination with Archean lithosphere that had experienced an early event of high Rb/Sr enrichment and subsequent rapid growth in $^{87}Sr/^{86}Sr$. This was followed by an episode of partial melting that substantially reduced the concentrations of most of the incompatible elements. Ultimately, both Yellowstone Plateau and Snake River Plain basalts have enriched Sr isotopic ratios and depleted Nd ratios compared to OIB. The basalts of the Norris-Mammoth corridor may also have been contaminated in the lithosphere as they rose from their mantle source, as revealed by their enriched Sr and depleted Nd isotopic ratios.

The future of volcanism in the Yellowstone

Plateau volcanic field

To determine if the most recent basaltic volcanism within the Norris-Mammoth corridor represents the initiation of a new caldera cycle, or the termination of the Yellowstone Caldera phase, isotopic values from Doe et al. (1982), Hildreth et al. (1991), and Smith (1997) of recent basalts (<2.2 Ma) were plotted against time and suggest a relationship of ε_{Nd} and

$^{87}Sr/^{86}Sr$ to periods of caldera formation (See Figure 41). For example, $^{87}Sr/^{86}Sr$ changed from 0.707 to 0.703 and ε_{Nd} from −7 to 0.1 at the inception of the first caldera cycle (2.1 Ma). This trend suggests injection of asthenospheric basalt into the crust at about the same time as caldera formation. Injection of basalt in the lithosphere may trigger partial melting of the crust that will ultimately lead to generation of large volumes of rhyolitic magma and caldera formation.

The isotopic signatures of the post-Yellowstone Caldera basalts (Osprey, Swan Lake Flat, Madison River, and Undine Falls) have both high and low values of $^{87}Sr/^{86}Sr$ and ε_{Nd}. Undine Falls basalt erupted after the eruption of the Lava Creek tuff that formed the Yellowstone Caldera and has an ε_{Nd} of −8.4 (lower flow) and −3.2 (upper flow) and a $^{87}Sr/^{86}Sr$ of 0.7059 (lower flow) and 0.7052 (upper flow). Madison River basalt has low ε_{Nd} (-5.5) and high $^{87}Sr/^{86}Sr$ (0.7065). Three vents of Swan Lake Flat basalt have varying ε_{Nd} and $^{87}Sr/^{86}Sr$. The Tower Road shield and Horseshoe Hill vents have ε_{Nd} −2.3 and −2.5 and $^{87}Sr/^{86}Sr$ of 0.7056 and 0.7060. The Panther Creek vent has the highest ε_{Nd} (0.20) in the corridor and $^{87}Sr/^{86}Sr$ of 0.7053. Osprey basalt has an ε_{Nd} of 0.14 and $^{87}Sr/^{86}Sr$ of 0.7054.

When the new dates, and the dates of Obradovich (1992) for post-Yellowstone caldera basalts, are plotted against Nd and Sr isotopes, there is a general trend of increasing ε_{Nd} with decreasing time. This trend suggests that the basalts of the Norris-Mammoth corridor may be recording a new influx asthenospheric mantle. The isotopic ratios of the Gerrit basalts are an exception. These basalts may: (1) signify the termination of Henry's Fork caldera cycle or (2) represent the transition of the Snake River Plain with the Yellowstone Plateau volcanic field. Ultimately, these EMORB-like basaltic partial melts are injected into the overlying

lithosphere, causing partial melting of the crust and the generation of rhyolitic magma, along

with the initiation of a new caldera cycle within the Yellowstone Plateau volcanic field.
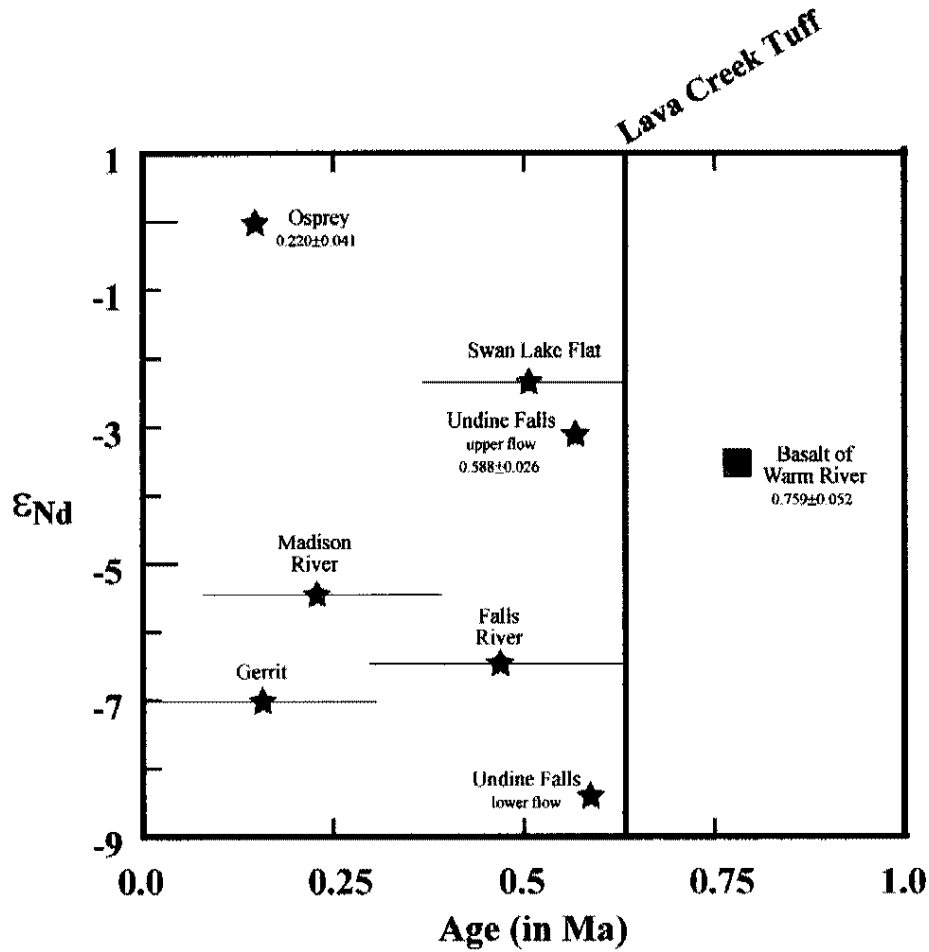
Figure 41: Epsilon Nd plotted against time. Red vertical line represents age of the Lava Creek ash-flow tuff. K/Ar ages of basalts shown, if known. Otherwise ages of basalts were constrained with K/Ar ages of comparative rhyolites; shown as black error bar through basalt symbol. Data from Doe et al. (1982) and Hildreth et al. (1991).

uncertainty

Correlative ?
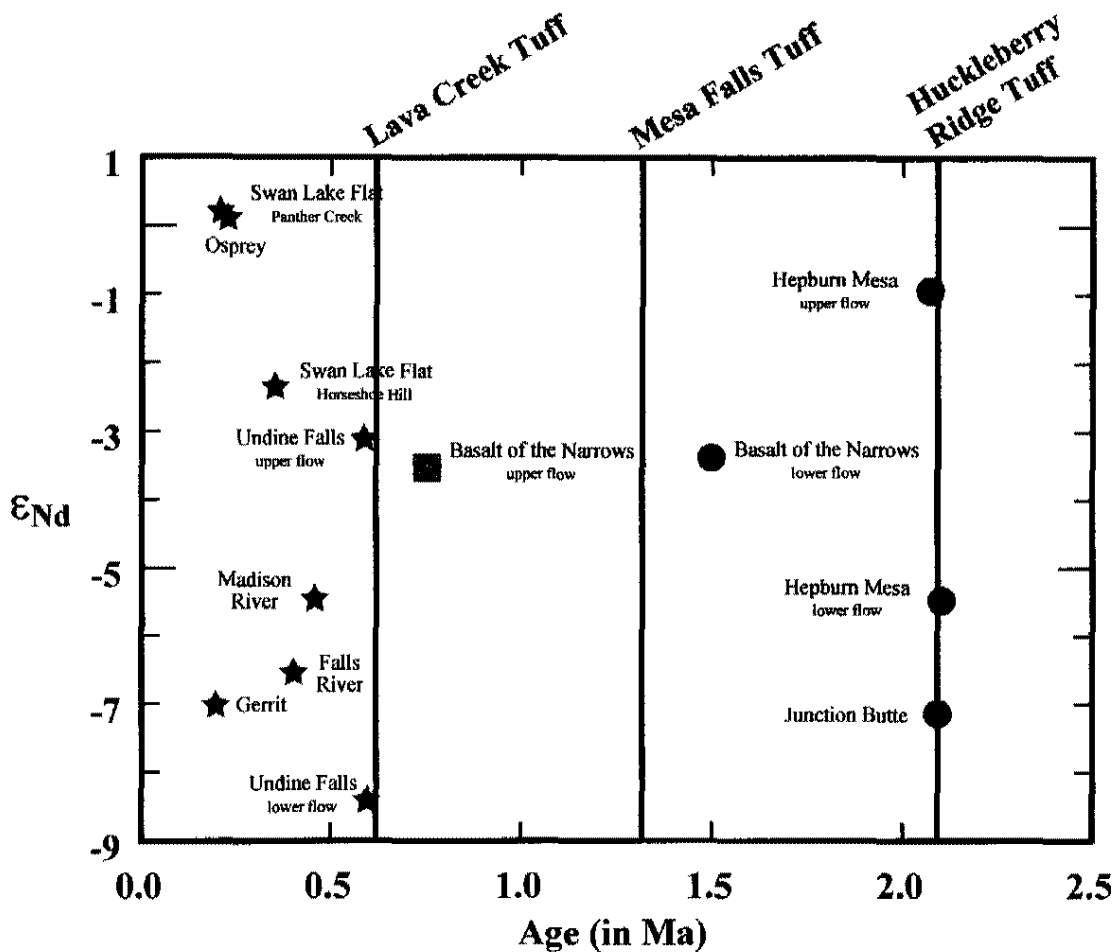
Figure 42. A plot of epsilon Nd values versus time in millions of years. This plot demonstrates that the basalts may incorporate a greater influx of a mantle-derived component at the start of a new caldera cycle. This larger contribution of mantle basalt may also represent the iniation of a new Yellowstone Plateau volcanic field caldera cycle.
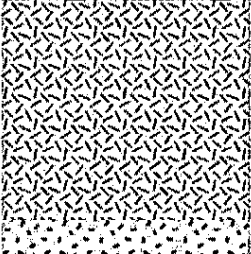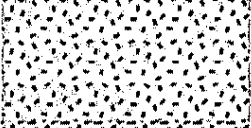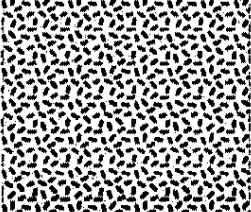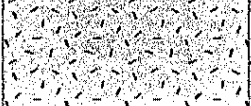
Age (in Ma)[1,2,3]	Rock Unit Name	Rock Unit Type	ε_{Nd} value of basaltic units
0.106	Obsidian Cliff rhyolite flow (Obsidian Creek member)		
0.174	Panther Creek cinder cone (Swan Lake Flat basalt)		-0.18 to 0.20
0.301	Gardner River mixed lavas (basalt and rhyolite)		
0.590	Tower Road shield (Swan Lake Flat basalt)		-2.4
	Cougar Creek rhyolite done (Roaring Mountain member)		
0.530	Madison River shield (Madison River basalt)		-5.5
	Riverside flow (Roaring Mountain member)		
0.588	Undine Falls flow (Undine Falls basalt)		-8.4 to -3.2

Figure 43: Stratigraphic section showing depletion in epsilon Nd in the NMC basalts with time. This depletion may be due to an increase of basalt injections into the crust. The ages of the rhyolite and mixed lava units also provide chronostratigraphic constraints on the ages of the basaltic units.

[1] ^{40}Ar/^{39}Ar dates completed as part of this Master's thesis.

[2] ^{40}Ar/^{39}Ar dates completed by Nicole Nastanski and Terry Spell as part of Nastanski's Master's thesis.

[3] K/Ar dates from Obradovich (1992).

CHAPTER 8

SUMMARY AND CONCLUSIONS

The basalts of the Norris-Mammoth corridor within the Yellowstone Plateau volcanic field have an erupted volume of ~94 km^3, but this estimate is conservative. The surface area of the erupted units experienced numerous glacial episodes during the Pleistocene. Basalt in the Yellowstone Plateau volcanic field is minor in volume compared to felsic rock types. The tholeiitic eruptive products predominantly formed small Hawaiian-style shield volcanoes that may terminate with a Strombolian phase in the summit crater. A newly identified volcanic vent, called the Panther Creek vent, within the Swan Lake Flat basalt stratigraphic unit, was primarily Strombolian in its eruption style. This vent is the first cinder cone recognized in Yellowstone National Park.

The oldest post-Yellowstone caldera basaltic unit in the Norris-Mammoth corridor is the Undine Falls basalt (588 ka) while the youngest is the Swan Lake Flat basalt that erupted from the Panther Creek volcano (174 ka). Basalt units within the Norris-Mammoth corridor, and the Yellowstone Plateau volcanic field, can be differentiated by isotopes and trace element geochemistry. Magma mixing, fractional crystallization, and/or assimilation/fractional crystallization models cannot generate one basaltic unit from another. The simplest model to explain source of the youngest basalt unit (Swan Lake Flat basalt that erupted from the Panther Creek vent) in the Norris-Mammoth

corridor is one of "source mixing." Partial melting produced EMORB-like basalt in the upper mantle. This basalt was contaminated within the lithospheric mantle by fractionated basalts from previous caldera cycles. This model is best illustrated with a simple mixing model between the youngest Gerrit basalt and an EMORB-like source. Also, there was some contamination with old (Archean) lithosphere.

The new, more precise $^{40}Ar/^{36}Ar$ ages for post-Yellowstone caldera basalts, along with Nd and Sr isotopes show a general Sr depletion and Nd enrichment with decreasing age of Norris-Mammoth corridor basalts. This suggests that the basalts within the Norris-Mammoth corridor may be recording a new influx asthenosphere-derived partial melts into he overlying lithosphere. Pooling of multiple basaltic partial melts in the lithosphere could be melting surrounding crust, generating rhyolitic magma that may coalesce to form a batholith-sized magma chamber and the initiation of a new caldera cycle.

APPENDIX A

PETROGRAPHY

All basalts within the Yellowstone Plateau volcanic field are tholeiites with sparse to abundant phenocrysts of plagioclase and olivine. YPVF basalts are hypersthene and olivine-normative tholeiites. They differ from basalts of the eastern Snake River Plain, which are quartz-normative basalts.

For this study, the unit names suggested by Christiansen (1974) and Christiansen and Blank (1974a; 1974b; 1975a; 1975b) are used to discriminate between basalt flows of the YPVF. Classification into local trends was determined by geochemistry in Chapter 4.

Hepburn Mesa basalt

Hepburn Mesa is porphyritic basalt with 10% phenocrysts of plagioclase (50%) and olivine (50%). The subhedral plagioclase (1.0 to 4.0 mm) crystals are sieved, slightly zoned, and somewhat rounded. Some of the euhedral olivine (0.5 to 2.0 mm) are fractured while others show at least one good crystal face. Some of the plagioclase and olivine phenocrysts occur in crystal "clots," which may be portions of mechanically broken crystal cumulates. Subhedral olivine and euhedral plagioclase are visible in the matrix. Amorphous iron oxide also exists in the matrix.

Gerrit Basalt

The Gerrit basalt flows are medium-gray to black and all exhibit a diabasic texture (Hamilton, 1965). The vesicle content ranges from 5 to 20% of the total volume of the rock. Some diktytaxitic vesicles are 0.5 to 2.0 cm in diameter and may be partially filled with white to tan zeolites.

These porphyritic basalts contain abundant plagioclase (61-71%) and olivine (29-39%). There are two types of plagioclase phenocrysts. The first and most abundant (~98%) are euhedral but fractured. These are 1.5 to 3.0 mm in length. Also, these plagioclase laths are intersertial with respect to the groundmass and show cloudy albite twinning (due to the presence of clay from secondary alteration). The second type of plagioclase is rare (~1%). These anhedral crystals may be up to 3.0 mm in length, have heavily sieved cores and are zoned. The anhedral olivine crystals are small (0.5 to 1.5 mm) and are highly fractured. Crystals within the groundmass are absent and the groundmass primarily consists of pale to dark brown amorphous iron oxide.

Basalt of Warm River and Shotgun Valley

The Warm River and Shotgun Valley basalt flows are medium-gray and holocrystalline. Vesicles exhibit a diktytaxitic texture and are 0.5 to 3.0 cm in diameter. The vesicle content ranges from 2 to 5% of the total volume of the rock. Warm River and Shotgun Valley basalts are phenocryst rich (80% of rock) and contain phenocrysts of plagioclase (50-60%) and olivine (40-50%). The 0.25-0.75 mm plagioclase laths are euhedral, although slightly fractured. Also, the plagioclase laths show cloudy albite twinning due to presence of secondary clay alteration. There are at least two generations of olivine. The first (~25%) is

larger (up to 0.75 mm), subhedral, and is predominantly fractured. The second, and dominant (~75%), olivine phase appear as small (0.1 to 0.25 mm) anhedral to subhedral crystals that appear to have grown after the plagioclase laths crystallized. The plagioclase and smaller olivine phenocrysts within the groundmass exhibit an "ophimottled" texture (MacKenzie et al., 1982). This texture is characterized by plagioclase laths that are intergrown in optically continuous olivine crystals. The groundmass also consists of pale to dark brown amorphous iron oxide.

Falls River basalt

The Falls River basalt flows are medium gray and holocrystalline. Vesicles are diktytaxitic, spherical, and are 0.5 to 3.0 cm in diameter. The vesicle content ranges from 2 to 5% of the total volume of the rock. The Falls River basalt is porphyritic (<5% phenocrysts) with 80% subophitic phenocrysts of intergrown plagioclase (46-61%) and olivine (23-39%). The 0.25-0.5 mm plagioclase laths are euhedral, although slightly fractured. Also, the plagioclase laths show cloudy albite due to secondary clay alteration. There are at least two sizes of olivine. The larger phase (~25%) is 0.75 to 1.5 mm in diameter, subhedral, and is fractured. Also this larger olivine phase contains oxides within their crystalline structure. The second, and dominant (~75%), olivine phase appears as small (0.1 to 0.25 mm) crystals in the matrix. The groundmass consists mainly of pale to dark brown amorphous iron oxide.

Madison River basalt

Madison River basalt is porphyritic, but contains fewer phenocrysts than the basalts described previously. This basalt contains 5 to 15% phenocrysts of plagioclase (65%) and olivine (35%). The plagioclase phenocrysts are 1.0-3.0 mm in length and are present as

individual crystals and as crystal "clots". The individual crystals are subhedral to euhedral and may be zoned and/or sieved. The plagioclase is not altered; there is have clear albite twinning and the crystals are not sieved. The subhedral olivine crystals are 0.25 to 1.0 mm in diameter and are fractured. Slight alteration to iddingsite occurs along fractures. Skeletal olivine is also present. Iron oxide crystals and plagioclase, along with microlites of olivine, are found within the matrix.

Undine Falls basalt

The Undine Falls basalt is similar to the Madison River basalts because they porphyritic with few phenocrysts. This basalt contains 2 to 5% phenocrysts of plagioclase (68%) and olivine (32%). The plagioclase phenocrysts are 1.0-4.0 mm in size, subhedral to euhedral and may be zoned and/or sieved. Some plagioclase crystals are no longer zoned and their crystal forms are partially replaced by minerals that are present in the matrix. The subhedral olivine crystals are 0.25 to 0.5 mm in diameter and are fractured. Alteration to iddingsite occurs along fractures and around the rims. The plagioclase and smaller olivine phenocrysts within the groundmass exhibit an "ophimottled" texture (MacKenzie et al., 1982). Abundant iron oxides (~15%) are also found within the matrix.

Swan Lake Flat basalt

Horseshoe Hill vents

The basalts associated with these vents are porphyritic and contain (50%) phenocrysts of plagioclase (62-67%) and olivine (33-38%). The plagioclase crystals occur in two phases. The dominant phase (~90%) consists of 0.25 to 0.75 mm plagioclase laths that are fractured but have clear albite twinning. The second phase (~10%) consists of subhedral, 0.75-2.0 mm individual crystals that are rounded, zoned, and/or sieved. In hand specimen, the crystals of

this phase are labradorescent. Crystal "clots" are also present and appear to be broken portions of olivine and plagioclase cumulates. The euhedral olivine crystals are 0.5 to 0.75 mm in diameter and are fractured. Iron oxide crystals (~5%), olivine, and plagioclase occur in the matrix.

Tower Road Shield

The basalts of this shield volcano are porphyritic with (5%) phenocrysts of plagioclase (75%) and olivine (25%). The plagioclase phenocrysts are 1.0-2.5 mm, subhedral to euhedral, broken, somewhat rounded, and zoned. Some plagioclase crystals are fractured and filled with minerals that are present in the matrix. The euhedral olivine is 0.25 to 0.5 mm in size and fractured. Skeletal olivine is also present. Iron oxide crystals (~10%) and plagioclase, along with microlites of olivine, are found in the matrix.

Panther Creek vent

The basalts of this cinder cone volcano are porphyritic (5 to 15%) with phenocrysts of plagioclase (75%) and olivine (25%). There are two phases of plagioclase phenocrysts. The dominant plagioclase phase (~95%) is euhedral, 0.5-1.50 mm in size, and has clear albite twinning. Crystals of the major phase are sometimes associated with olivine crystals, hence this phase may originate from olivine and plagioclase clots. The minor plagioclase phase (~5%) consists of rounded and/or broken, sieved or partially resorbed crystals. Some of these crystals are fractured and filled with minerals that are present in the matrix. The euhedral olivine crystals are 0.1 to 0.5 mm in diameter and are fractured. Iron oxide crystals (~10%), olivine, and plagioclase are found in the matrix.

Osprey basalt

Osprey Falls basalt flows are medium to dark gray. Additionally, they are massive, slightly vesicular, and holocrystalline. The vesicles range in size from 0.5 to 4.0 cm and the content ranges from 2 to 5% of the total volume of the rock. The porphrytic Osprey basalt flows are similar to the Swan Lake Flat, Madison River, and Undine Falls basalts. This basalt contains 2 to 5% phenocrysts of plagioclase (32%) and olivine (68%). The plagioclase phenocrysts are 2.0-4.5 mm, subhedral to euhedral and are zoned and/or sieved. Some plagioclase crystals are fractured and filled with minerals that are present in the matrix. The subhedral olivine crystals are 0.25 to 0.5 mm in diameter and are fractured. Slight alteration to iddingsite occurs along fractures and rims. Skeletal olivine is also present. Iron oxide (~5%) and plagioclase, along with microlites of olivine, are found in the matrix. Pilotaxitic flow textures occur around the only example of a disaggregated plagioclase masses in the thin section.

APPENDIX B: GEOCHEMICAL DATA

Precision and Accuracy

XRF and ICP-MS values and analytical precision of USGS basalt standard (BCR-1) for oxides, trace elements, and isotopic ratios.

Oxide	High	Low	Variation	Analytical Precision (2α)
SiO_2	50.89	48.00	2.89	+0.36
TiO_2	2.393	1.346	1.05	+0.008
Al_2O_3	16.3	15.02	1.28	+0.22
FeO^*	14.62	10.03	4.59	+0.02
MnO	0.232	0.159	0.07	+0.002
MgO	8.99	6.23	2.76	+0.2
CaO	11.73	9.00	2.73	+0.02
Na_2O	3.08	2.28	0.80	+0.1
K_2O	1.03	0.28	0.75	+0.14
P_2O_5	0.869	0.17	0.70	+0.004

Trace Elements	High	Low	Variation	Analytical Precision (2α)
Ni	459	64	395	+2
Cr	318	65	253	+4
Rb	21	3	18	+1.34
Ba	535	127	408	+25.36
Nb	31.6	7.8	24	+1
Hf	7.022	2.147	4.875	+0.14
Ta	2.425	0.718	1.707	+0.04
La	42.135	8.320	33.815	+0.98
Ce	79.786	17.465	62.320	+1.24
Nd	43.498	10.776	32.722	+0.96
Eu	3.481	1.262	2.219	+0.08
Gd	10.968	3.929	7.039	+0.16
Tb	1.742	0.724	1.018	+0.02
Y	37.297	21.736	15.560	+0.58
Yb	4.415	1.729	2.685	+0.06
Lu	0.690	0.262	0.428	+0.02

Isotopic Ratio	High	Low	Variation	Analytical Precision
$^{87}Sr/^{86}Sr$	0.708755	0.705224	0.003531	+0.018
$^{143}Nd/^{144}Nd$	0.512648	0.512206	0.000443	+0.023
$^{206}Pb/^{204}Pb$	17.893310	16.625125	1.268185	+0.076
$^{207}Pb/^{204}Pb$	15.546363	15.373502	0.172861	+0.00002
$^{208}Pb/^{204}Pb$	38.538114	37.111206	1.426907	+0.00001

APPENDIX B: GEOCHEMICAL DATA

Precision and Accuracy

XRF and ICP-MS test of contamination of pure quartz caused by grinding bowl of tungsten carbide (WC) from Washington State University GeoAnalytical Labratory. Tungsten carbide bowl causes significant contamination of Nb and Ta. From Johnson et al. (1999).

Major elements (XRF)	Unnormalized results (weight %)
SiO_2	98.25
Al_2O_3	0.18
TiO_2	0.02
FeO*	0.01
MnO	0.01
CaO	0.02
MgO	0.00
K_2O	0.01
Na_2O	0.00
P_2O_5	0.0009
Total	98.48

Trace Elements (XRF)	(in ppm)
Ni	9
Cr	0
Sc	1
V	5
Ba	2
Rb	4
Sr	3
Zr	10
Y	1
Nb	0
Ga	0
Cu	5
Zn	1
Pb	1
La	0
Ce	13
Th	0

Trace Elements (ICP-MS)	(in ppm)
La	0.00
Ce	0.20
Pr	0.03
Nd	0.11
Sm	0.02
Eu	0.01
Gd	0.02
Tb	0.00
Dy	0.02
Ho	0.00
Er	0.01
Tm	0.00
Yb	0.01
Lu	0.00
Ba	3.16
Th	0.07
Nb	1.38
Yb	0.11
Hf	0.05
Ta	1.62
U	0.01
Pb	0.03
Rb	0.28
Cs	0.01

APPENDIX B: GEOCHEMICAL DATA

Precision and Accuracy (continued)

Accuracy of X-ray Fluorescence Sprectrometry (XRF) from Washington State University GeoAnalytical Labratory. U.S.G.S. standard BCR-1 (basalt) was used as a reference. From Johnson et al. (1999).

Major elements (wt %)	BCR-1 WSU1	BCR-1 WSU2	BCR-1 U.S.G.S.
SiO_2	55.54	55.63	55.22
Al_2O_3	13.76	13.80	13.92
TiO_2	2.29	2.27	2.266
FeO*	12.16	12.03	12.32
MnO	0.19	0.18	0.184
CaO	7.12	7.09	7.09
MgO	3.49	3.53	3.55
K_2O	1.75	1.75	1.72
Na_2O	3.34	3.36	3.35
P_2O_5	0.37	0.37	0.367
Total	100.00	100.00	100.00

Trace Elements (ppm)			
Ni	0	0	13
Cr	27	27	16
Sc	29	32	33
V	405	415	407
Ba	727	726	681
Rb	45	45	47
Sr	329	324	330
Zr	176	175	190
Y	36	34	38
Nb	13	12	14
Ga	21	25	22
Cu	16	9	19
Zn	128	125	130
Pb	12	13	14
La	32	2	25
Ce	62	45	54
Th	5	9	6

APPENDIX B: GEOCHEMICAL DATA

Precision and Accuracy (continued)

Determination of X-ray Fluorescence Sprectrometry (XRF) precision from Washington State University GeoAnalytical Labratory. Seven repeat analyses of reference bead (BCR-1) during a single XRF run over a three week period. From Johnson et al. (1999).

Major Element (wt %)	Published concentration (USGS)	Mean of 7 replicated analyses	Standard deviation	coefficient variable
SiO_2	55.22	55.16	0.03	0.0
Al_2O_3	13.92	13.62	0.02	0.1
TiO_2	2.266	2.286	0.009	0.4
FeO*	12.32	12.73	0.02	0.2
MnO	0.184	0.184	0.001	0.4
CaO	7.09	6.99	0.02	0.2
MgO	3.55	3.52	0.05	1.4
K_2O	1.72	1.74	0.00	0.2
Na_2O	3.35	3.38	0.05	1.3
P_2O_5	0.367	0.378	0.001	0.3
Total	100.00	99.99	-	-

Trace Elements (ppm)

Ni	13	0	0	0
Cr	16	28	1	5
Sc	33	26	2	7
V	407	401	7	2
Ba	681	745	11	1
Rb	47	46	0	1
Sr	330	326	0	0
Zr	190	176	1	1
Y	38	36	0	1
Nb	14	13	0.6	5
Ga	22	23	1	3
Cu	19	12	2	18
Zn	130	124	2	1
Pb	14	10	2	19
La	25	19	8	41
Ce	54	51	11	21
Th	6	8	1	20

APPENDIX B: GEOCHEMICAL DATA

Major and Trace Element Abundances

Major elements in wt %	**Basalt of Warm River** HFWS-03-01	**Falls River Basalt** HFFR-03-01	**Gerrit Basalt**			
			HFGE-03-01	HFGE-03-02	HFGE-03-03	HFGE-03-04
SiO_2	48.45	49.56	47.42	45.42	48.13	48.62
Al_2O_3	16.38	15.27	15.73	15.22	16.30	15.02
TiO_2	1.35	1.89	2.00	3.31	1.38	2.39
FeO*	10.19	11.26	11.60	14.62	10.75	12.12
MnO	0.18	0.18	0.19	0.23	0.18	0.19
CaO	11.73	9.59	10.74	9.78	10.85	9.79
MgO	8.71	8.40	8.49	6.81	8.99	7.75
K_2O	0.28	0.56	0.53	0.50	0.33	0.71
Na_2O	2.28	2.42	2.38	2.67	2.37	2.51
P_2O_5	0.20	0.33	0.43	0.87	0.22	0.59
Total	99.74	99.46	99.51	99.43	99.51	99.70
Mg #	*60.4*	*57.1*	*56.61*	*45.37*	*59.86*	*53.26*

Trace elements in ppm	HFWS-03-01	HFFR-03-01	HFGE-03-01	HFGE-03-02	HFGE-03-03	HFGE-03-04
Zr (XRF)	86	147	174	300	101	222
La (ICP-MS)	8.32	19.86	21.97	42.13	11.89	28.55
Ce (ICP-MS)	17.47	39.07	44.09	79.79	23.95	56.91
Pr (ICP-MS)	2.26	4.79	5.30	10.03	3.02	6.90
Nd (ICP-MS)	10.78	21.05	23.22	43.50	13.78	30.52
Sm (ICP-MS)	3.18	5.43	5.77	10.69	3.79	7.60
Eu (ICP-MS)	1.26	1.96	1.99	3.48	1.47	2.59
Gd (ICP-MS)	3.93	5.75	6.04	10.97	4.26	7.64
Tb (ICP-MS)	0.68	0.95	0.98	1.74	0.75	1.24
Dy (ICP-MS)	4.31	5.88	5.88	10.38	4.60	7.34
Ho (ICP-MS)	0.91	1.17	1.18	2.07	0.97	1.45
Er (ICP-MS)	2.44	3.10	3.13	5.38	2.59	3.79
Tm (ICP-MS)	0.35	0.43	0.44	0.74	0.38	0.52
Yb (ICP-MS)	2.15	2.63	2.68	4.41	2.27	3.17
Lu (ICP-MS)	0.33	0.41	0.42	0.69	0.36	0.48
Ba (ICP-MS)	136.91	352.19	383.22	552.48	194.71	442.51
Ba (XRF)	146	353	403	535	202	452
Th (ICP-MS)	0.67	1.35	0.77	1.55	0.70	1.90
Nb (XRF)	7.8	14.4	19.3	31.6	8.8	21.4
Y (XRF)	23	29	31	51	25	36
Hf (ICP-MS)	2.15	3.81	3.96	7.02	2.56	5.31
Ta (ICP-MS)	0.72	1.20	1.51	2.42	1.04	1.64
U (ICP-MS)	0.14	0.26	0.21	0.28	0.14	0.37
Pb (ICP-MS)	1.50	3.95	2.76	4.92	2.05	4.93
Rb (XRF)	5	10	7	5	3	13
Cs (ICP-MS)	0.08	0.12	0.17	0.04	0.05	0.18
Sr (XRF)	191	282	280	277	225	285
Sc (ICP-MS)	41.53	34.47	36.29	38.49	38.24	34.04
Cr (XRF)	333	372	306	122	318	261
Ni (XRF)	108	135	78	64	159	112

APPENDIX B: GEOCHEMICAL DATA

Major and Trace Element Abundances (continued)

Major elements in wt %	Madison River Basalt		Osprey Basalt			
	YMR-03-02	YMR-03-03	YO-03-01	YO-03-02	YO-03-02A	YO-03-04
SiO_2	50.89	48.00	49.14	49.31	49.70	49.43
Al_2O_3	15.29	15.40	15.36	15.82	15.75	15.47
TiO_2	1.98	2.37	1.99	1.52	1.65	1.95
FeO*	11.64	13.23	10.96	10.43	10.03	10.87
MnO	0.17	0.20	0.17	0.16	0.17	0.17
CaO	9.00	9.48	10.87	11.20	11.10	10.96
MgO	6.33	6.71	7.52	8.13	8.01	7.72
K_2O	1.03	0.62	0.37	0.35	0.38	0.36
Na_2O	2.90	3.08	2.61	2.45	2.45	2.55
P_2O_5	0.26	0.32	0.26	0.17	0.18	0.25
Total	99.49	99.41	99.25	99.54	99.42	99.73
Mg #	49.22	47.49	55.02	58.19	58.76	55.88

Trace elements in ppm	YMR-03-02	YMR-03-03	YO-03-01	YO-03-02	YO-03-02A	YO-03-04
Zr (XRF)	157	166	131	92	99	125
La (ICP-MS)	25.09	20.45	14.47	9.45	10.08	13.72
Ce (ICP-MS)	48.15	40.56	30.19	20.25	21.74	28.99
Pr (ICP-MS)	5.68	5.09	3.94	2.69	2.88	3.77
Nd (ICP-MS)	24.29	22.95	18.24	12.76	13.83	17.72
Sm (ICP-MS)	6.25	6.24	5.22	3.78	4.05	4.97
Eu (ICP-MS)	1.97	2.22	1.88	1.45	1.56	1.83
Gd (ICP-MS)	6.55	6.71	5.65	4.38	4.54	5.58
Tb (ICP-MS)	1.08	1.12	0.94	0.72	0.76	0.93
Dy (ICP-MS)	6.54	6.85	5.73	4.32	4.49	5.49
Ho (ICP-MS)	1.30	1.35	1.10	0.83	0.90	1.07
Er (ICP-MS)	3.32	3.52	2.83	2.14	2.25	2.79
Tm (ICP-MS)	0.47	0.50	0.38	0.29	0.31	0.38
Yb (ICP-MS)	2.83	2.95	2.27	1.73	1.81	2.19
Lu (ICP-MS)	0.42	0.45	0.34	0.26	0.27	0.33
Ba (ICP-MS)	343.12	280.90	177.15	135.88	133.45	146.80
Ba (XRF)	341	269	174	127	135	139
Th (ICP-MS)	4.17	1.79	1.15	0.77	0.80	1.07
Nb (XRF)	17.7	16.6	14.5	9.0	10.3	14.3
Y (XRF)	33	34	28	21	22	26
Hf (ICP-MS)	4.33	4.34	3.38	2.42	2.61	3.28
Ta (ICP-MS)	1.40	1.30	1.12	0.75	1.13	1.11
U (ICP-MS)	0.67	0.36	0.26	0.21	0.21	0.26
Pb (ICP-MS)	5.07	2.83	1.77	1.41	1.52	1.64
Rb (XRF)	21	11	4	5	5	4
Cs (ICP-MS)	0.23	0.15	0.07	0.15	0.09	0.06
Sr (XRF)	289	284	318	338	332	307
Sc (ICP-MS)	28.01	30.49	32.69	31.73	31.41	34.85
Cr (XRF)	98	87	207	175	173	236
Ni (XRF)	81	81	100	110	107	100

APPENDIX B: GEOCHEMICAL DATA

Major and Trace Element Abundances (continued)

Major elements in wt %	Undine Falls Basalt			Horseshoe Hill vent Swan Lake Flat Basalt		
	YU-03-01	YU-03-03	YU-03-04	YSLF-03-04	YSLF-03-05	YSLF-03-07
SiO_2	48.89	49.01	49.80	49.88	50.08	50.47
Al_2O_3	15.96	15.96	15.46	15.66	15.69	15.69
TiO_2	1.87	1.85	1.85	1.62	1.60	1.67
FeO^*	11.30	11.79	11.22	10.33	10.33	10.04
MnO	0.17	0.18	0.16	0.16	0.16	0.16
CaO	10.41	9.76	10.11	10.57	10.54	10.55
MgO	6.23	6.84	6.82	7.44	7.45	7.42
K_2O	0.73	0.60	0.61	0.44	0.47	0.47
Na_2O	2.83	2.87	2.79	2.59	2.63	2.68
P_2O_5	0.29	0.25	0.26	0.20	0.20	0.21
Total	98.69	99.10	99.07	98.89	99.15	99.36
Mg #	*49.56*	*50.85*	*51.99*	*56.21*	*56.24*	*56.88*

Trace elements in ppm	YU-03-01	YU-03-03	YU-03-04	YSLF-03-04	YSLF-03-05	YSLF-03-07
Zr (XRF)	144	130	135	111	109	109
La (ICP-MS)	19.98	16.18	17.59	13.55	13.22	13.06
Ce (ICP-MS)	40.50	33.08	35.22	27.07	26.73	26.67
Pr (ICP-MS)	4.96	4.19	4.36	3.43	3.43	3.41
Nd (ICP-MS)	22.13	18.94	19.39	15.94	15.67	15.80
Sm (ICP-MS)	5.58	5.08	5.17	4.41	4.41	4.40
Eu (ICP-MS)	1.96	1.82	1.88	1.60	1.56	1.64
Gd (ICP-MS)	5.71	5.34	5.51	4.81	4.69	4.88
Tb (ICP-MS)	0.93	0.87	0.89	0.79	0.78	0.80
Dy (ICP-MS)	5.51	5.27	5.31	4.75	4.73	4.85
Ho (ICP-MS)	1.08	1.03	1.04	0.92	0.90	0.92
Er (ICP-MS)	2.82	2.62	2.68	2.35	2.28	2.31
Tm (ICP-MS)	0.39	0.37	0.37	0.32	0.31	0.33
Yb (ICP-MS)	2.26	2.18	2.10	1.86	1.84	1.90
Lu (ICP-MS)	0.35	0.34	0.32	0.28	0.29	0.29
Ba (XRF)	302	250	324	207	189	230
Ba (ICP-MS)	300.35	248.84	322.46	205.23	205.03	244.42
Th (ICP-MS)	1.11	1.35	1.45	1.41	1.37	1.13
Nb (XRF)	13.6	13.9	14.5	11.2	10.5	11.0
Y (XRF)	27	26	26	23	22	22
Hf (ICP-MS)	3.72	3.40	3.51	2.97	2.88	2.95
Ta (ICP-MS)	1.17	1.28	1.22	0.96	0.93	0.93
U (ICP-MS)	0.28	0.32	0.29	0.31	0.31	0.28
Pb (ICP-MS)	3.13	2.68	3.25	2.11	2.04	2.05
Rb (XRF)	10	10	7	8	9	6
Cs (ICP-MS)	0.27	0.15	0.36	0.15	0.17	0.12
Sr (XRF)	420	398	416	374	373	378
Sc (ICP-MS)	29.00	28.89	31.37	28.83	28.49	30.08
Cr (XRF)	66	65	80	132	135	124
Ni (XRF)	80	81	89	94	93	91

APPENDIX B: GEOCHEMICAL DATA

Major and Trace Element Abundances (continued)

Major elements in wt %	Tower Road shield Swan Lake Flat Basalt		Hepburn Mesa Basalt	Panther Creek cinder cone Swan Lake Flat Basalt		
	YSLF-03-02	YSLF-03-07	YHM-03-01	YSLF-03-01	YSLF-03-09	YSLF-03-10
SiO_2	49.52	50.47	48.40	49.46	50.08	50.47
Al_2O_3	16.10	15.69	15.97	15.26	15.69	15.69
TiO_2	1.69	1.67	1.97	1.85	1.60	1.67
FeO*	10.90	10.04	11.21	10.86	10.33	10.04
MnO	0.17	0.16	0.18	0.17	0.16	0.16
CaO	10.07	10.55	10.87	11.04	10.54	10.55
MgO	7.14	7.42	7.44	7.51	7.45	7.42
K_2O	0.65	0.47	0.50	0.43	0.47	0.47
Na_2O	2.95	2.68	2.59	2.52	2.63	2.68
P_2O_5	0.24	0.21	0.23	0.24	0.20	0.21
Total	99.42	99.36	99.37	99.34	99.15	99.36
Mg #	*53.88*	*56.88*	*54.19*	*55.21*	*55.39*	*55.58*

Trace elements in ppm	YSLF-03-02	YSLF-03-07	YHM-03-01	YSLF-03-01	YSLF-03-09	YSLF-03-10
Zr (XRF)	111	109	133	119	118	121
La (ICP-MS)	15.48	13.06	15.67	14.30	14.05	16.07
Ce (ICP-MS)	30.37	26.67	32.23	29.91	29.20	32.57
Pr (ICP-MS)	3.76	3.41	4.09	3.82	3.72	4.09
Nd (ICP-MS)	16.81	15.80	18.65	17.63	17.11	18.56
Sm (ICP-MS)	4.47	4.40	5.05	4.91	4.84	5.17
Eu (ICP-MS)	1.64	1.64	1.79	1.81	1.76	1.72
Gd (ICP-MS)	4.83	4.88	5.46	5.30	5.32	5.49
Tb (ICP-MS)	0.79	0.80	0.91	0.88	0.86	0.90
Dy (ICP-MS)	4.73	4.85	5.48	5.23	5.24	5.46
Ho (ICP-MS)	0.95	0.92	1.09	0.99	1.01	1.05
Er (ICP-MS)	2.35	2.31	2.84	2.54	2.53	2.72
Tm (ICP-MS)	0.32	0.33	0.39	0.36	0.35	0.37
Yb (ICP-MS)	1.89	1.90	2.34	2.08	2.02	2.13
Lu (ICP-MS)	0.30	0.29	0.36	0.31	0.30	0.33
Ba (ICP-MS)	325.51	244.42	235.51	167.35	163.83	175.92
Ba (XRF)	319	230	214	155	151	170
Th (ICP-MS)	1.12	1.13	1.16	1.07	1.07	1.74
Nb (XRF)	13.1	11.0	14.8	14.1	14.1	14.1
Y (XRF)	22	22	27	26	26	26
Hf (ICP-MS)	2.94	2.95	3.57	3.16	3.08	3.29
Ta (ICP-MS)	1.12	0.93	1.27	1.16	1.09	1.22
U (ICP-MS)	0.26	0.28	0.31	0.27	0.27	0.39
Pb (ICP-MS)	2.07	2.05	2.16	0.95	0.90	1.72
Rb (XRF)	11	6	8	7	8	13
Cs (ICP-MS)	0.14	0.12	0.07	0.11	0.10	0.19
Sr (XRF)	419	378	306	339	341	333
Sc (ICP-MS)	28.25	30.08	35.81	30.55	32.08	30.12
Cr (XRF)	106	124	115	257	252	253
Ni (XRF)	87	91	89	87	87	83

APPENDIX B: GEOCHEMICAL DATA

Major and Trace Element Abundances (continued)

Major elements in wt %	YSLF-03-11	YSLF-03-12	Panther Creek cinder cone Swan Lake Flat Basalt YSLF-03-13	YSLF-03-14	YSLF-03-16
SiO_2	49.50	49.83	49.40	49.94	49.58
Al_2O_3	15.14	15.26	15.04	15.40	15.23
TiO_2	1.80	1.82	1.73	1.77	1.84
FeO*	10.90	10.84	10.73	10.20	10.83
MnO	0.17	0.17	0.17	0.17	0.17
CaO	10.99	11.00	11.21	11.25	10.97
MgO	7.64	7.76	7.90	7.95	7.61
K_2O	0.43	0.42	0.41	0.38	0.43
Na_2O	2.52	2.54	2.46	2.48	2.58
P_2O_5	0.24	0.23	0.24	0.22	0.24
Total	99.32	99.87	99.28	99.76	99.48
Mg #	*55.54*	*56.09*	*56.79*	*58.15*	*55.61*

Trace elements in ppm	YSLF-03-11	YSLF-03-12	YSLF-03-13	YSLF-03-14	YSLF-03-15
Zr (XRF)	116	117	107	109	118
La (ICP-MS)	13.10	13.43	12.21	12.78	13.84
Ce (ICP-MS)	27.13	28.16	25.65	26.69	28.86
Pr (ICP-MS)	3.49	3.61	3.32	3.44	3.72
Nd (ICP-MS)	16.12	16.68	15.11	16.12	17.11
Sm (ICP-MS)	4.51	4.70	4.31	4.52	4.80
Eu (ICP-MS)	1.63	1.68	1.58	1.66	1.72
Gd (ICP-MS)	4.98	5.09	4.74	4.85	5.14
Tb (ICP-MS)	0.81	0.85	0.78	0.81	0.86
Dy (ICP-MS)	4.87	5.06	4.76	4.84	5.09
Ho (ICP-MS)	0.92	0.97	0.92	0.93	0.97
Er (ICP-MS)	2.40	2.44	2.29	2.38	2.50
Tm (ICP-MS)	0.33	0.33	0.32	0.32	0.35
Yb (ICP-MS)	1.94	1.97	1.84	1.90	1.99
Lu (ICP-MS)	0.29	0.30	0.27	0.28	0.30
Ba (XRF)	155	144	161	161	157
Ba (ICP-MS)	152.70	156.44	148.82	145.68	161.30
Th (ICP-MS)	1.02	1.05	0.94	0.92	1.05
Nb (XRF)	13.6	14.2	12.7	12.8	13.8
Y (XRF)	24	25	22	23	26
Hf (ICP-MS)	2.94	3.06	2.75	2.81	3.03
Ta (ICP-MS)	1.07	1.08	0.96	1.04	1.09
U (ICP-MS)	0.26	0.26	0.23	0.22	0.27
Pb (ICP-MS)	0.67	0.90	0.55	1.42	1.51
Rb (XRF)	7	6	8	5	6
Cs (ICP-MS)	0.09	0.09	0.08	0.11	0.09
Sr (XRF)	334	333	333	329	337
Sc (ICP-MS)	32.05	32.64	33.28	33.20	33.23
Cr (XRF)	268	283	328	330	257
Ni (XRF)	86	90	93	91	87

APPENDIX B: GEOCHEMICAL DATA

Major and Trace Element Abundances (continued)

Major elements in wt %	Panther Creek cinder cone Swan Lake Flat Basalt (xenoliths)	
	YSLF-03-10O	YSLF-03-10G
SiO_2	73.87	74.93
Al_2O_3	13.41	12.74
TiO_2	0.13	0.11
FeO*	1.74	1.34
MnO	0.02	0.03
CaO	0.96	0.70
MgO	0.26	0.10
K_2O	5.22	5.13
Na_2O	3.15	3.14
P_2O_5	0.02	0.04
Total	98.79	98.26
Mg #	20.8	11.5

Trace elements in ppm	YSLF-03-10O	YSLF-03-10G
Zr (XRF)	220	558
La (ICP-MS)	77.10	68.12
Ce (ICP-MS)	147.80	123.57
Pr (ICP-MS)	14.55	13.06
Nd (ICP-MS)	56.53	47.43
Sm (ICP-MS)	13.62	11.59
Eu (ICP-MS)	1.38	0.44
Gd (ICP-MS)	14.44	10.86
Tb (ICP-MS)	2.62	2.13
Dy (ICP-MS)	17.04	13.69
Ho (ICP-MS)	3.65	2.85
Er (ICP-MS)	10.10	8.08
Tm (ICP-MS)	1.42	1.22
Yb (ICP-MS)	8.08	7.61
Lu (ICP-MS)	1.19	1.11
Ba (XRF)	754	128
Ba (ICP-MS)	755.63	140.16
Th (XRF)	23	28
Nb (XRF)	45.9	59.3
Y (XRF)	106	72
Hf (ICP-MS)	7.66	13.95
Ta (ICP-MS)	3.36	4.58
U (ICP-MS)	4.60	6.88
Pb (ICP-MS)	21.71	28.59
Rb (XRF)	175	216
Cs (ICP-MS)	2.95	3.01
Sr (XRF)	62	30
Sc (ICP-MS)	2.61	2.28
Cr (XRF)	50	52
Ni (XRF)	5	7

APPENDIX B: GEOCHEMICAL DATA

Sr, Nd, and Pb Isotopic Ratios

Sample	Rb (ppm)	Sr (ppm)	Rb/Sr	$^{87}Sr/^{86}Sr$
YU-03-01	10	440	0.022727273	0.705224442
YU-03-04	7	416	0.016826923	0.705973948
HFFR-03-01	10	282	0.035460993	0.70875527
YMR-03-02	21	289	0.07266436	0.706523352
HFGE-03-04	13	285	0.045614035	0.707282358
YSLF-03-01	7	339	0.020648968	0.705385443
YSLF-03-02	11	419	0.026252983	0.705687445
YSLF-03-05	9	373	0.024128686	0.706060048
YSLF-03-09	8	341	0.023460411	0.705390943
YSLF-03-11	7	334	0.020958084	0.705372043
YSLF-03-12	6	333	0.018018018	0.705382343
YSLF-03-14	5	329	0.015197568	0.705278942
YSLF-03-16	6	337	0.017804154	0.705388
YO-03-04	4	307	0.013029316	0.705412343
YHM-03-01	8	306	0.026143791	0.705453144

APPENDIX B: GEOCHEMICAL DATA

Sr, Nd, and Pb Isotopic Ratios (continued)

Sample	Nd (ppm)	Sm (ppm)	$^{147}Sm/^{144}Nd$	$^{143}Nd/^{144}Nd$	ε_{Nd}
YU-03-01	5	22.899	0.136	0.51220567	-8.43339
YU-03-04	5	20.072	0.143	0.51247613	-3.15769
HFFR-03-01	5	21.718	0.139	0.51224212	-7.72238
YMR-03-02	6	25.060	0.138	0.51235765	-5.46876
HFGE-03-04	7	32.314	0.133	0.51227642	-7.05341
YSLF-03-01	4	17.877	0.150	0.51264734	0.18225
YSLF-03-02	4	17.245	0.143	0.51251585	-2.38286
YSLF-03-05	4	15.858	0.149	0.51250842	-2.52769
YSLF-03-09	4	17.710	0.150	0.51262858	-0.18382
YSLF-03-11	4	17.007	0.150	0.51263140	-0.12868
YSLF-03-12	4	17.285	0.150	0.51264841	0.20304
YSLF-03-14	4	16.661	0.152	0.51264411	0.11921
YSLF-03-16	4	17.509	0.149	0.51264316	0.10066
YO-03-04	5	18.290	0.153	0.51264515	0.13947
YHM-03-01	5	19.410	0.147	0.51261135	-0.51985

APPENDIX B: GEOCHEMICAL DATA

Sr, Nd, and Pb Isotopic Ratios (continued)

Sample	Pb	$^{206}Pb/^{204}Pb$	$^{207}Pb/^{204}Pb$	$^{208}Pb/^{204}Pb$
YU-03-01	4	16.625	15.374	37.111
YU-03-04	0	17.149	15.543	37.819
HFFR-03-01	6	17.094	15.539	38.143
YMR-03-02	5	16.825	15.423	38.147
HFGE-03-04	4	17.101	15.530	38.195
YSLF-03-01	0	17.804	15.529	38.516
YSLF-03-02	0	17.388	15.464	37.877
YSLF-03-05	4	17.194	15.500	38.152
YSLF-03-09	0	17.771	15.536	38.518
YSLF-03-11	0	17.788	15.526	38.515
YSLF-03-12	0	17.792	15.521	38.458
YSLF-03-14	0	17.749	15.500	38.415
YSLF-03-16	0	17.836	15.546	38.522
YO-03-04	0	17.893	15.533	38.538
YHM-03-01	2	17.345	15.508	37.993

APPENDIX C: SAMPLE LOCATIONS FOR PETROGRAPHIC ANALYSIS AND GEOCHEMICAL DATA

All locations were taken in the UTM coordinate system using the National Geodetic Vertical Datum of 1929. All coordinates are located in the northern hemisphere within zone 10. When coordinates were not taken with a GPS unit, approximate UTM coordinates were estimated from documented sample locations on 1:24,000 topographic map.

Sample #	Sample Description	Easting	Northing
YSLF-03-01	Swan Lake Flat basalt, Panther Creek flow	528000	4975600
YSLF-03-02	Swan Lake Flat basalt, Tower Road shield	528325	4975482
YSLF-03-03	Swan Lake Flat basalt, Horseshoe Hill vent	526646	4974165
YSLF-03-04	Swan Lake Flat basalt, Horseshoe Hill vent	522333	4965773
YSLF-03-05	Swan Lake Flat basalt, Horseshoe Hill vent	522804	4964896
YSLF-03-06	Swan Lake Flat basalt, Tower Road shield	527472	4976051
YSLF-03-07	Swan Lake Flat basalt, Horseshoe Hill vent	521241	4969306
YSLF-03-08	Swan Lake Flat basalt, Panther Creek agglomerate	520553	4971375
YSLF-03-09	Swan Lake Flat basalt, Panther Creek flow	520552	4371286
YSLF-03-10	Swan Lake Flat basalt, Panther Creek dike	520660	4971507
YSLF-03-11	Swan Lake Flat basalt, Panther Creek flow	520529	4971543
YSLF-03-12	Swan Lake Flat basalt, Panther Creek dike	520681	4971546
YSLF-03-13	Swan Lake Flat basalt, Panther Creek flow	520755	4971892
YSLF-03-14	Swan Lake Flat basalt, Panther Creek flow	520904	4970381
YSLF-03-15	Swan Lake Flat basalt, Panther Creek flow	520675	4971310
YSLF-03-16	Swan Lake Flat basalt, Panther Creek flow	520570	4971399
YMR-03-01	Madison River basalt, shield vent scoria	503776	4947981
YMR-03-02	Madison River basalt, shield vent flow	503761	4947837
YMR-03-03	Madison River basalt, unknown vent	497161	4943839
YU-03-01	Undine Falls basalt, lower flow	527387	4976753
YU-03-03	Undine Falls (Gardiner) basalt	524495	4986898
YU-03-04	Undine Falls basalt, upper flow	536164	4978240
YO-03-01	Osprey basalt, unknown vent	528593	4976574
YO-03-02	Osprey basalt, unknown vent	529035	4976315
YO-03-02A	Osprey basalt, unknown vent	525965	4977740
YO-03-04	Osprey basalt, unknown vent	529716	4976289
HFGE-03-01	Gerrit basalt, vent unknown	463910	4907035
HFGE-03-02	Gerrit basalt, NW of Snake River plain	464316	4893203
HFGE-03-03	Gerrit basalt, vent unknown	465809	4907570
HFGE-03-04	Gerrit basalt, Hatchery Butte vent	467560	4902099
HFFR-03-01	Falls River basalt	465816	4874155
HFWS-03-01	Warm River basalt	477334	4888732

APPENDIX D

GEOCHRONOLOGY

^{40}Ar/^{39}Ar Analytical Techniques

The following description of analytical techniques was provided by Kathy Zanetti and

Dr. Terry Spell of the Nevada Isotope Geochronology Laboratory (NIGL). "The whole rock

samples were crushed, sieved, treated with HNO3, and washed in distilled water and

handpicked to remove phenocrysts and weathered material leaving as pure as a groundmass

sample as possible. Selected samples were wrapped in Al foil and stacked in sealed 6 mm

(inside diameter) Pyrex tubes. Individual packets averaged 3 mm thick and neutron fluence

monitors (FC-2, Fish Canyon Tuff sanidine) were placed every 5-10 mm along the tube.

Synthetic K-glass and optical grade CaF_2 were included in the irradiation packages to

monitor neutron induced argon interferences from K and Ca. Loaded tubes were packed in

an Al container for irradiation. Samples were irradiated at McMaster Nuclear Reactor at

McMaster University, Ontario, Canada. The samples were in-core for 7 hours in the 5C

position where they were surrounded by fuel rods on all four sides. Correction factors for

interfering neutron reactions on K and Ca were determined by repeated analysis of K-glass

and CaF_2 fragments. Measured (^{40}Ar/^{39}Ar)$_K$ values were 0.0001 ($\pm$ 100%). Ca correction

factors were (^{36}Ar/^{37}Ar) Ca = 2.62 ($\pm$ 2.28%) x 10^{-4} and (^{39}Ar/^{37}Ar) Ca = 6.59 ($\pm$ 0.44%) x

10^{-4}. J factors were determined by fusion of 3-5 individual crystals of neutron fluence

monitors which gave reproducibility's of 0.05% to 0.41% at each standard position. Variation in neutron flux along the 100 mm length of the irradiation tubes was <4%.

Irradiated crystals together with CaF_2 and K-glass fragments were placed in a Cu sample tray in a high vacuum extraction line and were fused using a 20 W CO_2 laser. Sample viewing during laser fusion was by a video camera system and positioning was via a motorized sample stage. Samples analyzed by the furnace step heating method utilized a double vacuum resistance furnace similar to the Staudacher et al. (1978) design. Reactive gases were removed by a single MAP and two GP-50 SAES getters prior to being admitted to a MAP 215-50 mass spectrometer by expansion. The relative volumes of the extraction line and mass spectrometer allow 80% of the gas to be admitted to the mass spectrometer for laser fusion analyses and 76% for furnace heating analyses. Peak intensities were measured using a Balzers electron multiplier by peak hopping through 7 cycles; initial peak heights were determined by linear regression to the time of gas admission. Mass spectrometer discrimination and sensitivity was monitored by repeated analysis of atmospheric argon aliquots from an on-line pipette system. Measured $^{40}Ar/^{36}Ar$ ratios were 291.42 ± 0.24% during this work, thus a discrimination correction of 1.01400 (4 AMU) was applied to measured isotope ratios. The sensitivity of the mass spectrometer was ~6 x 10^{-17} mol mV^{-1} with the multiplier operated at a gain of 52 over the Faraday. Line blanks averaged 1.83 mV for mass 40 and 0.01 mV for mass 36 for laser fusion analyses and 2.54 mV for mass 40 and 0.01 mV for mass 36 for furnace heating analyses. Discrimination, sensitivity, and blanks were relatively constant over the period of data collection. Computer automated operation of the sample stage, laser, extraction line and mass spectrometer as well as final data reduction and age calculations were done using LabSPEC software written by B. Idleman (Lehigh

University). An age of 27.9 Ma (Steven et al., 1967; Cebula et al., 1986) was used for the Fish Canyon Tuff sanidine flux monitor in calculating ages for samples.

For $^{40}Ar/^{39}Ar$ analyses a plateau segment consists of 3 or more contiguous gas fractions having analytically indistinguishable ages (i.e. all plateau steps overlap in age at $\pm 2\sigma$ analytical error) and comprising a significant portion of the total gas released (typically >50%). Total gas (integrated) ages are calculated by weighting by the amount of ^{39}Ar released, whereas plateau ages are weighted by the inverse of the variance. For each sample inverse isochron diagrams are examined to check for the effects of excess argon. Reliable isochrons are based on the MSWD criteria of Wendt and Carl (1991) and, as for plateaus, must comprise contiguous steps and a significant fraction of the total gas released. All analytical data are reported at the confidence level of 1σ (standard deviation).

Cebula, G.T., M.J. Kunk, H.H. Mehnert, C.W. Naeser, J.D. Obradovich, and J.F. Sutter, The Fish Canyon Tuff, a potential standard for the ^{40}Ar-^{39}Ar and fission-track dating methods (abstract), *Terra Cognita (6th Int. Conf. on Geochronology, Cosmochronology and Isotope Geology)*, *6*, 139, 1986.
Staudacher, T.H., Jessberger, E.K., Dorflinger, D., and Kiko, J., A refined ultrahigh-vacuum furnace for rare gas analysis, *J. Phys. E: Sci. Instrum.*, *11*, 781-784, 1978.
Steven, T.A., H.H. Mehnert, and J.D. Obradovich, Age of volcanic activity in the San Juan Mountains, Colorado, *U.S. Geol. Surv. Prof. Pap.*, *575-D*, 47-55, 1967.
Wendt, I., and Carl, C., 1991, The statistical distribution of the mean squared weighted deviation, *Chemical Geology*, v. 86, p. 275-285.

NOTE: Discrimination values used during sample analyses are as follows:

$^{40}Ar/^{36}Ar$	4 AMU discrimination
291.24 $\pm$ 0.28%	1.01463
290.87 $\pm$ 0.12%	1.01593

Furnace Blank Averages

^{40}Ar	^{36}Ar	
6.35	0.019	for samples YSLF-2, YO1, YMR2, YMR3, YO4, YU4
5.34	0.017	for samples YSLF-1
6.18	0.026	for samples YSLF-12

REFERENCES CITED

Albardede, F., 1998, Time dependent models of U-Th-He and K-^{40}Ar/^{39}Ar evolution and the layering of mantle convection: Chemical Geology, v. 145, p. 413-429.

Bennett, K., and Smith, E.I., 2004, The Panther Creek volcano: A newly discovered basaltic vent in Yellowstone National Park: Geological Society of America *Abstracts with Programs*, Vol. 36, No. 4, p. 8.

Bradley, F.H., 1873, Report, *in* Hayden, F.V., Sixth annual report of the United States Geological Survey of the Territories: U.S. Geological and Geographical Survey of the Territories Sixth Annual Report [for 1872], p. 191-271.

Bradshaw, T.K., 1991, Tectonics and magmatism in the Basin and Range Province of the western United States [Ph. D. thesis]: Milton Keynes, Open University, 247 p.

Breddam, K. and Kurz, M., 2000, Mapping out the conduit of the Iceland mantle plume with helium isotopes: Earth and Planetary Science Letters, v. 176, 1, p. 45-55.

Budahn, J.R. and Schmitt R.A., 1985, Petrogenetic modeling of Hawaiian tholeiitic basalts: A geochemical approach: Geochimica et Cosmochimica Acta, v. 49, p. 67-87.

Bush, J.H., Jr., 1967, The basalts of Yellowstone Valley, southwestern Montana [Master's Thesis], Montana State University, 66 pp.

Carr, M.J., 2000, Igpet for Windows petrology software: Somerset, Terra Softa, Inc., Version: June 12, 2002.

Christiansen, R.L. and Blank, R.H., Jr., 1972, Volcanic Stratigraphy of the Quaternary Rhyolite Plateau in Yellowstone National Park: U. S. Geological Survey Professional Paper 729-B, 18 p.

Christiansen R.L. and Lipman, P.W., 1972, Cenozoic volcanism and tectonism in the western United States and adjacent parts of the spreading ocean floor: Transactions of the Royal Society of London, v. 271, p. 249-284.

Christiansen, R.L, 1974, Geologic map of the West Thumb Quadrangle, Yellowstone National Park, Wyoming: U.S. Geological Survey Geologic Quadrangle Map GQ-1191, scale 1:62,500.

Christiansen, R.L and Blank, R.H., Jr., 1974a, Geologic map of the Old Faithful Quadrangle, Yellowstone National Park, Wyoming: U.S. Geological Survey Geologic Quadrangle Map GQ-1189, scale 1:62,500.

Christiansen, R.L, and Blank, R.H., Jr., 1974b, Geologic map of the Madison Junction Quadrangle, Yellowstone National Park, Wyoming: U.S. Geological Survey Geologic Quadrangle Map GQ-1190, 1974, scale 1:62,500.

Christiansen, R.L, and Blank, R.H., Jr., 1975a, Geologic map of the Norris Junction Quadrangle, Yellowstone National Park, Wyoming: U.S. Geological Survey Geologic Quadrangle Map GQ-1193, scale 1:62,500.Christiansen, R.L, and Blank, R.H., Jr., 1975b, Geologic map of the Canyon Village Quadrangle, Yellowstone National Park, Wyoming: U.S. Geological Survey Geologic Quadrangle Map GQ-1192, scale 1:62,500.

Christiansen, R.L. and McKee, E.H., 1978, Late Cenozoic and tectonic evolution of the Great Basin and Columbia intermountain region: Memoirs of the Geological Society of America, v. 152, p. 283-311.

Christiansen, R.L., 2001, The Quaternary and Pliocene Yellowstone Plateau volcanic field of

Wyoming, Idaho, and Montana: U. S. Geological Survey Professional Paper 729-G, 144

p.

Christiansen, R.L., Foulger, G.R., and Evans, J.R., 2002, Upper-mantle origin of the

Yellowstone hotspot: Geological Society of America Bulletin, v. 114, 10, p. 1245-1256.

Clague, D.A., and Dalrymple, G.B., 1989, Tectonics, geochronology, and origin of the

Hawaiian-Emperor volcanic chain *in* Geology of North America, Vol. N, *eds*. Winterer,

E.L., Hussong, D.M., Decker, R.W., Boulder, CO: Geological Society of America, p.

188-217.

Condie, K., 2001, *Mantle plumes and their record in Earth history*, Cambridge University

Press: Cambridge, United Kingdom, 306 p.

Doe, B.R., Leeman, W.P., Christiansen, R.L., and Hedge, C.E., 1982, Lead and Strontium

isotopes and related trace elements as genetic tracers in the upper Cenozoic rhyolite-

basalt association of the Yellowstone Plateau Volcanic Field: Journal of Geophysical

Research, v. 87, p. 4785-4806.

Dueker, K., Yuan, H., and Zurek, B., 2001, Thick-structured Proterozoic lithosphere of the

Rocky Mountain region: GSA Today, v. 11, p. 4-9.

Duffield, W., Riggs, N., Kaufman, D., Champion, D., Fenton, C., Forman, S., McIntosh, W.,

Hereford, R., Plescia, J., and Ort, M., 2006, Multiple constraints on the age of a

Pleistocene lava dam across the Little Colorado River at Grand Falls, Arizona: GSA

Bulletin, v.118, no.3/4, p. 421-429.

Eaton, G.P., Christiansen, R.L., Iyer, H.M., Pitt, A.M., Mabey, D.R., Blank, J.R., Jr., Zietz, I., and Gettings, M.E., 1975, Magma beneath Yellowstone National Park: Science, v. 188, p. 787-796.

Feeley, T.C., 2003, Origin and Tectonic Implications of the Across-Strike Geochemical Variations in the Eocene Absaroka Volcanic Province: United States: Journal of Geology, v. 111, p. 329-346.

Fenner, C.N., 1938, Contact relationships between rhyolite and basalt on the Gardiner River, Yellowstone Park: Geological Society of America Bulletin, v. 49, p. 1441-1484.

Fenner, C.N., 1944, Rhyolite-basalt complex on Gardiner River, Yellowstone Park, Wyoming: A discussion: Geological Society of America Bulletin, v. 55, p. 1081-1096.

Fitton, J.G., James, D., and Leeman, W.P., 1991, Basic magmatism associated with late Cenozoic extension in the western United States: Compositional variations with space and time: Journal of Geophysical Research, v. 96, p. 13,693-13,711.

Gridley, D.J., and Smith, M.S., 2004, The Gardiner Basalts: petroogical and geochemical comparison with the Hepburn Mesa and Yellowstone National Park basalts: Abstracts with Programs-Geological Society of America, v. 36, no. 2, 103 p.

Hague, A., 1912, Geologic History of the Yellowstone National Park, United States of America: U.S. Department of the Interior, 24 p.

Hamilton, W., 1960, Late Cenozoic tectonics and volcanism in the Yellowstone region, Wyoming, Montana, and Idaho, in West Yellowstone earthquake area: Billings Geological Society Guidebook 11th Annual Field Conference, 1960, p. 92-105.

Hamilton, W., 1963, Petrology of rhyolite and basalt, northwestern Yellowstone Plateau, Article 80, *in* Short Papers in geology and hydrology: U.S. Geological Survey Professional Paper 475-C, p. C78-C81.

Hamilton, W., 1964, Volcanic rocks of the West Yellowstone and Madison Junction quadrangles, Montana, Wyoming, and Idaho, in the Hegben Lake, Montana, earthquake of August 17, 1959: U.S. Geological Survey Professional Paper 435-S, p. 209-221.

Hamilton, W., 1965, Geology and petrogenesis of the Island Park caldera of rhyolite and basalt, eastern Idaho: U.S. Geological Survey Professional Paper 504-C, 37 p.

Hamilton, W., and Wilshire, H.G., 1965, Liquid fractionation of basaltic magmas: Geological Society of America Special Paper 82, 331 p.

Hanan, B.B. and Graham, D.W., 1996, Lead and Helium isotope evidence form oceanic basalts for a common deep source of mantle plumes: Science, v. 272, p. 991-995.

Harry, D.L. and Leeman, W.P., 1995, Partial melting of melt metasomatized subcontinental mantle and the magma source potential of the lower lithosphere: Journal of Geophysical Research, v. 100, p. 10,225-10,269.

Hawkes, L., 1945, The Gardiner River rhyolite-basalt complex: Geological Magazine, v. 82, p. 182-184.

Hawkesworth, C., Turner, S., Gallagher, K., Hunter, A., Bradshaw, T., and Roger, N., Calc-alkaline magmatism, lithospheric thinning and extension in the Basin and Range: Journal of Geophysical Research, v. 100, p. 10,271-10,286.

Hayden, F.V., 1872, Report, *in* Hayden F.V., Preliminary report of the United States Geological Survey of Montana and Portions of Adjacent Territories: U.S. Geological and Geographical Survey of the Territories Fifth Annual Report [for 1871], p. 13-165.

Hayden, F.V., 1873, Report, *in* Hayden, F.V., Sixth annual report of the United States Geological Survey of the Territories: U.S. Geological and Geographical Survey of the Territories Sixth Annual Report [for 1872], p. 13-

Hildreth, W., Halliday, A.N., and Christiansen, R.L., 1991, Isotopic and chemical evidence concerning the genesis and contamination of basaltic and rhyolitic magma beneath the Yellowstone Plateau Volcanic Field: Journal of Petrology, v. 32, p. 63-138.

Hilton, D.R., Gronvold, K., Macpherson, C.G., and Castillo, P.R., 1999, Extreme $^3He/^4He$ ratios in northwest Iceland, constraining the common component in mantle plumes: Earth and Planetary Science Letters, v. 173, p. 53-60.

Hughes, S.S., Wetmore, P.H., and Casper, J.L., 2004, Evolution of Quaternary tholeiitic basalt eruptie centers on the eastern Snake River Plain, Idaho, *in* Bonnichsen, B., White, C.M. and McCurry, M., eds., Tectonic and Magmatic Evolution of the Snake River Plain Volcanic Province: Idaho Geological Survey Bulletin 30, p. 329-342.

Humphreys, E. D., Dueker, K.G., Schutt, D.L., and Smith, R.B., 2000, Beneath Yellowstone: Evaluating Plume and Non-Plume Models using Teleseismic Images of the Upper Mantle: GSA Today, v. 10, 12, p. 1-7.

Iddings, J.P., 1888, Obsidian Cliff, Yellowstone National Park: U.S. Geological Survey Annual Report, 7th, p. 249-295.

Iddings, J.P., 1899a, The rhyolites, *in* Hague, A., Geology of the Yellowstone National Park: U.S. Geological Survey Monograph 32, Part 2, p. 365-342.

Iddings, J.P., 1899b, Recent basalts, *in* Hague, A., Geology of the Yellowstone National Park: U.S. Geological Survey Monograph 32, Part 2, p. 433-439.

Johnson, D.M., Hooper, P.R., and Conrey, R.M., 1999, XRF Analysis of rocks and minerals for major and trace elements on a single low dilution Li-tetraborate fused bead: Advances in X-ray Analysis, v. 41, p. 843-867.

Josten, N.E., and Smith, R.P., 1997, Gravity evidence for buried calderas beneath the eastern Snake River plain, Idaho: Abstracts with Programs-Geological Society of America, v. 29, no. 6, 365 p.

Kaharka, Y.M., Sorey, M.L., and Thordsen, J.J., 2000, Large-scale hydrothermal fluid discharges in the Norris-Mammoth corridor, Yellowstone National Park, USA: Journal of Geochemical Exploration, v. 69-70, p. 201-205.

Keller, G.R., Karlstrom, K.E., and Farmer, G.L., 1999, Tectonic evolution in the Rocky Mountain region; 4-D imaging if the continental lithosphere: Eos, v. 80, no. 42, p. 493-498.

Kennedy, B.M., Reynolds, J.H., Smith, S.P., and Truesdell, A.H., 1978, Helium isotopes: Lower Geyser basin, Yellowstone National Park: Journal of Geophysical Research, v. 92, p. 12,477-12,489.

Klein, E.M. and Langmuir, C.H., 1987, Global correlations of ocean ridge basalt chemistry with axial depth and crustal thickness: Journal of Geophysical Research, v. 92, p. 8089-8115.

Kuntz, M.A., Champion, D.E., Spiker, E.C., Lefebvre, R.H., and McBroome, L.A., 1982, The Great Rift and the evolution of the Craters of the Moon lava field, Idaho, *in* Bonnichsen, B. and Breckenridge, eds., Cenozoic Geology of Idaho: Idaho Bureau of Mines and Geology Bulletin 26, p. 423-437.

Leeman, W.P., Menzies, M.A., Matty, D.J., and Embree, G.F., 1985, Strontium, neodymium, and lead isotopic compositions of deep crustal xenoliths from the Snake River Plain: evidence for Archaen basement: Earth and Planetary Science Letters, v. 75, p. 354-368.

Lehman, J.A., Smith, R.B., Schilly, M.M., and Braile, L.W., 1982, Upper crustal structure of the Yellowstone caldera from seismic delay time analyses and gravity correlations: Journal of Geophysical Research, v. 87, p. 2713-2730.

Lemarchand, F., Villemant, B., and Calas, G., 1987, Trace element distribution coefficients in alkaline series: Geochimica et Cosmochimica Acta, v. 51, p. 1071-1081.

Liotard, J.M., Briot, D., and Boivin, P., 1988, Petrological and geochemical relationships between pyroxene megacrysts and associated alkali-basalts from Massif Central (France): Contributions to Mineralogy and Petrology, v. 98, p. 81-90.

Loper, D.E., and Stacey, F.D., 1983, The dynamical and thermal structure of deep mantle plumes: Physics of the Earth and Planetary Interiors, v. 33, p. 304-317.

Love, J.D., and Keefer, W.R., 1975, Geology of the sedimentary rocks in southern Yellowstone National Park, Wyoming: U. S. Geological Survey Professional Paper 729-D, 60 p.

Lum, C.C., Leeman, W.P., Foland, K.A., Kargel, J.A., and Fitton, J.G., 1989, Isotopic variations in continental basaltic lavas as indicators of mantle heterogeneity: Examples from the western U.S. cordillera: Journal of Geophysical Research, v. 94, p. 7871-7884.

Mabey, D.R., Zietz, I., Eaton, G.P., and Kleinkopf, M.D., 1978, Regional magnetic patterns in part of the Cordillera in the Western United States, *in* Smith, R.B., and Eaton, G.P., Cenozoic tectonics and regional geophysics of the western Cordillera: Geological Society of America Memoir 152, p. 93-106.

MacKenzie, W.S., Donaldson, C.H., and Guiford, C., 1982, *Atlas of Igneous Rocks and Their Textures*, John Wiley & Sons: Oregon, 148 p.

McKenzie, D.P., 1984, The generation and compaction of partially molten rock: Journal of Petrology, v. 25, p. 713-765.

Morgan, L.A., Doherty, D.J., and Leeman, W.P., 1984, Ignimbrites of the eastern Snake River plain; evidence for major caldera-forming eruptions: Journal of Geophysical Research, v. 89, 10, p. 8665-8678.

Obradovich, J.D., 1992, Geochronology of the late Cenozoic volcanism of Yellowstone National Park and adjoining areas, Wyoming and Idaho: U.S. Geological Survey Open File Report 92-408, 45 p.

O'Brien, H.E, Irving, A.J., McCallum, I.S., Thirlwall, M.F., 1995, Strontium, neodymium, and lead isotopic evidence for the interaction of post-subduction asthenospheric potassic mafic magmas of the Highwood Mountains, Montana, USA, with ancient Wyoming craton lithospheric mantle: Geochimica et Cosmochimica Acta, v. 59, No. 21, p. 4539-4556.

Peale, A.C., 1873, Report, *in* Hayden, F.V., Sixth annual report of the United States Geological Survey of the Territories: U.S. Geological and Geographical Survey of the Territories Sixth Annual Report [for 1872], p. 99-187.

Pierce, K.L., 1979, History and Dynamics of Glaciation in the Northern Yellowstone National Park Area: U. S. Geological Survey Professional Paper 729-F, 90 p.

Reed, J.C., Jr., 1993, Map of the Precambrian rocks of the coterminous United States and some adjacent parts of Canada, *in* Reed, J.C., Jr., Sims, P.K.; Harrison, J.E.; and

Peterman, Z.E., Precambrian: Coterminous U.S.: Boulder, Colo., Geological Society of America, The Geology of North America, v. C-2, pl. 1, scale 1: 5,000,000.

Richards, M.A., and Griffiths, R.W., 1988, Deflection of plumes by mantle shear flow: Experimental results and a simple theory: Geophysical Journal of the Royal Astronomy Society, v. 93, p. 367-376.

Richter, D.H., and Moore, J.G., 1966, Petrology of the Kilauea Iki Lava Lake Hawaii: U.S. Geological Survey Professional Paper 537-B, 26 p.

Ruppel, E.T., 1972, Geology of the pre-Tertiary rocks in the northern part of Yellowstone National Park, Wyoming: U. S. Geological Survey Professional Paper 729-A, 66 p.

Sakimoto, S.E.H., Gregg, T.K.P., Hughes, S.S., and Chadwick, J., 2003, Re-Assessing Plains-style Volcanism on Mars [Abstract]: Sixth International Conference on Mars.

Sharma, M., 1997, Siberian traps: American Geophysical Union, Monograph 100, p. 273-295.

Smedes, H.W. and Prostka, H.J., 1972, Stratigraphic framework of the Absaroka Volcanic Supergroup in Yellowstone National Park, Wyoming: U. S. Geological Survey Professional Paper 729-C, 33 p.

Smith, A.D., 1993, The continental mantle as a source for hotspot volcanism: Terra Nova, v. 5, p. 452-460.

Smith, E.I., and Bennett, K., 2004, A geochemical and geochronological database for the Yellowstone Plateau volcanic field: Implications for the origin of post-caldera basalt and the future of the Yellowstone magmatic system: Geological Society of America *Abstracts with Programs*, Vol. 36, No. 4, p. 10.

Smith, M., Lageson, D., Heatherington, A., and Harlan, S., 1995, Geochronology, geochemistry and isotope systematics of the basalt of Hepburn Mesa, Yellowstone River valley, Montana: Rocky Mountain Section Abstracts-Geological Society of America, vol.27, no.4, pp.56.

Smith, R.B., and Braile, L.W., 1984, Crustal structure and evolution of an explosive silicic volcanic system at Yellowstone National Park, *in* Explosive volcanism: Washington, National Academy of Sciences, p. 96-109.

Spell, T.E., Smith, E.I., Nastanski, N., Bennett, K., 2004, Establishment and Evolution of a new Silicic Magma System North of Yellowstone Caldera: Geochronology, Geochemistry and Petrographic Relationships of Extracaldera Basalts and Rhyolites in the Norris-Mammoth Corridor: Eos Transactions of the American Geophysical Union, v. 85, no. 47, Abstract V52B-08.

Steinberger, B. and O'Connell, R.J., 1998, Advection of plumes in mantle flow: Implications for hotspot motion, mantle viscosity, and plume distribution: Geophysics Journal International, v. 132, p. 412-434.

Struhsacker, D., Mixed basalt-rhyolite assemblages in Yellowstone National Park: the petrogenetic significance of magma mixing: Geological Society of America Abstracts, Rocky Mountain Section Meeting, 1978: p. 239.

Wang, K., Plank, T., Walker, J.D., and Smith E.I., 2002, A mantle melting profile across the Basin and Range, SW USA: Journal of Geophysical Research, v. 107, p. 1010-1029.

White, C.M., Hart, H.K., Bonnichsen, B., and Matthews, D., 2002, Geochemical and Sr-isotopic variations in the western Snake River Plain basalts Idaho, *in* Bonnichsen, B.,

White, C.M. and McCurry, M., eds., Tectonic and Magmatic Evolution of the Snake River Plain Volcanic Province: Idaho Geological Survey Bulletin 30, p. 329-342.

White, R.S. and McKenzie, D., 1989, Magmatism at rift zones: The generation of volcanic and continental margins and flood basalts: Journal of Geophysical Research, v. 94, p. 7685-7729.

Whitehead, J.A., 1982, Instabilities in fluid conduits in flowing earth-Are plates lubricated by the asthenosphere?: Geophysical Journal of the Royal Astronomy Society, v. 70, p. 415-433.

Whitehead, J.A., and Luther, D.S., 1975, Dynamics of laboratory diapir and plume models: Journal of Geophysical Research, v. 90, p. 705-717.

Wilcox, R.E., 1944, Rhyolite-basalt complex on Gardiner River, Yellowstone Park, Wyoming: A discussion: Geological Society of America Bulletin, v. 55, p. 1047-1079.

Williams, H., 1932, Geology of the Lassen Volcanic National Park, California: University of California Publications: Bulletin of the Department of Geological Sciences, v. 21, no. 8, 385 p.

Wilson, J.T., 1963, A possible origin of the Hawaiian Islands: Canadian Journal of Physics, v. 41, p. 863-870.

Wilson, M., 1989, *Igneous Petrogenesis: A Global Tectonic Approach*, Chapman & Hall: London, 465 p.

Wolfgang, E.E., and Wohletz, K.H., 1987, Quaternary basalt fields of west-central New Mexico: McCartys pahoehoe flow, Zuni Canyon aa flow, Zuni ice cave, Bandera Crater, and Zuni Salt Lake maar: Centennial Field Guide Volume 2: Rocky Mountain Section of the Geological Society of America, vol: 2, p. 431-436.

Wooden, J.L., and Mueller, P.A., 1988, Pb, Sr, and Nd isotopic compositions of a suite of

Late Archaen, igneous rocks, eastern Beartooth Mountains: implications for crust-mantle

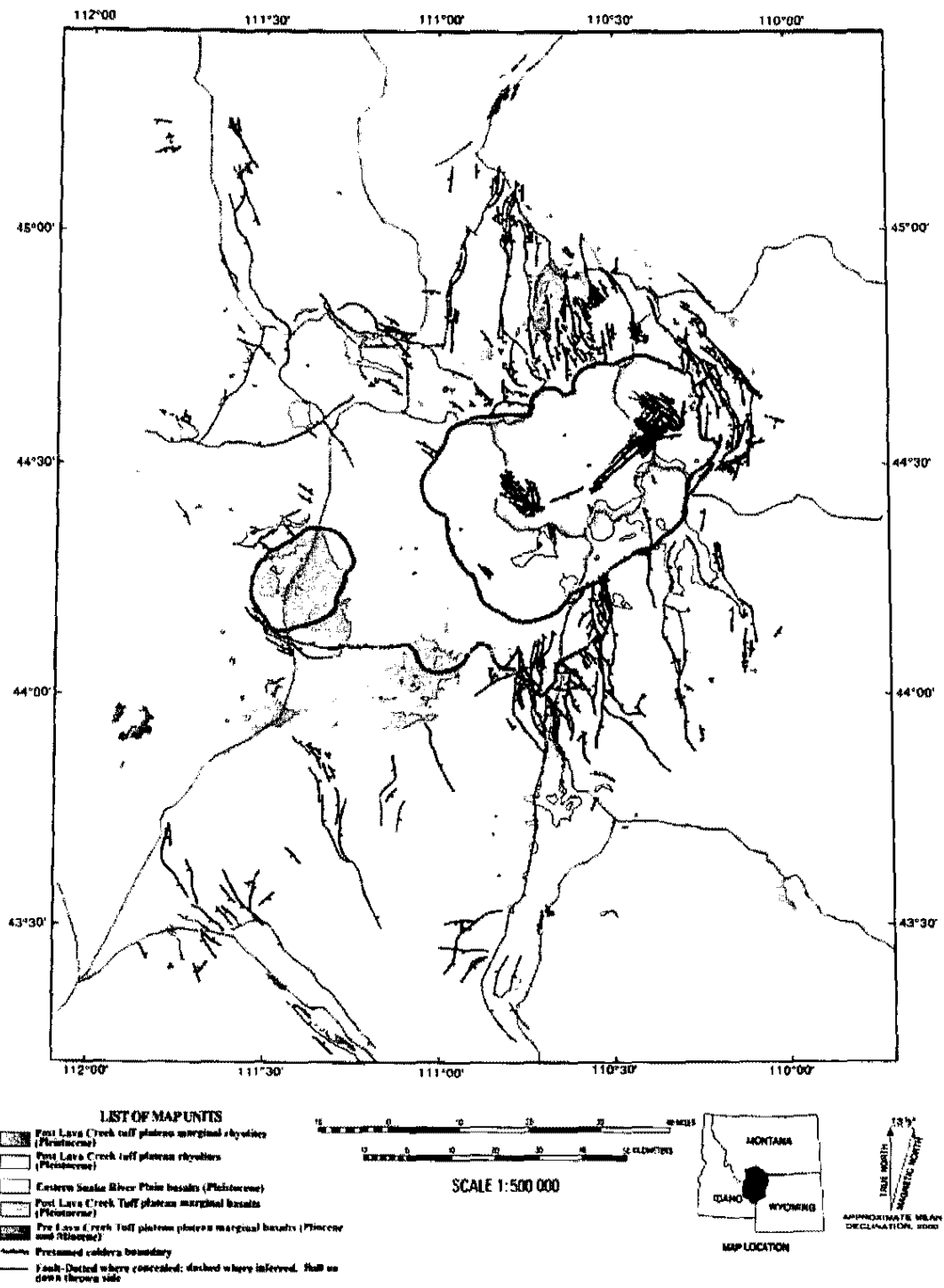evolution: Earth and Planetary Science Letters, v. 87, p.59-72.

LIST OF MAP UNITS

Post Lava Creek tuff plateau marginal rhyolites (Pleistocene)

Post Lava Creek tuff plateau rhyolites (Pleistocene)

Eastern Snake River Plain basalts (Pleistocene)

Post Lava Creek Tuff plateau marginal basalts (Pleistocene)

Pre Lava Creek Tuff plateau plateau marginal basalts (Pliocene and Pleistocene)

Presumed caldera boundary

Fault-Dotted where concealed; dashed where inferred. Ball on down thrown side

SCALE 1:500 000

MONTANA

IDAHO   WYOMING

MAP LOCATION

APPROXIMATE MEAN DECLINATION, 2000

Plate 1: Geologic map of selected basalt and rhyolite units within Yellowstone National Park. Modified *from* Christiansen, R.L., 2001, Geology of Yellowstone National Park-The Quaternary and Pliocene Yellowstone Volcanic Field of Wyoming, Idaho, and Montana: U.S. Geological Survey Professional Paper 729-G.